UNIVERSITAT DE BARCELONA

Role of TGFβ family members on physiological angiogenesis and ovarian cancer

Elisenda Alsina Sanchis

ROLE OF TGFβ FAMILY MEMBERS IN PHYSIOLOGICAL ANGIOGENESIS AND OVARIAN CANCER

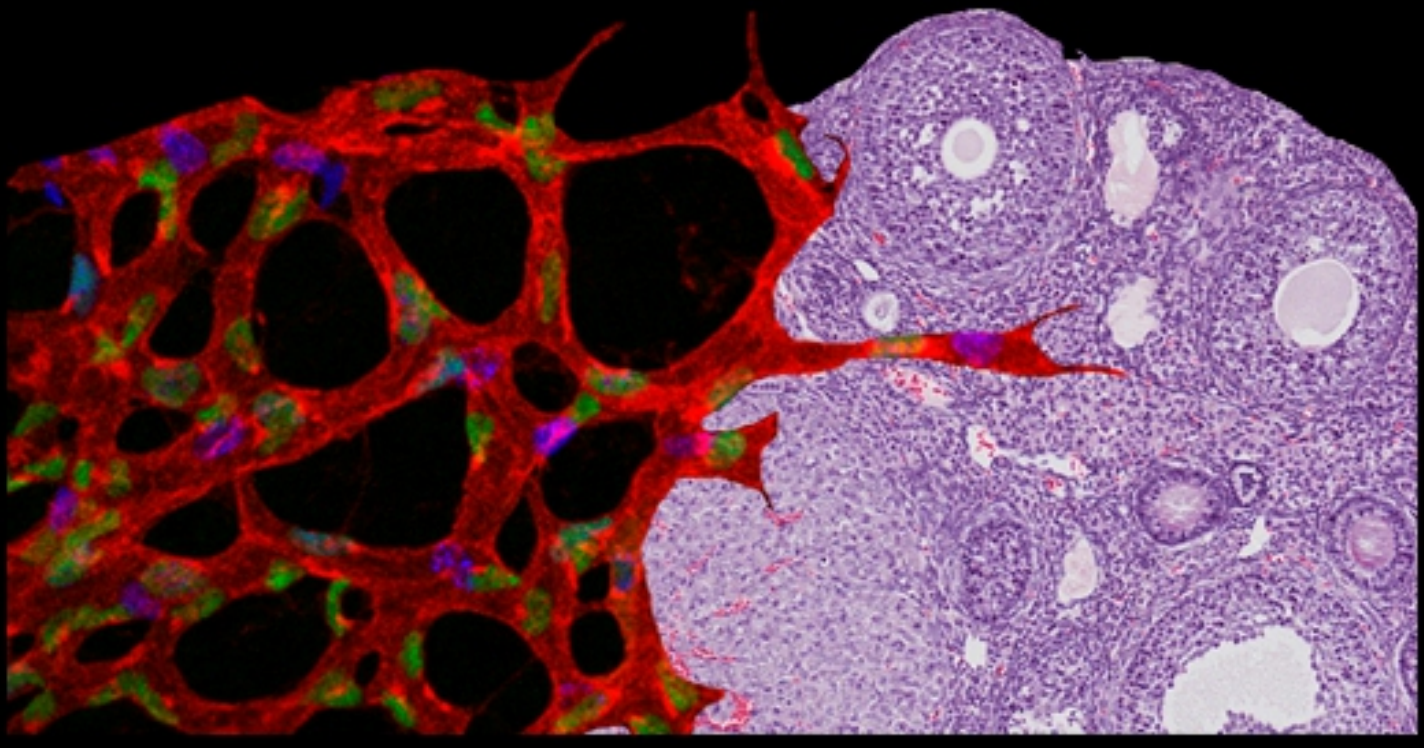

Elisenda Alsina Sanchis

Tesi Doctoral 2016

UNIVERSITAT DE BARCELONA

ROLE OF TGFβ FAMILY MEMBERS IN PHYSIOLOGICAL ANGIOGENESIS AND OVARIAN CANCER

PhD Thesis

Elisenda Alsina Sanchis

January 2016, Barcelona

IDIBELL
Institut d'Investigació Biomèdica de Bellvitge

ICO
Institut Català d'Oncologia

ROLE OF TGFβ FAMILY MEMBERS IN PHYSIOLOGICAL ANGIOGENESIS AND OVARIAN CANCER

Memòria de Tesi Doctoral presentada per

Elisenda Alsina Sanchis per optar al Grau de Doctor

Treball realitzat sota la direcció del Dr. Francesc Viñals i Canals
a l'Institut Català d'Oncologia i
l'Institut d'Investigacions Biomèdiques de Bellvitge

Tesi adscrita al Departament de Ciències Fisiològiques II
Programa de doctorat en Biomedicina
Facultat de Medicina, Universitat de Barcelona

Gener 2016, Barcelona

Francesc Viñals i Canals
Director de tesi

Elisenda Alsina i Sanchis
Doctoranda

This PhD thesis titled "*ROLE OF TGFβ FAMILY MEMBERS IN PHYSIOLOGICAL ANGIOGENESIS AND OVARIAN CANCER"* was performed at l'Institut Català d'Oncologia and l'Institut d'Investigacions Biomèdiques de Bellvitge and It has been founded by Ministerio de Economia y Competitividad with a FPI scholarship.

“A story has no beginning or end: arbitrarily one chooses that moment of experience from which to look back or from which to look ahead.”

Graham Greene

Aknowledgment/Agraïments

Sembla mentida, fa uns cinc anys vaig començar aquest camí i fa uns mesos la escriptura... i finalment arriba aquest moment, encara no m'ho acabo de creure. Mentre estic escrivint aquestes línies se'm passen pel cap moltes coses: molts pensaments, vivències, bons i mals moments... I es que una tesi dona per molt!!! Però, el que està clar es que sense tots vosaltres això no ho hagués pogut fer, una mica d'aquest tesis també és vostra.

Primer de tot voldria agrair al Francesc Viñals per haver confiat en mi i haver-me donat la oportunitat d'entrar en aquest projecte. Per saber-me motivar i transmetrem aquestes ganes de saber més, sense perdre el bon humor en cap moment. Per ensenyar-me que en la ciència també pot haver-hi bellesa, perquè encara que la foto sigui d'uns vasos sanguinis... també pot ser bonica. Simplement, gràcies per haver sigut tant proper i educador però alhora exigent, ja que sense treball no hi ha resultats. Ha estat un plaer realitzar la tesis sota la teva direcció, on he aprés tant professional com personalment.

També voldria agrair a l'ajuda incondicional de la meva "mare científica" Agnès Figueras. Ja se que no ets amant d'aquests elogis, però sense tu aquesta tesi no hagués sigut possible de cap manera. Tant pel que m'has ensenyat professionalment, la reina de les immunos, els ratolins i tantes altres tècniques... com per les grans converses que hem tingut l'una amb l'altre, per tot això i molt més, moltes gràcies.

Tampoc podria deixar-me la gent que m'ha ajudat al llarg d'aquest treball, ja que el grup d'Angio és molt gran. Tant l'Oriol Casanovas per les aportacions als labs meetings com la Mariona Graupera, per les aportacions als labs meetings i especialment per l'ajuda en el projecte de les retines, al principi he de reconèixer que em feia una mica de por cada vegada que havia d'anar a agafar anticossos.. però després aquesta por s'ha convertit en simpatia, perquè no és tant seria com sembla... A l'Alberto Villanueva pels seus super ratolins, no només per deixar-me treballar amb els seus models sinó també per les seves explicacions a l'estabulari. També voldria agrair el suport a l'August Vidal pels seus coneixements histològics sobre el càncer d'ovari.

Parlant del projecte de les retines... no puc deixar de mencionar i agrair el gran COM3, on les bogeries, rialles i bons moments són el que més m'emporto. Moltes gràcies pels grans moments des del principi a l'Helena (Pixurri), pel gran suport en el món de l'aïllament i les tincions de les retines, i a l'Adri, tb per aquest últims moments bojos d'escriptura, anava bé saber que no estava sola. Por las grandes incorporaciones de las Anas las loquis (Angulo y Fonsi) sois muy grandes y para el pequeñín Iñigo que trajiste un poco de orden al COM3 i también, para Erica la morenaza. No puedo dejar de mencionar a Clara, Raffa y Gaby, que aún sin formar parte de Angio, me han hecho sentir como en casa en el COM3.

Tornant al LRT i seguint amb el grup d'angio, voldria agrair a tots els membres del grup que m'han ajudat a realitzar aquest treball, tant els que no hi son com la Mercè, de la qual vaig aprendre molt, la Vives, la Laura, la Lidia i especialmente a Lara, que fuiste un gran apoyo para mí en muchos momentos, tanto buenos como malos. Com dels que segueixen formant part: Gaby, Nick, Susana, Patricia, Iratxe, Júlia i especialment a la Mar, pel seu coneixement i suport pel que fa al món ratonil i l'Alba per la extra vigilància de la meva mini colònia que per mi ja era gran. Tampoc puc deixar de nombrar a les meves "Xaperonines", Roser i Mariona, uns grans fitxatges per angio i per la meva vida. Tampoc les incorporacions de l'Ali, la Carla, la Zas i el iogurín Álvaro amb els que he disfrutat aprenent a comentar i debatre de tu a tu sobre projectes per a treure més suc als experiments i als diferents projectes.

Però, per sort el LRT, és un gran laboratori amb molts grups que a part de tenir coneixements varis també permet conèixer a moltes grans persones. Perquè sense tots vosaltres i el gran ambient tampoc hagués sigut possible, tant a la sala de becaris, cultius, com pel mig del lab o a la Flama, Salamandra o sopars varis. Al Luis con sus borderias-dulces, al Marcel , per les grans converses de camí o tornada del lab o de festa..., al Carlos, por nuestras grandes conversaciones, ayudas varias y porque todo lo sabes, la ciencia tiene suerte de tenerte. A l'Alba (Pelmins) per les grans converses i pels moments musicals compartits amb el Carlos a les tantes a la sala de becaris. A Curro por los buenos momentos tanto en la comida como fuera del lab, a la Marta i al Raúl, por ser o no como eres. També a les tres flors de

l'Alberto que sempre estan allà; Maria, Sara i Mónica. A la Sònia pel descobriment del convent... i al Derek per l'ajuda amb l'anglès. Tampoco puedo olvidarme de todos los "Borja", tanto los de ahora como los de antes, que han hecho de estos años unos grandes momentos, tanto cenas como excursiones o escapadas: Ahmed, Arianne, Carmen, Edu, Eric, Dani, Gorka, Iris, Jack, Joan, Martí, Miguel, Natalia, Nerea, Paco, Samuel, Silvia. També m'agradaria agrair a la Nadia i el Rafa per ser tant divertits i a l'Olga, pels seus bon dia i les imprescindibles ajudes amb els materials del laboratori cada dia, sense tu el LRT no seria el mateix. I també voldria agrair a la Thais, gracias por nuestras charlas y por siempre estar allí.

No vull deixar-me tampoc a tots aquells que tot i no estar al laboratori, sense vosaltres aquesta tesis tampoc hagués sigut capaç. Perquè durant aquests anys de tesis també he après molt al vostre costat.

A les Bionenes, pels nostres afterworks, els nostres sopars i simplement pels nostres moments. Per tot això i molt més que no puc explicar.... és una gran sort tenir-vos a la meva vida. A la Ruth, la sandra Ba, la Marina, la Xell, la Cris, la Maria, l'Alba, la Sandra Bo i la juli. També al Marcus que encara que et resisteixis, ets una Bionena més.

A les meves U..... fa molts anys que ens coneixem i molts més que seguiran. Perquè hem passat grans coses i hem crescut i madurat juntes. No podria haver-ho fet sense vosaltres. Per totes les nostres anades d'olla, els sopars mensuals i els riures inacabables. A les meves petites Saigí i Anna (Ru), a la Sara, Mercè, Amanda, Raquel i Montse.

I would like to thank all my International LUMC friends. It has been really nice to catch up with you all from time to time here in Barcelona or in Holland: Jelrik, Roel, Yahya, Malin and Fleur. Fleur and Malin our skypes dates have been always such fun. Fleur, I'm so grateful that I don't have enough words to describe it. Not only for your last help with all the English corrections of this thesis but for your support in my "old Dutch life", and for being always there.

I per acabar a tu Pere, sense tu aquest últims mesos haurien sigut insuportables. Moltes gràcies per ser com ets, per estar al meu costat encara que sigui una clara tortura, escoltar-me i animar-me a no defallir. Però sobretot per fer-me riure constantment, perquè al teu costat la vida sembla més fàcil.

Finalment voldria agrair als meus pares, sou els millors pares que podria tenir. Sense vosaltres i el vostre suport no ho hauria pogut aconseguir. Soc tot el que soc gràcies a vosaltres.

Moltíssimes gràcies a tots.

Abbreviations

µg	microgram
µl	microlitre
µM	micromolar
ml	millilitre
AKT	Protein Kinase B
ALK1	Activin receptor-like kinase 1
ALK5	TGFβ receptor type 1
BMP	bone morphogenetic protein
BSA	Bovine serum albumin
CCC	Clear-cell carcinoma
CDDP	Cisplatin
DMEM	Dulbecco's modified Eagle's medium
DMSO	Dimethyl sulfoxide
EC	Endothelial Cell
ECACC	*European Collection of Cell Cultures*
ECM	Extracellular matrix
EMC	Endometrioid carcinoma
EMT	epithelial-mesenchymal transition
EOC	Epithelial ovarian cancer
ERK 1/2	Extracellular-signal-regulated kinase-1/2
FBS	Foetal bovine serum
HGSC	High-grade serous carcinoma
HHT	hereditary haemorrhagic telangiectasia
H&E	Haematoxylin & Eosin
IF	Immunofluorescence
IGF	Insulin-like growth factor
IGF1R	Insulin-like growth factor 1 receptor
IHC	immunohistochemistry
LGSC	Low-grade serous carcinoma
MAPK	Mitogen-activated protein kinase
MC	Mucinous carcinoma
MTT	3-(4,5-dimethylthiazol-2-yl)-2,5-diphenyltetrazolium bromide
OSE	Ovarian surface epithelium
PBS	phosphate buffered saline
PCR	Polymerase chain reactions
PDGF	Platelet-derived growth factor
PI3K	Phosphoinositide 3- kinase
PTEN	Phosphatase and tensin homolog
RPMI	Roswell Park Memorial Institute medium
RTK	Receptor tyrosine kinase
SDS	sodium dodecyl sulfate
SEM	standard error of the mean
shRNA	Short-hairpin RNA
TBS	Tris buffered saline
TGFβ	Transforming growth factor β
TGFβRI	TGF-β type I receptor
TGFβRII	TGF-β type II receptor
TMA	Tissue macro array
TUNEL	Terminal deoxynucleotidyl transferase dUTP nick end labelling
VEGF	Vascular endothelial growth factor

List of Figures

List of Tables

Introduction

Introduction

1. TGFβ signalling pathway

Transforming growth factor-β (TGFβ) is a large family of cytokines involved in a wide range of cellular processes such as proliferation, differentiation, angiogenesis, migration and homeostasis. This family can be further divided into two subfamilies depending on the signal pathways they activate: the TGFβ/Activin/Nodal subfamily and the Bone Morphogenetic Protein (BMPs) subfamily (Heldin et al., 1997).

The TGFβ/Activin/Nodal includes TGFβs, Activins, Nodals and some Growth and Differentiation Factors (GDFs). TGFβ, one of ligand of this subfamily, is a multifunctional cytokine secreted in a latent form by many cell types. Its latent form is complexed with two other polypeptides; latent TGFβ binding protein (LTβP) and latency-associated peptide (LAP), both of which undergo activation and release of the active cytokine. The TGFβ ligand exists in three isoforms (TGFβ1, TGFβ2 and TGFβ3), which share a receptor complex and signal in similar ways but vary in expression levels depending on the tissue.

The subfamily Bone Morphogenetic Protein (BMPs) represents almost one third of the TGFβ superfamily, with more than 30 members already described. It is comprised of BMPs, most GDFs and Anti-Müllerian Hormone (AMH), also known as Müllerian Inhibitory Substance. Many processes in early development are dependent on BMP signalling for cell growth, apoptosis, and differentiation. BMPs also play important roles in maintaining adult tissue homeostasis, such as the maintenance of joint integrity, the initiation of fracture repair and vascular remodelling (Wang et al., 2014).

1.1 Canonical TGFβ signalling pathway

Each subfamily of the TGFβ ligands (TGFβ or BMP) binds to TGFβ receptor type I (TβRI) and type II (TβRII); both receptors are transmembrane serine/threonine kinases with a single transmembrane domain.

Seven type I receptors, also termed *Activin receptor-like kinases* ((ALK1, ALK2, ALK3 (BMPRIA), ALK4 (ActRIB), ALK5 (TGFβRI), ALK6 (BMPRIB) and ALK7) and five type II receptors (ActRIIA, ActRIIB, TGFβRII, BMPRII and MIS/AMHRII) have been identified (Akhurst and Hata, 2012).

The sequence similarity among the type I receptors is strikingly higher than among type II receptors. Type I receptor extracellular domains are shorter than the type II receptor, including a three-cysteine cluster which is also present in both types. A short cytoplasmic segment is followed by the serine/threonine domain. In the type I there is a short segment (the Gs domain) just N-terminal to the kinase domain that provides a switch for kinase activation, into a site that binds the substrate proteins for its phosphorylation after ligand binding (Derynck and Feng, 1997; Huse et al., 2001) (Figure I1).

The signalling of TGFβ ligand, independent of isoform, is mediated by the formation of a heterodimeric complex formed by TβRII and I (mainly ALK4, ALK5 and ALK7) on the cell surface (Figure I1).

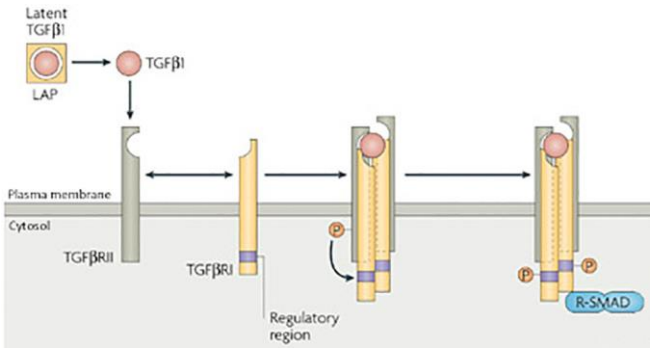

Figure I1. Schematic representation of TGFβ mediated activation of TGFβRI & II. TGFβ is produced in a latent, inactive form, which undergoes activation and release of the active cytokine. Active TGFβ binds the TGFβRII on the cell surface. This binding induces the assembly of the activated receptor-ligand heteromeric complex, which results in an autophosphorylation of the receptor followed by phosphorylation of R-Smad. Figure adapted from (Rubtsov and Rudensky, 2007).

Four different type I receptors have been implicated in BMP signalling: ALK1, ALK2, ALK3, and ALK6 (Wang et al., 2014). Certain BMPs have been shown to have a higher affinity for certain type I receptors. For example, BMP4 preferentially binds to ALK3 and ALK6, whereas BMP6 and 7 preferentially bind to ALK2, but can also engage with ALK3. Another cytokine is BMP9, a ligand which specifically binds ALK1 with high affinity to activate signalling pathways that promote endothelial cell, quiescence and vessel maturation. Interestingly, it has been demonstrated as well that BMP9 can bind to ALK2 and activate the signalling in ovarian cancer cell lines (Herrera et al., 2009).

In addition, auxiliary co-receptors (also known as type III receptors) that regulate the access of TGFβ superfamily members to signalling receptors also exist (Akhurst and Hata, 2012). The type III receptors Betaglycan and Endoglin are naturally present as homo-oligomers, presumably homodimers, at the cell surface. These co-receptors add an additional layer of complexity to the regulation of ligand/receptor activation. The high affinity of the type III receptors for the TGFβ isoforms (TGFβ1, TGFβ2 and TGFβ3) suggests that functions as reservoir for readily available TGFβ that can be presented with high affinity to the type II receptors. Ligand presentation in the case of TGFβ2 is especially important, which only interacts with TβRII when bound to TβRIII (Tian et al., 2011). While membrane-bound type III receptors promote signalling by presenting ligands to the signalling receptors, cleavage of the extracellular domain yields soluble proteins that can sequester ligands to inhibit signalling (Bernabeu et al., 2009). The increased affinity of the type II receptors in the presence of type III receptors may have an important developmental significance (Cheifetz and Massague, 1989).

To initiate the signalling, TGFβ or BMP binds to TβRI (signalling propagating) and TβRII (signalling activator) and form the heterodimeric complex. In the complex, type II receptors phosphorylate the type I components, which in turn transduce the signal through phosphorylation of the receptor-regulated R-Smads (Smad1/5/8 and Smad2/3). Then, these R-Smads form complexes with the common-mediator Smad (Co-Smad), Smad4 and these complexes then enter the nucleus where they regulate transcription of various target genes (e.g., Id1, Id3, fibronectin, PAI).

Moreover, there are two inhibitory Smads (I-Smads), Smad6 and Smad7, that both inhibit TGFβ signalling through competition with R-Smads for Co-Smad or receptor interaction and target receptors for degradation (Shi and Massague, 2003).

In this work, we have been focused on two of these receptors; the TβRI called ALK5, which is ubiquitously expressed, and a different member ALK1, which is preferentially expressed in endothelial cells (EC). In the SMAD-dependent pathway, activation of ALK5 leads to phosphorylation of Smad2 and Smad3, whereas ALK1 phosphorylates Smad1, Smad5 and Smad8. It has been demonstrated that TGFβ has a major affinity for ALK5 but that it can also stimulate ALK1 at high concentrations. It is not clear how the balance of both cytokines (TGFβ and BMP9) influence the ALK1 signalling functions (Bertolino et al., 2005). Several lines of evidence suggest that TGFβ members regulate a fine balance between ALK1 and ALK5 signalling in the endothelium (Seki et al., 2006).

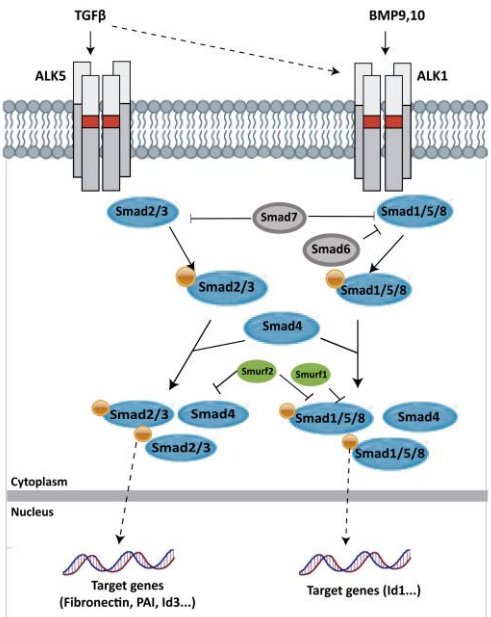

Figure I2. TGFβ signalling pathway in Endothelial cells (EC). ALK5 is a TGFβRI ubiquitously expressed that signals through phosphorylation of Smad2/3, binding to Smad4. Then this complex enters the nucleus and regulates transcription of various genes like fibronectin, PAI, Id3 and others. Whereas ALK1, a TGFβRI preferentially expressed in EC, signals through phosphorylation of Smad1/5/8, which binds to Smad4 and enters the nucleus regulating transcription of various genes like Id1 and others. In both cascades, Smad6 or 7 can inhibit the signalling.

1.1 Non-canonical signalling

Although TGFβ signals mainly via the SMAD pathway, TGFβ can also activate other pathways called: non-canonical TGFβ signalling pathways, which work independently of R-Smad activation. Some examples are observed below (Figure I3).

To initiate these non-canonical pathways, the activated TGFβ receptor complex transmits a signal through other factors, such as tumour necrosis factor (TNF) receptor-associated factor 4 (TRAF4), TRAF6, TGFβ-activated kinase 1 (TAK1; also known as MAP3K7), p38 mitogen-activated protein kinase (p38 MAPK), RHO, extracellular signal-regulated kinase (ERK), JUN N-terminal kinase (JNK) or nuclear factor-κB (NF-κB), phosphoinositide 3-kinase (PI3K) or AKT (also known as protein kinase B).

Unlike the canonical pathway, modulation of these pathways by TGFβ is often cell type specific and context dependent (Massague, 2008; Moustakas and Heldin, 2009; Wu and Derynck, 2009; Ikushima and Miyazono, 2010).

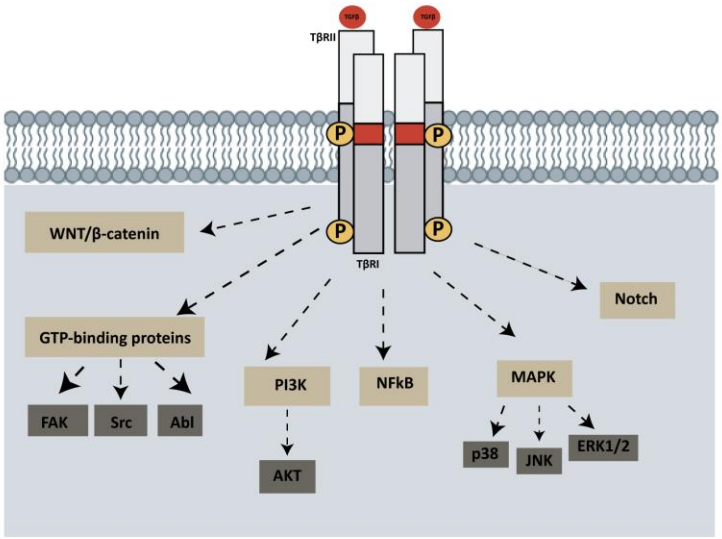

Figure I3. Schematic representation of the TGFβ non-canonical signalling pathway. After ligand binding, several different signalling pathways can be activated such as Notch signalling, MAPK, PI3K/AKT, NF-kB and Wnt/β-catenin pathways.

For instance it has been described that besides acting as serine/threonine kinases, the type I and II receptors display dual specificity, and as such are able to phosphorylate tyrosine residues (Zhang, 2009). Type I receptor mediated phosphorylation of Shc1 (better known as ShcA) or tyrosine phosphorylation of TGFβRII, either by auto-phosphorylation or via TGFβ-activated Src kinase, can lead to the recruitment of SH2-domain proteins such as Grb2 and Shc1 and results in activation of ERK or p38 MAPK pathways (Weiss and Attisano, 2013).

Mitogen activated protein kinases (MAPK) control different cellular processes like metabolism, survival, mitosis and apoptosis. MAPK is the last kinase of the sequentially signalling kinase cascade; MAPKKK phosphorylates MAPKK, which in turn phosphorylates MAPK. In mammals there are three MAPK groups: JNK, p38 and ERKs (FigureI4).

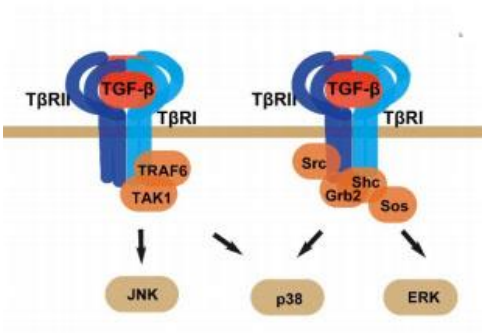

Figure I4. Schematic representation of the TGFβ non-canonical activation of MAPKs. Activation of MAPKs can be achieved via the TRAF6-TAK1 axis or the Grb2/Shc-Ras axis. Adapted from (Huang and Chen, 2012).

ERK1 and ERK2 are activated by growth factors by the MAPK signalling cascade: RAS-RAF-MEK-ERK. As previously explained, TGFβ-activated Src kinase can lead to the recruitment of SH2-domain proteins such as Grb2, an adaptor protein that recruits *Son Of Sevenless* (SOS) in the cytoplasm in the absence of ligand stimulation.

Upon receptor activation, Grb2/Sos complex is recruited, which brings SOS to the plasma membrane, where it activates Ras by catalysing the exchange of *Guanosine diphosphate* (GDP) for *Guanosine Triphosphate* (GTP). Ras:GTP then recruits Raf to the membrane where it becomes activated. Raf is responsible for serine/threonine phosphorylation of mitogen activated protein kinase kinase-1 (MEK1). MEK1 phosphorylates ERK1 and 2 at specific Thr and Tyr residues. ERK1/2 phosphorylates and activates a variety of substrates and even upstream substrates. The number of ERK1/2 targets is easily in the hundreds (>600) (Steelman et al., 2011; Santarpia et al., 2012).

Another non-canonical example is observed when TGFβ can rapidly activate PI3K, as indicated by the phosphorylation of its downstream effectors, which include AKT (Bakin et al., 2000; Shin et al., 2001; Viñals and Pouyssegur, 2001). In addition, in immunoprecipitation experiments, the TβRII receptor was found to be constitutively associated with p85, the regulatory subunit of PI3K, while association of the TβRI receptor with p85 requires TGFβ stimulation (Yi et al., 2005).

PI3K (phosphatidylinositol 3-Kinase) signalling has a critical role in regulating diverse cellular functions including metabolism, growth, proliferation, survival and protein transcription and synthesis (Manning and Cantley, 2007; Pearce et al., 2011). PI3Ks have been divided into three classes according to their structural characteristics and substrate specificity. Of these, the most commonly studied are the class I enzymes that are activated directly by cell surface receptors.

Class IA PI3Ks are heterodimers consisting of a p110 catalytic subunit and a p85 regulatory subunit, which mediates receptor binding, activation, and localization of the enzyme. The activated p110 catalytic subunit generates phosphatidylinositol-3,4,5-trisphosphate (PIP_3), which in turn activates multiple downstream signalling pathways (Liu et al., 2009). The cellular level of PIP_3 is tightly regulated by the opposing activity of PTEN, which functionally antagonizes PI3K activity. Via its intrinsic lipid phosphatase activity, PTEN reduces the cellular pool of PIP_3 by converting PIP_3 back to PIP_2 (Engelman et al., 2006; Liu et al., 2009).

AKT (PKB) is a serine/threonine kinase that interacts with PIP3 on the cell membrane. This binding produces a conformational change, which allows the phosphorylation of the residue Thr308 by PDK1. This phosphorylation gives a partial activity to AKT. Not until mTORC2 (mammalian target of rapamycin complex 2) phosphorylates Ser473 is AKT fully activated (Pearce et al., 2011).

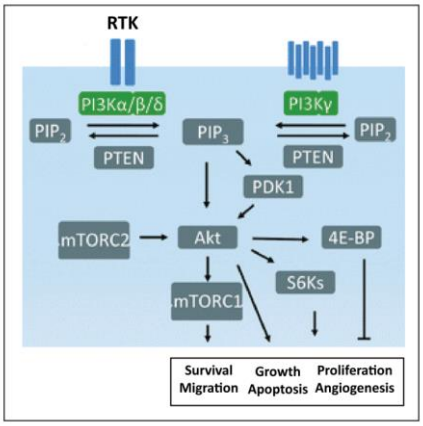

Figure I5. Schematic representation of the PI3K/AKT signalling pathway. Figure modified from (Wu 2012).

1.3 TGFβ signalling and Angiogenesis

As previously explained, TGFβ is involved in different cellular processes such as proliferation, differentiation, angiogenesis, migration and homeostasis.

1.3.1 Angiogenesis

Angiogenesis is the generation of new blood vessels from already pre-existing ones (Carmeliet, 2000). This is a process extremely important during embryonic development and is also required for other physiological and pathological situations during human life: female reproduction, tissue repair, inflammatory diseases, tumour growth and metastasis (Choi et al., 2014).

There are different mechanisms of angiogenesis that are generally divided into non-sprouting and sprouting angiogenesis. The former can occur by proliferation of ECs inside a vessel, producing a wide lumen that can be split by transcapillary pillars (Risau, 1997; Makanya et al., 2009; Fang and Salven, 2011). The latter refers to the strict sprouting of new blood vessels from walls of existing ones (Risau, 1997; Carmeliet, 2000). Although non-sprouting and sprouting angiogenesis might occur simultaneously, sprouting angiogenesis likely accounts for the majority of vascular growth (Graupera and Potente, 2013).

An essential step that happens during sprouting angiogenesis is the selection of ECs to occupy specific positions in the newly formed sprouts. In this sense, sprouting blood vessels are made up of three different ECs populations: leading tip cells, stalk cells and phalanx cells (Figure I6).

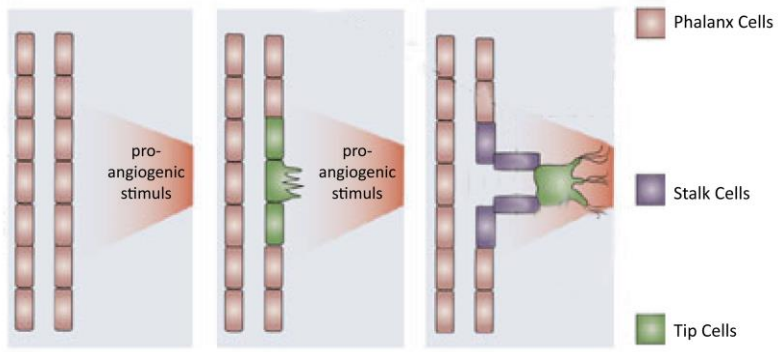

Figure I6. Schematic representation of the three different ECs populations on an sprouting vessel. ECs exposed to a pro-angiogenic stimulus are induced to migrate, but only the middle (future tip) cell (green) should take the lead to prevent ECs moving as a sheet instead of forming a branch. Following the tip cell, the stalk cells (blue) constitute the base of the sprout and maintain the connection to the parental vessel. Figure modified from (Carmeliet et al., 2009).

During sprouting angiogenesis, some ECs are specifically selected for sprouting after a pro-angiogenic stimulus, becoming a single leading tip cell which guide the sprouts (Adams and Alitalo, 2007; Jakobsson et al., 2010). These so-called tip cells are characterized for highly polarized, tubeless and low proliferating status.

The tip cell is highly motile, and uses their long and dynamic filopodia to guide a sprouting vessel towards an angiogenic stimulus (Phng and Gerhardt, 2009). Following the tip cells are the stalk cells, which constitute the base of the sprout and maintain the connection to the parental vessel (Phng and Gerhardt, 2009; Siekmann et al., 2013). Stalk cells produce fewer filopodia and are considered to proliferate when stimulated with pro-angiogenic factors to form an elongating stalk, and create lumen (Gerhardt et al., 2003; Blanco and Gerhardt, 2013). Next, beneath the stalk cells are the phalanx cells that promote vessel maintenance. Phalanx cells are lumenized, non-proliferating, immobile tube cells with a stable quiescent phenotype that sense and regulate perfusion in the persistent sprout and align in a smooth cobblestone monolayer, becoming the innermost cell layer in the new blood vessel (De Bock et al., 2009). Thereby, both stalk and phalanx cells are also responsible for the formation of a vascular lumen and the establishment of adherent and tight junctions to maintain the integrity of the new sprout (Gerhardt et al., 2003; Dejana et al., 2009).

This EC specification begins in response to pro-angiogenic signals that stimulate quiescent EC. Among all the signalling pathways involved in the angiogenic process, the Vascular Endothelial Growth Factor (VEGF)/VEGFR is almost totally endothelial-specific. The VEGF/VEGFR signalling plays a key role in EC specification into tip and stalk cells during sprouting angiogenesis. Studies involving mosaic endothelial cell cultures derived from embryonic stem cells have showed that the position of a cell within a growing blood vessel sprout can be determined by the levels of VEGF receptors (Jakobsson et al., 2010). The EC exposed to the highest VEGF concentration is selected to become a tip cell and then leads the sprout at the forefront and invades the surrounding tissue by extending numerous filopodia.

The sprout elongates via proliferation of endothelial stalk cells trailing behind the tip (Figure I7A). Next, the new branch connects with another branch via tip‑cell fusion (Figure I7B). Formation of a vascular lumen allows initiation of blood flow and, in turn tissue oxygenation which reduces VEGF expression levels (Figure I7C).

Maturation and stabilization of the nascent plexus relies on the recruitment of pericytes, also known as mural cells, and the deposition of extracellular matrix (ECM) (Figure I7D). In the established vasculature, ECs adapt a quiescent endothelial phalanx phenotype (Figure I7E).

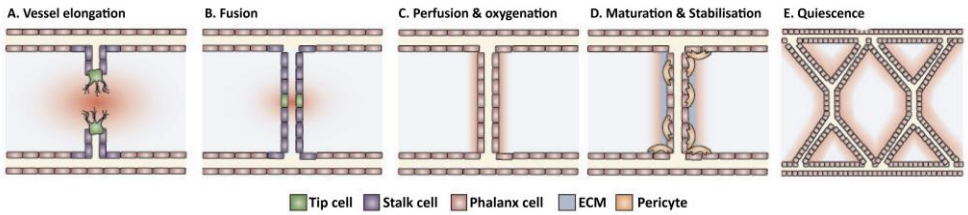

Figure I7. Scheme of vessel elongation and maturation after VEGF stimulus. A) ECs exposed to VEGF are induced to migrate and form branches. B) Tip-cell fusions connecting new branches. C) Formation of vascular lumen. D) Vessel maturation by recruitment of pericyte coverage and deposition of ECM. E) Quiescent cells in an established vasculature. Figure modified from (Carmeliet et al., 2009).

1.3.2 VEGF/VEGFR signalling pathway

The VEGF/VEGFR signalling is a highly enriched pathway in the endothelium. The VEGF family is a group of secreted growth factors with carefully regulated activity and is essential for multiple aspects of the formation and modelling of the vasculature (Olsson et al., 2006). There are five VEGF family members: VEGFA (commonly referred as VEGF), VEGFB, VEGFC, VEGFD and the placenta growth factor PLGF (Shibuya, 2013). Among the different ligands, VEGFA is the most prominently involved in the angiogenic process (Carmeliet et al., 1996; Ferrara, 1996). A particular feature of VEGFA ligand its dramatic up-regulation under hypoxic conditions. VEGFs ligands bind in an overlapping pattern to three receptor tyrosine kinases, known as VEGF receptor 1 (VEGFR1 or Flt1), receptor 2 (VEGFR2, KDR or Flk1) and receptor 3 (VEGFR3 or Flt4). VEGFR1 and VEGFR2 are most strongly expressed in vascular endothelial cells but are also expressed in myeloid cells and neurons (Blanco and Gerhardt, 2013). Whereas VEGFR3 is restricted to the lymphatic endothelium in the adult, while in the embryo and during

postnatal and tumour angiogenesis is up-regulated in vessels (Kaipainen et al., 1995; Kukk et al., 1996; Jussila and Alitalo, 2002).

The VEGFs/VEGFRs ligand-receptor interaction induces the formation of both homodimers and heterodimers of VEGFRs (Dixelius et al., 2003). Dimerization of the VEGFRs is accompanied by activation of the receptor-kinase activity, which in turn, results in the auto-phosphorylation of the receptors.

Phosphorylated receptors recruit SH-2-containing adaptors and downstream kinases, inducing the activation of a variety of downstream signalling pathways like MAPK and PI3K/AKT among others that regulate endothelial cell migration, survival, proliferation and tube formation (Olsson et al., 2006; Blanco and Gerhardt, 2013). It is worth mentioning that the potential biological responses of VEGFs/VEGFRs interaction depend not only on which of the three receptors is being activated, but also on the ligand to which the receptors bind.

Apart from the VEGF/VEGFR signalling pathway, other more widely active pathways, such as the PDFG /PDGFRβ, the Ephrin/Eph, the FGFR, the Notch, the PI3K or TGFβ signalling pathways, which have also been reported to perform specific vascular roles.

In the case of TGFβ there are functional evidences of its importance as a pro-angiogenic factor although its molecular processes have not yet been identified (Vinals and Pouyssegur, 2001; Viñals and Pouyssegur, 2001; Bertolino et al., 2005). The TGFβ/ALK5 and TGFβ/ALK1 pathways have been observed to be implicated on EC behaviour. Gene ablation studies in mice have revealed the importance of TGFβ, ALK5, ALK1, and Smad5 in angiogenesis (Goumans and Mummery, 2000). Together, these observations have encouraged us to study the specific role of ALK1 on the sprouting angiogenesis.

1.3.3 Hereditary Haemorrhagic Telangiectasia (HHT)

There is a human autosomal dominant disorder that affects 1 in 5000-8000 people worldwide known as *hereditary haemorrhagic telangiectasia-2* (*HHT2*), also known as *Rendu-Osler-Weber syndrome*; caused by heterozygous loss-of-function mutations on ALK1 gene (Johnson et al., 1996). This loss-of-function causes an adult-onset vascular dysplasia characterized by dilated, leaky capillaries that manifest in patients as mucocutaneous telangiectasia and arteriovenous malformations (AVM) in the brain, lungs, liver, and gastrointestinal tract (Govani and Shovlin, 2009). Interestingly, a second form of *HHT* known as *HHT1,* results from loss of Endoglin a co-receptor that directly interacts with ALK1 and modulates TGFβ and bone morphogenetic protein (BMP) signalling (Mitchell et al., 2010; Young et al., 2012), other genes can produce HHT in a lower prevalence as Smad4 mutated gene.

Clinical diagnosis of *HHT* by the Curacao criteria (Shovlin, 2010), remain the mainstay of *HHT* clinical diagnosis. A definitive diagnosis can be made if at least three separate manifestations of this list are present:

- Spontaneous recurrent nosebleeds.

- Mucocutaneous telangiectasia (multiple at characteristic sites: fingertip pulps, lips, oral mucosa or tongue).
- Visceral involvement (gastrointestinal, pulmonary, hepatic, cerebral or spinal AVM).
- Family history: a first-degree relative affected according to these criteria.

At the moment, the standard treatment for HHT patients is very invasive and is only short-term; with surgical treatments and embolization on the tissue most affected by the AVM (Govani and Shovlin, 2009). An example of this treatment on the lung is embolization that consists of inserting a tiny metal coil or a small balloon to block off the artery that leads into or “feeds” the pulmonary arteriovenous malformations (PAVM). This stops the blood flow to the PAVM which eliminates the occurrence of a potentially life-threatening complication.

The embolization is accomplished by passing a small catheter through a vein in the leg and then passing it up to the arteries of the lungs. This procedure is usually performed under conscious sedation. It is well-demonstrated that embolization is safe, though it cannot be expected to provide a long-term cure in most patients with HHT. It can reduce the severity and duration of bleeding in some patients and can be performed in emergency situations for control of severe epistaxis until patients are stabilized (Illum and Bjerring, 1988; Funaki, 2007). However, there is not yet a way to prevent the telangiectasia or AVMs from occurring.

Several small research studies have suggested that various oral therapies can help some patients for whom the local therapies (i.g. home moisturizing care and laser therapy) have not been successful. Birth control pills have been used the most, and while they do seem to help some patients, they have significant side effects. Drugs that affect either the formation of clots or blood vessels are being investigated (i.g., estrogens and tamoxifen)(Yaniv et al., 2011). Moreover, in a phase II clinical trial of bevacizumab (Avastin®), a monoclonal antibody to VEGF, it was reported in HHT patients with severe liver disease that hyperdynamic cardiac output secondary to intrahepatic arteriovenous shunting was significantly improved in treated patients (Dupuis-Girod et al., 2012; Chavan et al., 2013). In light of this, we considered important to continue working to elucidate new therapies for these patients. Nevertheless, the molecular mechanisms implicated in the regulation of angiogenesis by ALK1 and BMP9 and their relevance in HHT remains to be clarified.

1.3.3.1 ALK1$^{+/-}$ deficient mice as HHT mouse model

Interestingly, it has been described that ALK1 mutated animals mimic the same vascular defects observed by *HHT2* patients. Complete ALK1 deficiency results in early embryonic lethality at E11.5 as a result of defects in the remodelling of the primary capillary plexus into a functional network of arteries, capillaries, and veins (Oh et al., 2000; Urness et al., 2000). Furthermore, ALK1$^{+/-}$ mice presented severe vascular abnormalities, such as;

dilated vessels and HHT-like vascular lesions in liver, nail bed, intestine, or skin that developed between 7 and 20 months (Srinivasan et al., 2003). However, these lesions occur at incomplete penetrance (approximately 40% of ALK1$^{+/-}$ mice have one or more lesions) and in an unpredictable manner (Tual-Chalot et al., 2015). Nevertheless, these vascular defects are associated with enhanced expression of angiogenic factors, so probably these defects are present in a pro-angiogenic tissue. In summary, these mice are appropriated to study the role of BMP9/ALK1 signalling on the sprouting angiogenesis and are also a good tool to study possible therapies to treat *HHT* patients.

1.3.3.2 Retina mouse model for studying vascular development

To study angiogenesis many different *in vitro* techniques can be useful, including wound healing migration and proliferation assays, network formation assays in Matrigel or aortic ring formation assay. However, the common limitation is that they focus on isolated steps of the angiogenic process and are affected by artificial experimental settings (Pitulescu et al., 2010). Thereby, to faithfully recapitulate angiogenesis, most of the investigations have moved to *in vivo* assays, from which we can highlight the post-natal mouse retinal model.

The retina is a vascularized tissue that in mice develops after birth. During gestation, it is the hyaloid vasculature that supplies the inner eye and lens with nutrients and oxygen. But right after birth, the hyaloid vessels regress and the retinal vascular plexus is rapidly formed on top of a pre-existing migratory astrocyte plexus (Fruttiger et al., 1996). Retinal vasculature develops from birth in a well-defined sequence of events. Retinal plexus emerges from the optic nerve disc and sprouts radially to the peripheral margin during the first days after birth (from birth until post-natal day 10) (Figure I8).

Immunostaining of the retinal vasculature using vascular markers or in-situ hybridization, followed by three-dimensional imaging of whole-mounted tissue, allows a profound analysis of physiological vessel development. IsolectinB4, VE-cadherin, platelet-endothelial cell adhesion molecule (PECAM)-1 or CD31, endomucin and VEGFR-2 are the most common vascular markers used to label vascular structures in the mouse retina model.

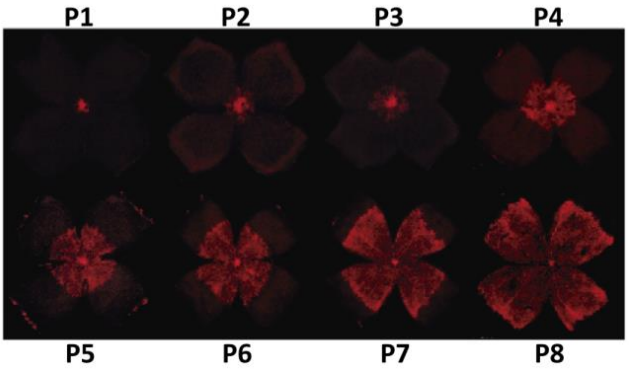

Figure I8. Retina mouse model. Development of the superficial vascular plexus in C57Bl/6 mouse retinas during first days after birth. Retinal whole mounts from postnatal day P1 to P8 were stained for endothelial cells with isolectin B4-Alexa 594 (red). Figure modified from (Stahl et al., 2010).

1.4 TGFβ signalling and cancer

We have explained the role of TGFβ signalling members, specifically the ALK1 receptor, in angiogenesis, but TGFβ signalling is important in a wide range of other cellular processes, as well, both from a physiological and pathological point of view. Regarding the role of TGFβ in cancer, it is widely believed that TGFβ switches its role from a tumour suppressor in normal cells to a tumour promoter in advanced cancers favouring invasiveness and metastasis depending on the tumour stage (Tian et al., 2011).

TGFβ tumour suppressor properties are acquired late in the G1 phase of the cell cycle and result in suppression of cell proliferation and induction of apoptosis. Firstly, TGFβ downregulates the expression of the growth-promoting transcription factors like c-Myc and Id1-3. In addition, TGFβ prevent cell cycle progression by enhancing the expression of the cyclin-

dependent protein kinase (CDK) inhibitors, p15 and p21 (Siegel et al., 2003; Massague and Gomis, 2006). Yet, during tumour progression, sensitivity to these effects of TGFβ is frequently lost and, in later stages, TGFβ signalling becomes even a pro-oncogenic signalling pathway (Siegel et al., 2003) (Figure I9A-B).

One aspect that contributes to this cancer progression is the epithelial-mesenchymal transition (EMT), which has been observed in early tumour stages or carcinoma in situ, where the inhibitory effects of TGFβ are often lost. EMT is characterized by a change in cell shape from a polarized epithelial cell to a flattened fibroblast-like cell, a decrease in cell-cell contacts and increased cell motility (Tian et al., 2011). TGFβ-induced EMT is associated with the downregulation of E-Cadherin expression, which in turn enhances tumour cell migration as it is observed in transformed epithelial progenitor cells with tumour-propagating ability (Mani et al., 2008). Consequently, other aspects of cancer progression like invasion and metastasis are potentiated (Lahn et al., 2005; Tian et al., 2011)(Figure I9C). Regardless of its role in migration and invasion, induction of EMT either by TGFβ or its downstream targets, Snail or Twist, has been reported to prompt the expression of cell surface markers associated with cancer stem cells (CSCs), such as: $CD44^{+}/CD24^{lo}$ cells (Shipitsin et al., 2007). This is also important given that CSCs are known to have enhanced chemotherapeutic drug resistance (Connolly et al., 2012).

Another of the oncogenic roles of TGFβ is the forementioned explained pro-angiogenic function (Derynck et al., 2001). Tumour angiogenesis provides the developing neoplasia with an efficient supply of nutrients and ultimately with a route for their metastatic spreading. TGFβ has been reported to regulate the activation and resolution phases of angiogenesis and affects ECM production and remodelling in EC microenvironments, impacting the interaction and communication between ECs and their supporting mesenchymal cells (Bertolino et al., 2005)(Figure I9D).

Last but not least, TGFβ can suppress or modulate the immune response since many of the TGFβ signalling effects act on both adaptive and innate immune cells (Figure I9D).

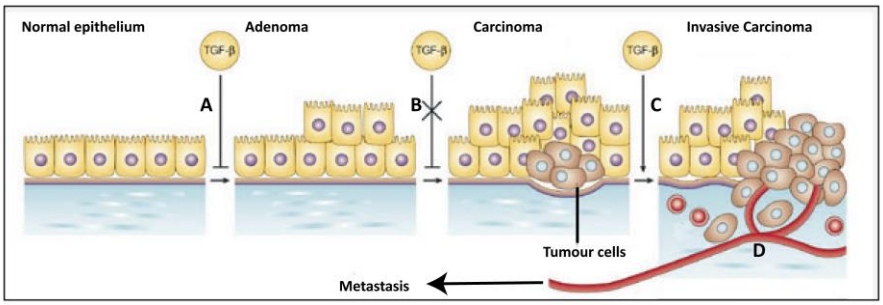

Figure I9. Representation of the TGFβ action during tumour progression. A) TGFβ limits the growth of normal epithelium and early-stage tumours. B) Loss of TGFβ sensitivity during tumour progression. C) TGFβ signalling becomes pro-oncogenic with for example the EMT transdifferentiation becoming more invasive. D) TGFβ signalling produces an immunosuppressive environment and can induce an angiogenic response that sustains tumour growth, systemic spread (extravasation of tumour cells at sites of metastasis) and metastasis. Adapted from (Siegel and Massague, 2003).

1.4.1 TGFβ Inhibitors in cancer

Throughout, TGFβ dual role has been the major concern in deciding if inhibiting TGFβ and/or its downstream signalling pathway would be beneficial in the treatment of cancer. Nowadays, TGFβ signalling factors have been considered a useful therapeutic target. However, the challenge remains to identify which group of patients and which cancer type are the best to target. Treatments against TGFβ signalling pathway are now under clinical development (Seoane, 2008; Akhurst and Hata, 2012; Neuzillet et al., 2015)(Table I1).

Based on the current understanding of TGFβ and its signalling pathway, three approximations have been investigated to inhibit the pathway for new cancer therapies. These approximations consist of inhibition at the transcriptional level using antisense oligonucleotides (ASOs), inhibition of the ligand-receptor interaction using monoclonal antibodies (MoAbs), and the inhibition of the receptor-mediated signalling cascade using inhibitors of

TGFβR kinases (SMIs)(Lahn et al., 2005; Nagaraj and Datta, 2010; Connolly et al., 2012).

Firstly, the approximation for ASOs is designed to hybridize their complementary RNA sequence and accelerate mRNA degradation (Nagaraj and Datta, 2010). Unpredictable RNA binding affinity, possible non-specific/off-target effects, and the challenge of delivery of relatively large molecules into the target cell are all factors that limit the feasibility of ASOs. In fact, it has been recently shown in clinical tests that ASOs have specific pharmacokinetic behaviour that may limit their ability to reach tumour tissue (Connolly et al., 2012). However, AP-12009 (Trabedersen), ASO directed against mRNA of TGFβ2 produced promising results for treatment of glioblastoma in the clinic (Vallieres, 2009; Bogdahn et al., 2011). As a result, while these limitations need to be taken into account, the use of ASOs can be effective depending on tumour type.

The other approximation consists of using large-molecule inhibitors that block receptor-ligand interaction, these monoclonal antibodies are antagonists of TGFβ ligand binding to the heteromeric receptor complex. One example is metelimumab (CAT/Genzyme), a human monoclonal antibody against TGFβ1 that antagonizes TGFβ ligand binding to the heteromeric receptor complex. Although studies in cancer were not very promising, this drug is currently undergoing Phase I/II trials in patients with diffuse scleroderma (Denton et al., 2007). Some antibodies failed in oncologic trials and are currently being investigated in fibrosis rather than cancer. The significant physical barriers that block penetration of a solid tumour may be an important cause of the failure of antibody treatments such as metelimumab (Christiansen and Rajasekaran, 2004).

The last approximation consists of small molecule inhibitors that block the receptor-mediated signalling cascade. Targeting receptor kinases by small molecules has been an area of prolific experimental drug development in the last few years largely because of the practicality of small molecule drug delivery by the oral route (Nagaraj and Datta, 2010; Connolly et al., 2012).

These molecules are not as specific as ASO because they can bind to different kinase receptors of the TGFβ pathway. Despite this risk of not being specific, dual inhibitors such as LY2109761, which inhibits TβRI/II, have been shown to reduce tumour growth in glioblastoma (Anido et al., 2010).

Table I1. Some TGFβ inhibitors and their state of clinical development.

	Name	Drug target	Clinical studies	Company
ASOs	Trabedersen (AP-12009)	mRNA TGFβ2	Phase III in oncology treatment	Antisense Pharma®
	Lucanix™ (Belagenpumatucel-L)	TGFβ1 & TGFβ2	Phase III in advanced NSCLC	NovaRx Corporation
	AP-11014	mRNA TGFβ1	Pre-clinical	Antisense Pharma®
MoAbs	metelimumab® (CAT-192)	TGFβ2	Development stopped	Cambridge Antibody Technology
	Fresolimumab® (GC-1008)	Pan TGFβ	Phase I/II in oncology and sclerosis treatment	Cambridge Antibody Technology/Genzyme Corp./Sanofi
	ID11	Pan TGFβ	Pre-clinical	Genzyme Corp., Sanofi
SMIs	Galunisertib® (LY215299)	TβRI Kinase	Phase I/II in oncology treatment	Eli Lilly & Co.
	PF-03446962	(ALK1) TβRI Kinase	Phase II in oncology treatment	Pfizer®
	TEW-7197	TβRI Kinase	Phase I	MedPacto®
	IMC-TR1 (LY3022859)	TβRII Kinase	Phase I	Eli Lilly & Co.
	LY2109761	TβRI & II Kinase	Pre-clinical	Eli Lilly & Co.
Others	Esbriet® (pirfenidone)		FDA approved 2014 for Idiopathic Pulmonary fibrosis	Roche Pharma

NSCLC: Non-small Cell Lung Cancer.

1.4.1.2 LY2109761

LY2109761 (Eli-Lilly & Co) is a dual tyrosine kinase TGFBRI and TGFBRII inhibitor, which is relatively metabolically stable and suitable for *in vivo* studies (Lacher et al., 2006). It has been effective in pre-clinical models for the treatment of liver metastasis from colon cancer (Zhang et al., 2011b) and in suppressing pancreatic cancer metastasis (Melisi et al., 2008). In addition, it has been really effective in the treatment of glioblastoma, reducing tumour growth and its glioma-initiating cell population (Anido et al., 2010). Furthermore, it has been demonstrated that LY2109761 in combination with Temozolomine (clinical standard) and radiotherapy in glioblastoma model delayed tumour growth compared to controls (Bouquet et al., 2011).

Another drug from Lilly & Co called Galunisertib® (LY2157299) that specifically inhibits TGFβRI is being tested in some clinical trials. Currently, Phase I studies on hepatocellular carcinoma and pancreatic cancer. In addition, Phase II studies are being developed in Glioma, hepatocellular carcinoma, pancreatic cancer and Myelodysplastic Syndromes (http://www.lillyoncologypipeline.com/).

2. Ovarian cancer

2.1. The ovary

The ovary is an organ of the female reproductive system; each ovary is a small glandular organ about the shape and size of an almond. They are located on the opposite end of the pelvic wall, on either side of the uterus. Each ovary is connected to the fallopian tube through the fimbriae. The open ends of the fallopian tubes rest just beyond the lateral surface of the ovaries to transport ova, to the uterus.

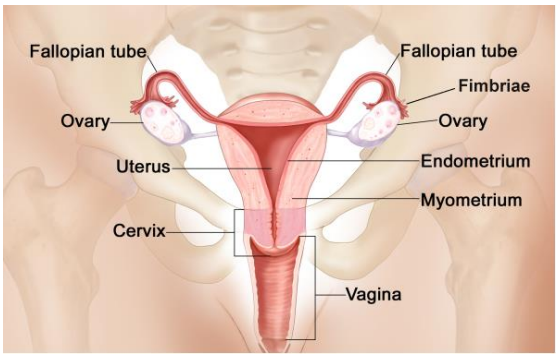

Figure I10. Female reproductive anatomy. Figure modified from National cancer institute (NCI) website.

The ovaries have two central roles in the female reproductive system by acting as both glands and gonads. The ovaries produce and release two groups of sex hormones; progesterone and oestrogen. At birth the ovaries contain between several hundred thousand to several million circular bundles of cells known as follicles. Each follicle surrounds and supports a single oocyte that has the ability to mature into an ovum, the female gamete. Despite this large number of potential ova, only around 4,000 oocytes survive to puberty and only 400 oocytes mature into ova in a woman's lifetime.

The ovaries are made up of 3 main kinds of cells: the surface epithelial cells known as ovarian surface epithelium (OSE), the sex-cord stromal cells which comprise the bulk of ovarian tissue with a peculiar spindle-shaped similar to fibroblast, and the germ cells that produce the eggs (ova).

The female reproductive system modulates and adapts for the ovulation and gestation process each month. These monthly changes in fact make the ovarian system susceptible of possible errors, and as a consequence can produce different pathologies, such as polycystic syndrome, ovarian cyst, endometriosis or ovarian tumours. Ovarian tumours can be further subdivided into those that are clearly benign (cystadenomas), those that are frankly malignant (carcinomas), and those that have features intermediate, called borderline tumours (Cho and Shih Ie, 2009). It is important to specify that in ovarian cancer there is no the same progression as in colorectal cancer and tumours from the beginning can be carcinoma without a cystadenoma phase.

An ovarian carcinoma can be originated from different cell types. The germ cells, which develop into germ cell tumours (dysgerminomas, yolk sac tumours, and immature teratomas (3% of ovarian cancers) and the sex cord-stromal tumour (1–2% of ovarian cancer), which start from structural tissue cells that hold the ovary together and produce the female hormones oestrogen and progesterone (granulose-theca cells)(Feeley and Wells, 2001).

Nevertheless, more than 90%, of ovarian tumours are localized in the ovarian surface, have an epithelial histology and are called ovarian epithelial tumours. The cell of origin is very controversial and there are some different theories. Traditionally, it was believed that these tumours came from the ovarian surface epithelium (OSE) and differenciate to the different tumour histological types (Kurman, 2002). Although the mesothelial origin cannot be excluded, there is now compelling evidence that a number of what have been thought to be primary ovarian cancers are actually originated in other pelvic organs, for instance in the digestive tube, and involve the ovary secondarily.

Recently, there have been proposed the origin from precursor epithelial lesions in the distal fimbriated end of the fallopian tube (Medeiros et al., 2006; Lee et al., 2007), whereas other ovarian tumour types originate from ovarian endometriosis (Obata et al., 1998; Sato et al., 2000) through the process of retrograde menstruation (Halme et al., 1984) or an endometriosis generated after neoplastic transformation from a tubal origin (Yuan Z, 2013). More research has to be done in order to gather a deeper understanding of the mechanism linking these morphologic transformations.

2.2. Epidemiology and etiology of ovarian cancer

Among all cancer types, ovarian cancer is the second most common gynaecological cancer by incidence (≈6 per 100,000 individuals) and the fifth most common cause of cancer death in women in western countries. Even though breast cancer is the most frequent one, as observed in Figure I11, the mortality rate of ovarian cancer remained fairly static during the past last years (Berrino et al., 2007; Ferlay et al., 2010).

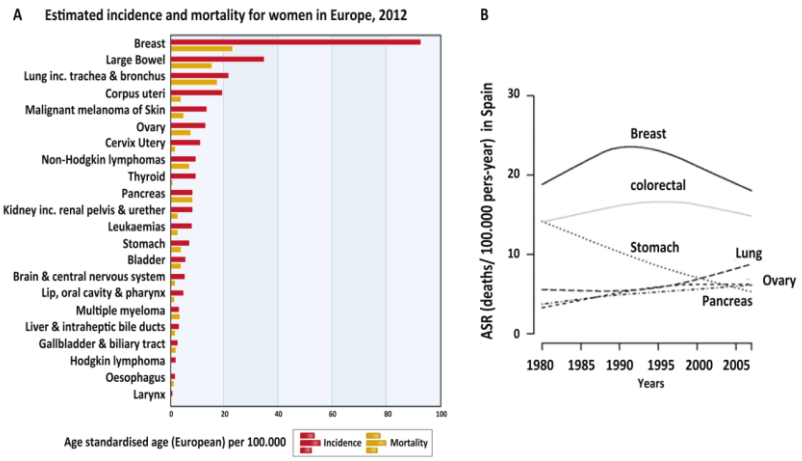

Figure I11. Incidence and mortality of cancer for women in Europe. A) Estimated incidence and mortality for women of different cancers in Europe on 2012. Ovarian cancer has lower incidence than other cancers but its mortality is more frequent than 50 % of the cases. Figure modified from the *European Cancer Observatory* webpage (ECO, 2015). B) The mortality rate of ovarian cancer in Spain remained fairly static among the last years. Figure modified from (Cabanes et al., 2010).

Despite the accumulating information from epidemiological studies which link several risk factors to ovarian cancer, the overall pathogenesis remains controversial (Doufekas and Olaitan, 2014):

It has been demonstrated that the incidence of ovarian cancer increases with aging, being more prevalent in the eighth decade of life and younger women have a better prognosis. Thus, with an aging population in the Western countries, the total number of ovarian cancer cases can be expected to rise in the coming years (Doufekas and Olaitan, 2014).

There are different possible risk factors that play a role in ovarian cancer progression; hormones such as oestrogen and progesterone are believed to be involved in promoting ovarian carcinogenesis. In contrast, breast-feeding, pregnancy or oral anticonceptive that suppress ovulation are suggested to have a protective effect (Casagrande et al., 1979). Additionally, obesity and increasing body mass index (BMI) have been associated with ovarian cancer risk. Moreover, it has been observed a slightly association between smoking or some particular diet and cancer risk but results are still controversial (Daniilidis and Karagiannis, 2007).

Genetic studies on ovarian cancer indicate that most of the cases are sporadic while 10 % are inherited, generally due to germline mutations. Two types of ovarian cancer susceptibility genes have been identified: the breast and ovarian cancer tumour suppressor genes (BRCA1 and BRCA2), which explain the majority of hereditary ovarian cancer cases and the mismatch repair genes associated with Hereditary Nonpolyposis Colorectal Cancer (HNPCC)(Daniilidis and Karagiannis, 2007).

2.3. Histologic classification of ovarian tumours.

Ovarian cancer is a general term for different tumours types which its unique clinical and pathological common feature is the anatomical localization. At histological and molecular levels, ovarian cancers are remarkably heterogeneous.

The normal ovary is a complex tissue with several distinct components. Ovarian tumours can be reproducibly diagnosed by light microscopy and are essentially different diseases, as indicated by differences in epidemiologic and genetic risk factors, precursor lesions, ways of spread, and molecular changes during oncogenesis and response to chemotherapy or outcome (Stewart BW, 2003).

As described above, ovarian cancer can be divided on germ cell tumours (3%), sex-cord stroma (2%) and epithelial tumours (95%).

2.3.1 Types of Epithelial ovarian cancer (EOC)

The current classification of ovarian epithelial tumours used by pathologists is based entirely on tumour cell morphology according to the predominant pattern of differentiation and is divided into five main histotypes (Figure I12):

- Low-grade serous carcinoma (LGSC)

- High-grade serous carcinoma (HGSC)

- Endometrioid carcinoma (EMC)

- Clear-cell carcinoma (CCC)

- Mucinous carcinoma (MC).

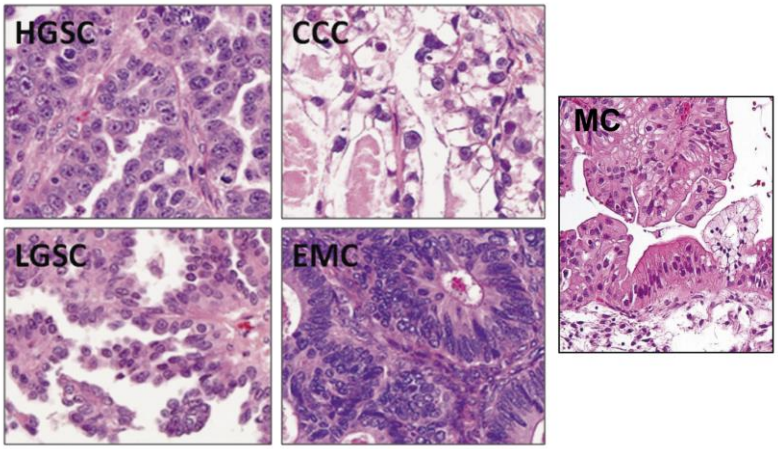

Figure I12. Epithelial ovarian cancer types. H&E of the five EOC types. HGSC: High-grade serous carcinoma, LGSC: Low-grade serous carcinoma, CCC: Clear cell carcinoma, EMC: Endometrioid carcinoma and MC: Mucinous carcinoma. Figure modified from (Kuhn et al., 2011).

Low-grade serous carcinoma (LGSC) (less than 5%)(Figure I12)

Low-grade serous carcinoma is thought to arise in many cases in a stepwise fashion from a benign serous cystadenoma through a serous borderline tumour to an invasive low-grade serous carcinoma.

The cells of LGSC are charcaterized by uniform nuclei with mild or moderate atypia and less than or equal to 12 mitoses per 10 high power fields (the mitotic count is usually approximately two per 10 high power fields or less than this). There is no necrosis or multinucleation. It is worth pointing out that prominent nucleoli and intracytoplasmic mucin are not uncommon in this type of tumours (McCluggage, 2012).

KRAS or BRAF mutations are present in over half of LGSC, whereas mutations in TP53 are rare (Kupryjanczyk et al., 1993; Wen et al., 1999; Chan et al., 2000; Singer et al., 2005). Overall, 70–80% of low-grade serous carcinomas express active ERKs (Hsu et al., 2004).

Patients with low-grade serous ovarian tumours are diagnosed at a younger age, have a longer overall survival but have lower response rates to conventional chemotherapy.

High-grade serous carcinoma (HGSC) (68%)(Figure I12)

It is now believed that most HGSCs arise from the distal, fimbriated end of the fallopian tube. HGS cells exhibit moderate to marked nuclear atypia and greater than 12 mitoses per 10 high power fields. Necrosis and multinucleate cells are often present. It is generally not necessary to count mitotic figures as these are typically abundant (McCluggage, 2012).

Unlike LGSC, mutations of *KRAS*, *BRAF*, or *ERBB2* are rare in HGSC, while *TP53* is mutated in 50% of the cases (Singer et al., 2005; Galic et al., 2007). In addition, this tumour type has a highly chromosome instability (Meinhold-Heerlein et al., 2005). For example, a high level DNA copy number gain/amplification of *CCNE1*, *NOTCH3*, *RSF1*, *AKT2*, and *PIK3CA* loci in 36.1%, 32.1%, 15.7%, 13.6%, and 10.8% have been observed repectively (Cho and Shih Ie, 2009).

HGSC is the predominant histotype associated with hereditary breast-ovarian cancer, seen in 16% of cases (Bell et al., 2011), and women with these inherited mutations have a lifetime risk of 40–60% (*BRCA1*) and 11–27% (*BRCA2*)(George and Shaw, 2014). In addition, although somatic mutations of *BRCA1* and *BRCA2* are known to be rather uncommon in sporadic ovarian carcinomas (about 6% of the cases), accumulated studies suggest that these genes may be inactivated, particularly in serous carcinomas, through mechanisms other than mutations (Cannistra, 2007).

Almost all serous carcinomas that have previously been classified as moderately or poorly differentiated represent high-grade neoplasms, while those that have been classified as well-differentiated may be either low-grade or high-grade using the actual classification. For example, some architecturally well-differentiated serous carcinomas have high nuclear grade and represent examples of high-grade serous (McCluggage, 2012).

Endometrioid carcinoma (EMC) (20%)(Figure I12)

The Endometrioid ovarian tumours are bilateral in 28% of the cases. It is formed by glandular structures resembling endometrial epithelium characterized by the presence of epithelial, stromal elements, or a combination of both. These tumours are solid masses with a soft, firm, or fibrous consistency, containing distinctive tubular glands lined by single or pseudostratified columnar cells with large atypical oval nuclei and basophilic cytoplasm. Foci of squamous differentiation are often seen (Kaku et al., 2003).

Somatic mutations of the β-catenin (CTNNB1) and PTEN genes are the most common genetic abnormalities identified in ovarian ECs. Furthermore, mutations on ARID1A and RAS genes as well as microsatellite instability are also present in this tumour type (Obata et al., 1998; Palacios and Gamallo, 1998; Catasus et al., 2004).

Clear cell (CCC) (4%)(Figure I12)

These tumours are rarely bilateral. CCCs are associated with an unfavourable prognosis when diagnosed at advanced stages (Sugiyama et al., 2000). It resembles the well-differentiated normal cells that form nest within the vagina. At the histological level, CCC is characterized by multiple complex papillae, densely hyaline basement membrane material expanding the cores of the papillae and hyaline bodies, whith mitoses being less frequent than in other types of ovarian carcinomas (Prat, 2012). The cells have a clear or eosinophilic cytoplasm (that contains glycogen), protruding into glandular lumen.

CCCs have PTEN, ARID1A and PBK genes. There is a lack of the BRCA abnormalities, chromosomal instability, or complex karyotypes of HGSC (Press et al., 2008).

Mucinous (MC) (3%)

MC resembles the well-differentiated normal cells from the endocervix. Primary ovarian mucinous carcinomas affect a wide age range, including occasionally children and adolescents. They are relatively uncommon, accounting approximately 3% of primary epithelial ovarian carcinomas. Most primary MCs are unilateral. It has been stated that when a mucinous carcinoma is diagnosed in the ovary, further investigations, such as colonoscopy and detailed imaging of the upper abdomen, should be undertaken to exclude a primary neoplasm elsewhere. This is done so, as many presumed primary ovarian mucinous carcinomas, especially of advanced stage, were metastases from extraovarian sites. It has irregular glands that are composed of cell with atypical nuclei and intracytoplasmic mucin (McCluggage, 2011).

KRAS and ERBB2 mutations, which are an early event in mucinous tumorigenesis, are frequent in ovarian MCs (Cuatrecasas et al., 1997).

2.4. Staging of the ovarian tumours.

Ovarian cancer remains largely a surgically staged disease, for this reason is important to define extensively the region of lesion. The prognosis is based on histologic type (section 2.3.), radiographic, and operative extent of the disease.

The *Féderation Internationale de Gynécologie et d'Obstétrique* (FIGO) and *the American Joint Committee on Cancer* (AJCC) have designated staging to define ovarian epithelial cancer depending on how far the tumour is spread. It is organized in four steps at the same time subdivided to define better the staging of ovarian cancer progression. FIGO recently approved a new staging system for ovarian, fallopian tube, and primary peritoneal cancer (2014 FIGO), described in Table I2.

Table I2. 2014 FIGO ovarian, fallopian tube, and peritoneal cancer staging system and corresponding TNM.

Stage	Description	ID
I	Tumour confined to ovaries or fallopian tube(s)	T1
IA	Tumour limited to one ovary (capsule intact) or fallopian tube. No tumour on ovarian or fallopian tube surface. Nonmalignant cells in the ascites or peritoneal washings	T1a
IB	Tumour limited to both ovaries (capsules intact) or fallopian tubes No tumour on ovarian or fallopian tube surface No malignant cells in the ascites or peritoneal washings	T1b
IC	Tumour limited to one or both ovaries or fallopian tubes, with any of the following: IC1 Surgical spill intraoperatively IC2 Capsule ruptured before surgery or tumour on ovarian or fallopian tube surface IC3 Malignant cells present in the ascites or peritoneal washings	T1c
II	Tumour involves one or both ovaries or fallopian tubes with pelvic extension (below pelvic brim) or peritoneal cancer (Tp)	T2
IIA	Extension and/or implants on the uterus and/or fallopian tubes/and/or ovaries	T2a
IIB	Extension to other pelvic intraperitoneal tissues	T2b
III	Tumour involves one or both ovaries, or fallopian tubes, or primary peritoneal cancer, with cytologically or histologically confirmed spread to the peritoneum outside the pelvis and/or metastasis to the retroperitoneal lymph nodes	T3
IIIA	Metastasis to the retroperitoneal lymph nodes with or without microscopic peritoneal involvement beyond the pelvis. IIIA1 Positive retroperitoneal lymph nodes only (cytologically or histologically proven). IIIA1(i) Metastasis ≤ 10 mm in greatest dimension (note this is tumour dimension and not lymph node dimension) IIIA1(ii) Metastasis N 10 mm in greatest dimension	T1,T2, T3aN1
IIIA2	Microscopic extrapelvic (above the pelvic brim) peritoneal involvement with or without positive retroperitoneal lymph nodes	T3a/T 3aN1
IIIB	Macroscopic peritonealmetastases beyond the pelvic brim ≤ 2 cmin greatest dimension,with orwithoutmetastasis to the retroperitoneal lymph nodes	T3b/T 3bN1
IIIC	Macroscopic peritoneal metastases beyond the pelvic brim N 2 cm in greatest dimension, with or without metastases to the retroperitoneal nodes (Note 1)	T3c/T 3cN1
IV	Distant metastasis excluding peritoneal metastases Stage IV A: Pleural effusion with positive cytology Stage IV B: Metastases to extra-abdominal organs (including inguinal lymph nodes and lymph nodes outside of abdominal cavity) (Note 2)	Any T, Any N, M1

(Note 1: Includes extension of tumour to capsule of liver and spleen without parenchymal involvement of either organ, and Note 2: Parenchymal metastases are Stage IV B. Figure adapted from (FIGO 2014).

2.5. Detection of ovarian cancer

Ovarian cancer has been termed the “silent Killer” because women are diagnosed with already advanced disease. Even though, 80% of patients have symptoms, even when the disease is still limited to the ovaries (Goff et al., 2000). Unfornately, these symptoms are, however, shared with many common gastrointestinal, genitourinary and gynaecological conditions and have not proved useful for early diagnosis and many patients are diagnosed after the cancer has already metastasised. Metastases can occur through lymphatics to nodes at the renal hilus or blood vessels to liver and lung. Moreover, and unlike other type of cancers, the absence of anatomical barriers favours the spread of metastases and dissemination throughout the peritoneal cavity in the case of ovarian cancer. This is one of the reasons elevated mortality rate in ovarian cancer (up to 70%), because only 20-30% of patients are diagnosed at the initial stage. Five-year survival rates for women with advanced disease range from 20% to 30%; however, for women who are diagnosed when the disease is confined to the ovary, cure rates are approximately 70% to 90% (Cannistra, 2004). At that point, early detection of ovarian cancer represents the best hope for mortality reduction and long-term disease control.

The identification of patients with genetic risk currently offers the most effective measure for prevention and early detection, but, as mentioned before, this represents only a low percentage of all patients since the majority suffer from ovarian cancers of sporadic origin. There is therefore an urgent need to determine new screening tests for those patients.

Since its discrovery in 1981, Cancer antigen 125 (CA-125) has become well established as a tumour marker for epithelial ovarian cancer (Bast et al., 1981). CA-125 is a high molecular weight glycoprotein that is expressed by a large proportion of epithelial ovarian cancers. However, the sensitivity and specificity of CA-125 is known to be poor. It is only raised in approximately 50% of stage I epithelial ovarian cancers and in 75% to 90% of patients with advanced disease (Woolas et al., 1993; Fritsche and Bast, 1998). In addition, the specificity of the test is poor, and it produces a high number of false-

positive results (Ozguroglu et al., 1999). Lately, it has been described that the expected CA-125 profile is flat at an individual's baseline level (variable between women), whereas in women with undiagnosed ovarian cancer, the expected CA-125 profile is initially flat, but increases significantly, presumably because of tumour growth (Skates et al., 2001).

Despite the efforts to identify new markers, the chances of discovering an ideal and unique marker for epithelial ovarian cancer is low, given the biologic heterogeneity of the disease . There is therefore an urgent need to improve the conventional therapies to reduce its mortality in more advanced cases, while identifying new possible biomarkers for an earlier detection.

2.6. Treatment of ovarian cancer

In patients with organ-confined cancers, surgery alone is curative in more than 90% of the cases. However, most of the patients (>80%) have disseminated tumours beyond the ovaries by the time it is diagnosed. For these cases, a combination of surgery and chemotherapy are applied as the standard treatment.

Surgery is the initial therapeutic approach and excising or biopsying any suspicious peritoneal area and the sampling of the lymph nodes are also recommended practices (Ledermann et al., 2013; Morgan et al., 2014). The goal of primary surgery, defined as optimal cytoreduction, is to achieve the full elimination of residual cancer. Primary surgery is recognized around the world as a standard treatment for EOC, and optimal cytoreduction remains the main prognostic factor for survival and risk of recurrence (Chi et al., 2011). However, interval debulking surgery (IDS) (residual disease of 1 cm or more) has progressively become more popular, mainly due to its intent to reduce the volume of residual disease after primary surgery plus chemotherapy or after chemotherapy alone as much as possible, in cases with advanced stages, or early stages with a high risk of recurrence.

No major changes in the last decades have been achieved in the treatment of ovarian cancer as chemotherapy is still the standard treatment since 1985 (Figure I13). Platinum agents have been considered the major resource in the medical treatment of EOC as better results were observed with cisplatin-cyclophosphamide compared with cyclophosphamide alone (Lambert and Berry, 1985). Later, the combination of cisplatin-paclitaxel showed better efficacy (McGuire et al., 1996). Eventually, it was demonstrated that replacing cisplatin for carboplatin led to similar efficacy results but a significant reduction in drug-associated toxicities. (du Bois et al., 2003; Ozols et al., 2003). Nowadays, carboplatin-paclitaxel is the standard of care in the adjuvant and first-line treatment.

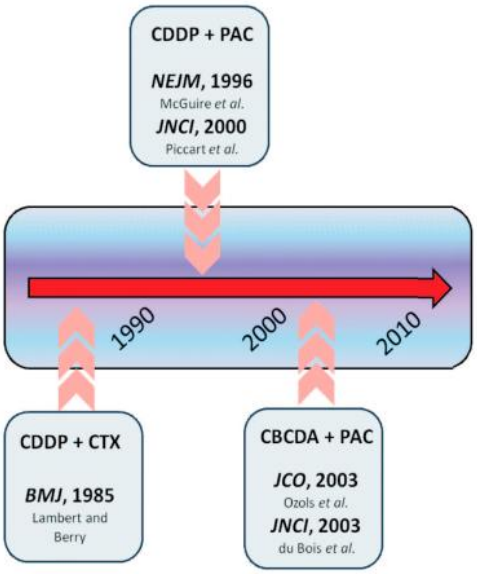

Figure I13. Ovarian cancer treatment changes over the last decades. CDDP + CTX: cisplatin and cyclophosphamide; CDDP + PAC: cisplatin and paclitaxel; CBCDA + PAC: carboplatin and paclitaxel. Adapted from (Della Pepa et al., 2015).

An alternative to the standard treatment is the combination of carboplatin with carboplatin-liposomal pegylateddoxorubicin (LPD). This treatment, although not being superior to the carboplatin-paclitaxel, has shown reduced side effects which represent an advantage for patients wanting to avoid alopecia or peripheral neuropathy.

It has been recently suggested that the use of intraperitoneal (IP) chemotherapy in the treatment of EOC can be a promising improvement for the treatment of ovarian cancer. Initially, it was postulated that delivering chemotherapy directly to the peritoneal cavity might reduce the risk of myelotoxicity. However, clinical trials have demonstrated the opposite, as different drug-related toxicities have been observed. Despite this adverse events, a phase III clinical trial comparing IV or IP chemotherapy patients that received debulking surgery has shown promising results (Mackay et al., 2011).

Even though survival rates of patients with advanced disease have improved over the past decade, there is still an urgent need for a better improvement. It is essential that we understand that ovarian cancer is a general term for a series of molecularly and etiologically distinct tumour.

By now, the same treatment is established for all histological types of ovarian cancer as just one tumour type. In the era of personalized cancer medicine, reproducible histopathological diagnosis of tumour cell type is requerid for successful treatment. For instance, it has been found that different tumour types respond differently to chemotherapy. The poor response rate of CCC (15%) contrasts notably with that of HGSCs (80%), resulting in a lower 5-year survival for clear cell compared with HGSC in patients with advanced stage tumours (20% versus 30%) (du Bois et al., 2003; Takano et al., 2006). The clear cell and mucinous types, in particular, are candidates for clinical trials to identify more active therapy than what is presently used (Fountain et al., 2006).

Table I3. Clinical and molecular features of the five EOC.

	HGSC	LGSC	EMC	CCC	MC
Pattern of spread	early transcoelomic spread	Transcoelomic spread	confined to pelvis	confined to pelvis	confined to ovary
Molecular abnormalities	BRCA, p53	BRAF, KRAS	PTEN, ARID1A	HNF1, ARID1A	KRAS, HER2
Chemosensitivity	High	Intermediate	Low	High	Low
Prognosis	Poor	Intermediate	Favorable	Intermediate	Favorable

Transcoelomic: “across the peritoneal cavity”. Adapted from (Prat, 2012).

2.6.1. Resistance to chemotherapy

Although progress has been made in the treatment of epithelial ovarian cancer (EOC) by improved surgical debulking and the introduction of platinum-taxane regimens, the overall 5-year survival rate is only 29% in advanced-stage disease (Oberaigner et al., 2012). For instance, for patients with low residual disease (all lesions < 1 cm in size following surgical debulking), the risk for recurrence after completion of primary therapy is 60% to 70%, whereas; for women with large-volume residual disease, the risk is estimated at 80% to 85% (Foley et al., 2013). This low survival rate can be attributed to the frequent diagnosis at an advanced stage and to intrinsic and acquired resistance to platinum-based chemotherapy. The efficacy of conventional platinum-based chemotherapy for EOCs is limited and although; most patients show an initial response to treatment, upon relapse (around 85% of the patients), the platinum response rates progressively diminish and they ultimately die (Galluzzi et al., 2012; Foley et al., 2013).

In the recurrent disease setting, those patients who experience progression through first-line platinum-based therapy (platinum refractory), or those who experience relapse within 6 months of receiving platinum therapy (platinum resistant) are typically treated with a second-line non–platinum-based regimen, such as doxorubicin (Muggia et al., 1997), gemcitabine (Lund et al., 1994), paclitaxel, topotecan (ten Bokkel Huinink et al., 1997), vinorelbine (Rothenberg et al., 2004), or trabectedin plus pegylated liposomal doxorubicin (Poveda et al., 2010). Agents yielding responses in the range of 15% to 20% that last a median of approximately 4 months (Alberts et al., 2008; Ushijima, 2010), emphasize the great need for novel effective therapeutic strategies to overcome cisplatin resistance as 85% of patients will relapse in five years.

2.7. Targeted therapies for ovarian cancer

Different biological molecules have been investigated in the first-line setting to overcome cisplatin resistance. Although at present the data on

bevacizumab are more mature, other antiangiogenic agents and tyrosine-kinase inhibitors (TKis) may be emerging as future therapeutic options.

For instance, **Bevacizumab** (Avastin®) is a humanized monoclonal antibody that binds to vascular endothelial growth factor A (VEGF-A) and is recognized as a potent antiangiogenic agent. After its approval for the treatment of many solid malignancies (e.g., colorectal and lung cancers), bevacizumab has proven to be highly active in EOC as well. It is reported that the addition of bevacizumab to carboplatin and paclitaxel, followed by maintenance therapy with bevacizumab alone, significantly prolonged the progression-free survival (PFS) of EOC patients (Perren et al., 2011). Nevertheless, not all patients benefit from adding bevacizumab to the standard treatment and some patients overcome resistance as well (Weber et al., 2012). For this reason, interesting biomarkers are currently under development as predictive factors of response to bevacizumab (e.g., circulating levels of Ang1 and Tie2)(Backen et al., 2014).

Another effective strategy to treat EOC patients and overcome resistance to bevacizumab is targeting other pathways involved in cell proliferation and carcinogenesis, which, in addition of being antiangiogenic, have also effects over the tumoral cell. One example of this is **Pazopanib** (Votrient®), an orally administered, multi-targeted kinase inhibitor; which target the VEGF receptors 1, 2 and 3, platelet derived growth factor receptors (PDGFRs), and the fibroblast growth factor receptor (FGFR)(Sonpavde and Hutson, 2007).

Furthermore, the clinical development of Poly(ADP-ribose) polymerase (PARP) inhibitors has been accelerated again following encouraging data on their efficacy in EOC treatment. PARP is a family of nuclear proteins involved in DNA repair. Most studies focus on maintenance treatment after chemotherapy rather than combinations with antineoplastic drugs (Della Pepa et al., 2015). **Olaparib** (Lynparza®) is certainly the best known PARP inhibitor, although a number of agents in the same class are currently under evaluation. In a study, olaparib, which is given as a maintenance treatment after platinum-based chemotherapy, was compared with placebo in patients with platinum-sensitive, recurrent, BRCA-positive HGSC resulting in a

significantly longer PFS, which was the primary end of the study. (Ledermann et al., 2013) and a phase III trial is being tested. In addition, the FDA approved the use of Olaparib in women with BRCA ovarian cancer. Other PARP inhibitors are also under development, namely **niraparib** and **rucaparib**, both of which are currently being tested in platinum sensitive recurrence.

Nevertheless, other target therapies are being tested in order to find new possible solutions for this highly percentage of relapse on ovarian cancer:

In recent years, there are several clinical trials using the ERK-MAPKK (MEK) inhibitors for the treatment of LGSC patients (Diaz-Padilla et al., 2012). Activation of the ERK signalling pathway may be very important as BRAF and KRAS mutations were initially reported in up to 68% of cases. **Selumetinib** (AZD6244) or **Trametinib** are being tested on two phase III clinical trials for the treatment of patients with recurrent or progressive LGSC or peritoneal cavity cancer, comparing these inhibitors with a standard therapy (Farley et al., 2012). In primary mucinous ovarian cancer, which is frequently resistant to conventional chemotherapy, the Ras/Raf pathway is also an appropriate therapeutic target (Banerjee and Kaye, 2013). Multiple other signalling molecules are also implicated in overcoming resistance to chemotherapy and targeted agents in ovarian cancer; including the insulin-like growth factor (IGF) receptor (Singh et al., 2014).

3. IGF signalling pathway

Insulin and Insulin-like growth factor (IGF) signalling regulates cellular growth, proliferation, metabolism, and survival. IGF1R belongs to the insulin receptor (IR) family that includes the IR, IGF1R, IGF1R/ IR, and the mannose 6phosphate receptor (also known as IGF2R), which is a non-signalling receptor (Pollak, 2004; Pollak, 2008).

IGF1R can be activated by the ligands insulin like growth factor1 (IGF1) or insulin like growth factor2 (IGF2). IGF1R/IR hybrids preferentially signal with

the IGF ligands. IR exists in two isoforms: IRB, traditional insulin receptors, and IRA, a fetal form that is re-expressed in selected tumours and preferentially binds IGF2 (Frasca et al., 2008). These receptors may coexist in a given cell, with relative abundance and activation status varying by cell type, tissue type, and physiologic or pathologic conditions.

Following co-translational insertion into the endoplasmic reticulum (ER) as a 220KDa proreceptor, the IGF1R is cleaved in the trans-Golgi network to generate mature α (135KDa) and β (98KDa) subunits linked by disulfide bonds (Adams et al., 2000). After trafficking to the plasma membrane, IGF1Rs are activated by IGFs, and then internalized and degraded, or recycled to the cell surface (Vecchione et al., 2003; Romanelli et al., 2007).

IGF1R works as homodimer, formed by 2 subunits α and 2 subunits β. Activation of IGF1R leads to phosphorylation of IR substrates-1 (IRS1) and Src-homology collagen protein (Shc) (Baserga, 1999),which in turn mediates the activation of the ERK pathway and the PI3K/AKT pathway (Pollak, 2008), which is considered the predominant downstream signalling pathway for the IR family. PI3K activation results in translocation of the glucose transporter, Glut4, and phosphorylation of the protein kinase AKT, which in turn influence cell survival pathways. At the same time, IRS1 activation also leads to activation of Ras/Raf/MEK/ERK pathway (Clayton et al., 2011) (Figure I14).

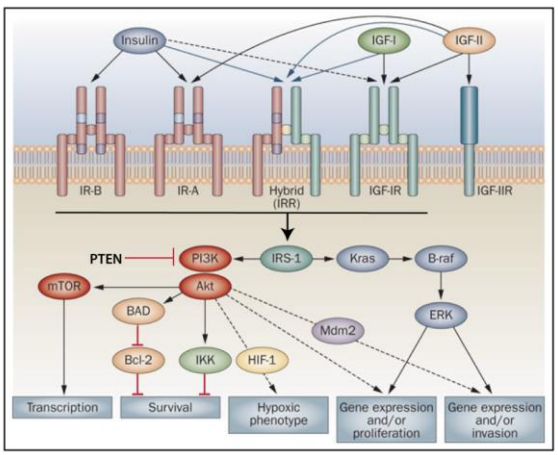

Figure I14. IGF signalling pathway. Adapted from (Clayton et al., 2011)

Extensive studies have implicated IGF1R, IGF1, and IGF2 signalling in cancer development, maintenance, and progression. IGF1R expression is critical for anchorage independent growth, a well-recognized property of malignant cells in different tumour types, ovarian cancer (Cullen et al., 1990; Gooch et al., 1999; Nickerson et al., 2001; Hassan and Macaulay, 2002; Koti et al., 2013).Moreover, the IGF pathway has also been shown to modulate paclitaxel resistance (Huang et al., 2010).

3.1 IGF1R inhibitors in cancer

Through its anti-proliferative activity, inhibitors of the IGF1R system have been considered to provide a number of clinically important benefits. For instance, maintenance therapy, aimed at suppressing growth of residual, subclinical disease, could have a major impact if IGF system signalling is a critical factor, as suggested by prognostic data in patients with breast and ovarian cancer (Vadgama et al., 1999; Lu et al., 2006; Pasanisi et al., 2008).

Linsitinib (OSI-906), a small-molecule dual kinase inhibitor of both IGF1R and insulin receptor, has entered phase II clinical trials in combination with weekly paclitaxel in platinum-resistant ovarian cancer. Furthermore, overexpression of IGF1 and growth inhibition with OSI-906 was reported in preclinical models of LGSOC (King et al., 2011) and, therefore, in addition to MEK inhibition, targeting the IGF pathway may be another potential therapeutic approach in this setting. Several approaches to inhibit IGF1R signalling have been investigated (Table I4).

However, some clinical trials showed some undesirable side effects. For example, a dose-escalation phase I study of **IMC-A12** *(Cixutumumab*), a monoclonal antibody against IGF1R that blocks the activity of this receptor, has revealed good results but some adverse events included hyperglycemia, which was dosing limiting (Higano et al., 2015). Nevertheless, and as observed in TableI4, despite this dosing limiting problems a Phase II is being performed as benefits are encouraging over this manageable side effects.

Table I4.IGF1R inhibitors in clinical trials.

	Agent	Target	Clinical trials	Company
SMIs	Linsitinib (OSI-906)	IGF1R & IR r	Phase III	OSI
	BMS-754807	IGF1R & IR	Phase II	BMS
	XL228	IGF1R & AURORA & SRC	Phase I	Exelixis
	INSM-18 (NDGA)	IGF1R	Phase I	Insmed
MoABS	Cixutumumab (IMC-A12)	IGF1R	Phase II	ImClone
	Figitumumab (CP-75 1,871)	IGF1R	Discontinued after Phase III	Pfizer
	Dalotuzumab (MK-06 46; h7C10)	IGF1R	Phase III	Pierre Fabre and Merck
	Ganitumab (AMG 479)	IGF1R	Phase III	Amgen
	SCH 717454 (19D12)	IGF1R	Discontinued after Phase III	Schering Plough
	AVE1642 (EM164)	IGF1R	Discontinued	ImmunoGen /Sanofi

SMIs: small molecules tyrosine inhibitors. MoABS:monoclonal antibodies.

Overall, there is still a lot to sort out in order to find new possible therapies for ovarian cancer as 85% of patients relapse between five years and this work try to demonstrate a new candidate for its use on ovarian cancer treatment.

Objectives

Objectives

One of the general objectives of this work has been to evaluate the role of ALK1 receptor, member of the TGFβ signalling pathway, on physiological angiogenesis. Inside this objective there are some specific objectives to be evaluated:

a) Analysis of the influence of ALK1 lack on the sprouting angiogenesis using the $ALK1^{+/-}$ retina mouse model.

b) Use of this $ALK1^{+/-}$ mice model, which mimics HHT, to find possible therapies to treat these patients.

On the other hand there is the second general objective to study the role of TGFβ family members, ALK1 and ALK5 on the progression of ovarian cancer. From this one there are these derived objectives:

c) Evaluate the activation levels of the Smad2/3 pathway levels on human ovarian cancer samples and its extrapolation to orthotopic mouse models.

d) Analyse the antitumor activity of the TGFβ inhibitor, LY2109761, on the ovarian orthotopic mouse models as a possible target therapy to treat ovarian cancer.

Materials and methods

Materials and methods

1. Animal studies

All mice used in this work were kept in individually ventilated cages on constant temperature (20-25ºC), in a SPF (Specific Pathogen Free) conditions and sterility. Mice obtained water and food by libitum. All experiments were done on a laminar flow cabinet, and all procedures were done in accordance to the guidelines and legislation and approved by the committee for animal care on IDIBELL and la Generalitat de Catalunya.

For the retina mouse model; we investigated the loss of ALK1 on $ALK1^{+/-}$ mice (C57BL6 background)(Srinivasan et al., 2003). When indicated ALK1 heterozygous animals were crossed with $p110\alpha^{D933A}$ knock-In (KI) allele mice from Dr. M.Graupera´s group (Foukas et al., 2006).

To assess the ovarian cancer study, we used female un/un Swiss mice of 5-6 weeks and 20-22 gr of body weight purchased from Janvier (France).

1.2 Orthotopic implantation of ovarian tumours in Athymic mice

In this work it has been used three orthotopic mouse models from human origin; one endometrioid tumour model (OVA15) and two high-grade serous ovarian tumour model; OVA8 and OVA17, this last tumour model metastasized on liver and lung tissues. All three were established in the Laboratori de Recerca Translacional (LRT) at Institut Català d'Oncologia (ICO) by Dr. Alberto Villanueva. The ovarian tumours were perpetuated in nude mice by consecutives passages orthotopically into the same original organ where came from the patient, in our case into the ovary of the mice.

Firstly, the tumour was extracted from the donor mouse just in the moment of the sacrifice and cleaned with cell culture medium DMEM 10% FBS, 50 U/ml penicillin and 50 µg/ml streptomycin in order to avoid possible contaminations. Then, we fragmented the tumour in pieces of 6 mm^3 approximately, which stayed in the medium until implantation moment.

For the surgical implantation mice were anesthetized by isoflurane inhalation. Its skin was disinfected with Betadine and a small incision was made and the ovaries were exteriorized. A piece of 6 mm^3 tumour was implanted in one ovary of the mouse (unilaterally) using Prolene 7.0 surgical sutures. The ovary was returned to the abdominal cavity and the incision was closed with wound clips (Becton-Dickinson). The animal was then located under a lamp in order to warm the mouse until it woke up.

Afterwards, Buprex was administered i.p to the mouse (200 ul) the day of the surgical intervention and for two days after the implantation. Wound clips were extracted after 8-10 days from the implantation, when wound healed was observed.

1.2.1 Ovarian tumours orthotopic mouse model

In particular we maintained and used three ovarian tumours *in vivo*, and samples were used as well for protein and RNA analysis.

OVA15: Endometrioid tumour model.

OVA8: High-grade serous tumour model.

OVA17: High-grade serous tumour model which metastasises to liver and lung.

1.2.2 *In vivo* treatment

As the tumours had different growth behaviours the treatment schedules were different. Treatments started when a palpable intra-abdominal mass was detected. When all mice presented an approximated 100 mm^3 tumour size, mice were randomized in the different treatment groups taking into consideration the possible differences of tumour volume. The studies were terminated when tumours in vehicle-treated animals were judged to be adversely affecting their wellbeing.

Oral administrations were done using animal feeding needles.

1.2.2.1 Treatment schedule of the experiments with LY2109761 (Results section 2.2.1)

LY2109761 was kindly provided by Lilly and Co. It was dissolved in 1% carboxymethylcellulose, 0.5% sodium lauryl sulphate (Sigma), 0.085% Polyvinylpyrrolidone (Sigma) and 0.05% antifoam (Sigma) solution. Drug aliquots were prepared every two weeks and kept in the dark at 4°C.

Mice were treated with LY2109761, administered twice daily with gavage as an oral dose of 100 mg/kg (Anido et al., 2010). Control mice were treated with the vehicle oral solution as the treated groups.

Treatment of the high-grade serous tumour models OVA8 and OVA17 started 5 weeks after implantation and continued for one further month. Treatment of the OVA15 endometrial model started six weeks after tumour implantation and continued for another month more. These treatments had no significant effect on mouse body weight and the animals appeared healthy and active throughout the study.

OVA15: We used five mice for each group. In this work, not all tumour implanted grow for this reason when randomized we had to use only five per group.

OVA8: We used sixe mice for each group.

OVA17: We used nine mice for each group.

1.2.2.2 Treatment schedule of the experiments with Linsitinib (Results section 2.3)

Linsitinib (OSI-906) was obtained from LC Laboratories (MA, USA) and was dissolved in 25 mM tartaric acid (Sigma) solution.

Treatment of OVA8 started 4 weeks after implantation. Linsitinib was administered daily (5 days) with an oral dose of 40 mg/kg by gavage (Leiphrakpam 2013), 1 week without treatment followed by a new cycle of treatment for 5 days to six mice.

These treatments had an effect on mouse body weight for this reason we performed an intermittent treatment. Control mice (8 mice) were treated with the vehicle oral solution as the treated groups.

1.2.2.3 Treatment schedule of the experiments with Cixutumumab (Results section 2.3)

IMC-A12 (Cixutumumab) was obtained from ImClone (NJ, USA). IMC-A12 (Cixutumumab) treatment of OVA17 started 5 weeks after implantation. The antibody was administered i.p. three times a week for 4 weeks at a dose of 12 mg/kg to four mice. Control group (six mice) was treated three times a week for 4 weeks with i.p injection of PBS.

At the end of the treatment a mouse body weight reduction was observed but the animals appeared healthy and active throughout the study.

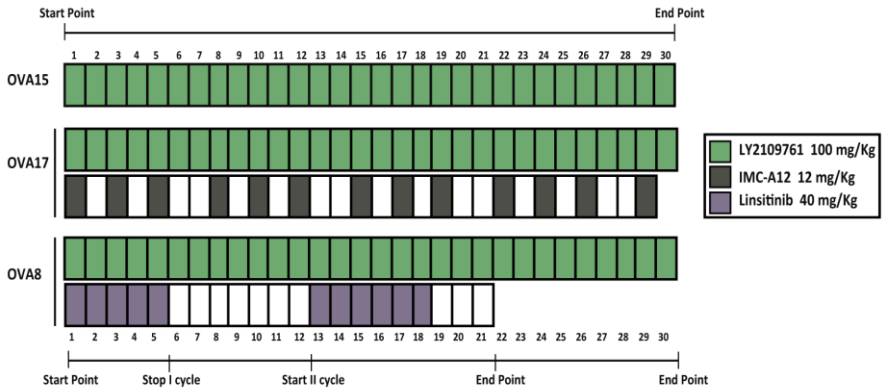

Figure M1. Schedule and drug dose of the different *in vivo* treatments.

1.2.3 Tumour sample extraction and process

At the end of the experiment, all mice were sacrificed by cervical dislocation. After sacrifice the effects of the different treatments on tumour response were evaluated by determining tumour weight and volume, where volume = (length)(width^2/2)(Jensen et al., 2008).

From each tumour sample were taken frozen pieces into crio-tubes for RNA and protein extraction at -80ªC; Froze samples in OCT (Tussue-TEK® Sakura) to obtain frozen slides and analyse by IF later.

In addition, other tumour pieces were paraffin embedded to analyse with H&E and IHC following the embedded protocol: first fixation phase where tumour samples were kept O/N (over-night) on 4% Formol (pH=7,4), then a dehydration process with a alcohol battery to finally arrive to a xylene (1 hour in Ethanol 70%, 1 hour in Ethanol 96%, O/N Ethanol 96%, and 1h 30' in each steps: 3 ethanol of 100% and xylene). Finally, a liquid paraffin bath at 60ºC O/N and the next day samples were embedded in paraffin in a block sharp ready to cut and dried at Room Temperature (RT).

1.2.4 Dissemination study by bioimaging

In order to perform the bioimaging *in vivo* study we used the SKOV3-GFP cell line generated by DR. Agnès Figueras (section 3 of materials and methods).

The cell line was seeded in two groups of Petri dish; the control group with DMSO and the treated group with LY2109761 for three days. Afterwards, 1 million of SKOV3-GFP cells were collected in 200µl of DMEM medium without any supplement, and were I.P. injected to each athimic mice, six mice per group.

To analyse cell attachment *in vivo* between groups, pictures of the different mice were taken with the *IVIS Imaging System* (*Caliper LifeSciences*) at different time points (24, 48 and 72 hours).

We quantified for each mice the number of different number of ROIs for each mice and the average of the luminescence radiance divided by pixel for second and by surface (p/s(cm^2).

1.3 ALK1 mice characterization

1.3.1. PI3K inhibition through LY294002 injection

LY294002 (Calbiochem, Millipore, Billerica, MA) was re-suspended in dimethyl sulfoxide (DMSO, Sigma) 4:1 PBS at final 15 mM stock concentration. Half of the litter was injected intraperitoneally with 20µl of LY294002 stock solution at P6 (16:00 hours (h)) and P7 (9:00h). Same volume of DMSO + PBS was injected to the other half of the litter to obtain the control condition. Retinas were isolated at P7 (16:00h) for experiment.

1.3.2 Mice genotyping

1.3.2.1 Tissue digestion

New born mice were weaned once they turned 4-weeks old. Upon weaning, ear or tail biopsies were kept for genotyping. Tissue was lysed with 600 µl of 50 mM NaOH (Sigma). Samples were incubated at 100 ºC for 15 min and were vortexed and kept at room temperature (RT) until they reached 50-70ºC. To neutralize the samples, 100 µl of 1M Tris (Sigma) HCL pH 7.4 were added to each sample. Samples were vortexed, centrifuged at maximum speed for 1 min and kept at 4 ºC until samples were processed for DNA amplification.

1.3.2.2 PCR

Polymerase chain reactions (PCR) were performed using two different protocols referred as PCR reaction WT and PCR reaction HET to genotype the WT strain or the $ALK1^{+/-}$ (HET) strain and a third one to detect p110α Ki mice.

Table M1. Table of PCR primer sequences.

PCR	Primer sequence
ALK1 WT	ALK1-WT-Fw 5'-ACCACAGCTGTTCCTACCTTCT-3' ALK1-WT-RV 5'- AACTGTTCTTCCTCGGAGCCTT-3'
ALK1 HET	ALK1-nul-Fw 5'-GCAACATCCACTGAGGAGCAG-3' ALK1-nul-RV 5'- GTGGCTGGAGAGGAACAGTAG-3'
p110α KI	M36-Fw 5'-CCTAAGCCCTTAAAGCCTTAC-3' M47-Rv 5'-ACTGCCATGCAGTGGAGAAGCC-3'

PCR reaction WT (to a final volume of 25 l): 2µl DNA sample, 17.4 µl H2O, 0.8 µl MgCl2 15mM (diluted from MgCl2 50mM Ecogen), 2.5 µl of 10x reaction buffer without Mg (Ecogen), 0.3 µl of 10 µM primer pool (forward + reverse), 2.5 µl dNTPs and 0.25 µl Ecotaq DNA polymerase (Ecogen).

PCR reaction HET (to a final volume of 25 l):2µl DNA sample, 17.4 µl H2O, 1.3 µl MgCl2 15mM (diluted from MgCl2 50mM Ecogen), 2.5 µl of 10x reaction buffer without Mg (Ecogen), 0.3 µl of 10 µM primer pool (forward + reverse), 2.5 µl dNTPs and 0.25 µl Ecotaq DNA polymerase (Ecogen).

PCR reaction p110αKI (to a final volume of 25 l): 1.5 µl DNA sample, 15.875 µl H2O, 2.5 µl 10x Titanium Taq reaction buffer, 2.5 µl of 10 µM primer pool (forward + reverse), 2.5 µl dNTPs and 0.125 µl 50x titanium Taq (Clontech).

Table M2. Table of PCR conditions.

	WT		**HET**			**p110α KI**	
	Tº	**Time**	**Tº**	**Time**		**Tº**	**Time**
	94	2 min	94	2 min		94	2 min
35 cycles	94	20 sec	94	20 sec	39 cycles	94	30 sec
	55	30 sec	65	30 sec		65	30 sec
	72	1 min	72	1 min		72	30 sec
	72	10 min	72	10 min		72	7 min

2. Post-natal mouse retina isolation and IF staining of whole-mount tissue

2.1 Eyes extraction and retina isolation

Pups were sacrificed by decapitation and eyes were quickly removed using scissors and forceps. Eyes were fixed in a solution of 4 % paraformaldehyde (PFA) (Sigma) in phosphate-buffered saline (PBS) for 1h and 15 min at 4 ºC. Once the fixation time was over, 4 % PFA was changed to PBS and retinas were harvested from the rest of the eye following the protocol described below.

The procedure of retina isolation was done with the help of a binocular dissecting microscope (Carl Zeiss). Briefly, eyes were collected in a clean culture dish filled with PBS and the cornea (the clear tissue that covers the anterior part of the eye, opposite to the optic nerve) was incised with the help of a needle (Figure M2b).

Using micro-scissors (Fine Science Tools), the cornea was cut and removed. Next, the iris was also removed using two forceps (Fine Science Tools) and the outer layer of the eye, the sclera and the pigmented retina layer started to be separated. The outer layer should be dissected carefully, in small increments, to avoid damaging the retina layer beneath. At this point, the lens and the vitreous humour, which appears as a single jelly-like structure (Figure M2e) need to be removed. Finally, the hyaloids vessels (Figure M2f) were carefully detached from the inner side of the eye using fine movements. Retinas were then fixed for 45 min more and were kept in PBS at 4ºC until they were processed for immunofluorescence (IF).

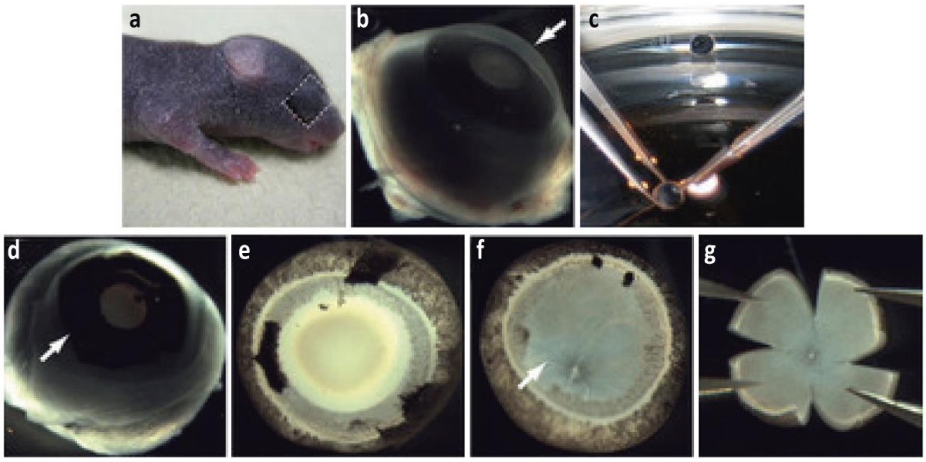

Figure M2. Eye and retina dissection. a, Image showing where to make the incisions around the eye of the pup.b, Dissected eyeball from a P6 pup. Arrow points to the cornea surface. c, Overview of cornea dissection d, Eyeball without cornea. Arrow indicates dissected cornea. e, Image showing eye without sclera, choroid, cornea layers, pigmented layers and without the iris. f, Dissected eye without lens. Arrow shows hyaloid vessels. g, Retina with four radial incisions. Figure modified from (Pitulescu et al., 2010b).

2.2 Immunofluorescent staining of whole-mount retinas

2.2.1 Simple staining with conjugated IsolectinB4

Retinas were incubated 30 min, at RT in Pblec buffer (1% Triton X-100, 1mM CaCl2, 1mM MgCl2, 1mM MnCl2 in PBS pH6.8). Retinas were then incubated with conjugated isolectinB4 in appropriate dilution (Table M3) in Pblec buffer ON at 4ºC with gently agitation. The following day, Pblec containing isolectinB4 antibody was removed and retinas were washed 3 times (10 min each) with PBT buffer at RT (PBS containing 0.1% Tween-20). After the final washing steps with PBT, retinas were incubated with DAPI in appropriate dilution (Table M3) and then were post-fixed using 4 % PFA, at RT for 2 min. A last wash with PBS was done before retinas were flat-mounted on glass slides using Mowiol (Calbiochem) as mounting medium.

2.2.2 Staining with primary antibodies different than conjugated IsolectinB4

Retinas were blocked and permeabilised with permeabilization buffer (1% bovine serum albumin (BSA) (Sigma), 0.3% Triton X-100 in PBS) ON at 4 ºC with gentle rocking. Retinas were then incubated with primary antibodies in appropriate dilutions (Table M3) in permeabilization buffer ON at 4ºC with gentle rocking. The following day, primary antibodies were removed and retinas were washed 3 times (10 min each) with PBT buffer. Retinas were further incubated 30 min, at RT in Pblec buffer (% Triton X-100, 1mM CaCl2, 1mM MgCl2, 1mM MnCl2 in PBS pH6.8) and incubated ON at 4ºC with the appropriate dilution of secondary antibodies in Pblec buffer (Table M4). In addition, conjugated isolectinB4 was added together with the secondary antibodies in the appropriate dilution (Table M3). The day after, retinas were washed 3 times (10 min each) with PBT, were incubated with DAPI in appropriate dilution (Table M3) and then were post-fix for 2 min with 4% PFA and were flat-mounted on glass slides using Mowiol as mounting medium.

Table M3. List of primary antibodies used for mouse retina immunostaining.

Antibody	Conjugated	Host	Dilution	Company
Erg 1,2 3,	-	Rabbit	1:100	Santa Cruz
Desmin	-	Rabbit	1:200	Abcam
Isolectin-GS-B4	Alexa Fluor 568	-	1:300	Molecular Probes
Isolectin-GS-B4	Alexa Fluor 647	-	1:300	Molecular Probes
DAPI	-	-	1:300	Invitrogen

Table M4. List of secondary antibodies used for mouse retina immunostaining.

Antibody	Conjugated	Dilution	Company
Goat Anti-Rabbit	Alexa Fluor 488	1:200	Molecular Probes
Goat Anti-Rabbit	Alexa Fluor 568	1:200	Molecular Probes

2.2.3 *In vivo* proliferation assay, EdU detection

EdU is a synthetic analogue of thymidine, and thereby, it can be incorporated into DNA during S phase. Click-iT EdU Imaging Kit was bought from Invitrogen and was used for EdU injection and detection. To determine the number of proliferating ECs in the growing retinal vasculature, pups were injected intraperitoneally with 60 µl of EdU component A from the kit (diluted to 2mM in 1 DMSO: 1 PBS) 2h before they were culled for retina extraction.

Retinas were isolated following the instructions described in section (4.1.). Thereafter, the reaction for EdU detection was performed following the instructions described in the Click-iT Imaging Kit. Briefly, retinas were incubated for 1h at RT with gentle rocking in 100 µl (for each pair of retinas) of EdU detection solution.

For 1ml of EdU detection solution:

- 860µl of 1x Click-iT EdU reaction buffer (obtained from appropriate dilution of component D)

- 40 µl of CuSO4 (component E)

- 2 µl of azyde-conjugated Alexa-Fluor (component B). Alexa fluor 488 and 647 were used for this thesis work.

- 100 µl of 1x Click-iT EdU buffer additive (obtained from the appropriate dilution component F)

Retinas were washed twice with PBS and were then incubated with permeabilisation buffer (described in section 4.2.2) ON at 4ºC with gentle agitation. Thereafter, retinas were incubated in appropriate dilution of Erg 1,2,3 (Table M3) in permeabilisation buffer ON at 4ºC with gentle agitation. The day after, retinas were washed 3 times with PBT at RT, followed by 30 min incubation with Pblec buffer at RT (described in section 4.2.1). Secondary antibody against Erg1,2,3 and isolectinB4 were incubated ON agitating at 4ºC in appropriate dilutions (Tables M3 and M4). Retinas were washed 3 times (10 min each) with PBT, were post-fix for 2 minutes with 4% PFA at RT and were flat-mounted on glass slides using Mowiol.

2.2.4 Retina imaging and quantification of vascular parameters

2.2.4.1 Confocal microscopy

All images shown of retina characterization were taken using a Leica confocal or a Nikon 801 microscope. Images were processed using Volocity 3D PerkinElmer software and Adobe Photoshop CS5 software. Images were quantified using Image J. 1.47h software with the proper scale set up.

2.2.4.2 Analysis of the vascular parameters

2.2.4.2.1 Number of sprouts

The number of sprouts was expressed as nº of sprouts / 100 µm of sprouting membrane. For this, the total vessel length at the sprouting front was determined using images taken with the 40x objective. Thereafter, the number of sprouts present throughout the sprouting membrane was quantified (Figure M3A).

2.2.4.2.2 Vessel width

A visual field of 100x100 µm was determined behind the vascular sprouting front of images taken with the 40x objective. The vessel widths of six representative branches were quantified per image (Figure M3B).

2.2.4.2.3 Radial expansion

For radial expansion quantification, images with 4x objective in Nikon 801 microscope were taken. The migratory length of the vascular plexus was analysed by measuring the total length of the retinal vasculature from the optic nerve towards the retinal periphery as shown in figure M3C.

2.2.4.2.4 Vascular branching

For quantification of number of branch points per area, images were taken with the 40x objective. A visual field of 100x100 µm was determined behind the vascular sprouting front and the number of branch-points was quantified as shown in Figure M3D**.**

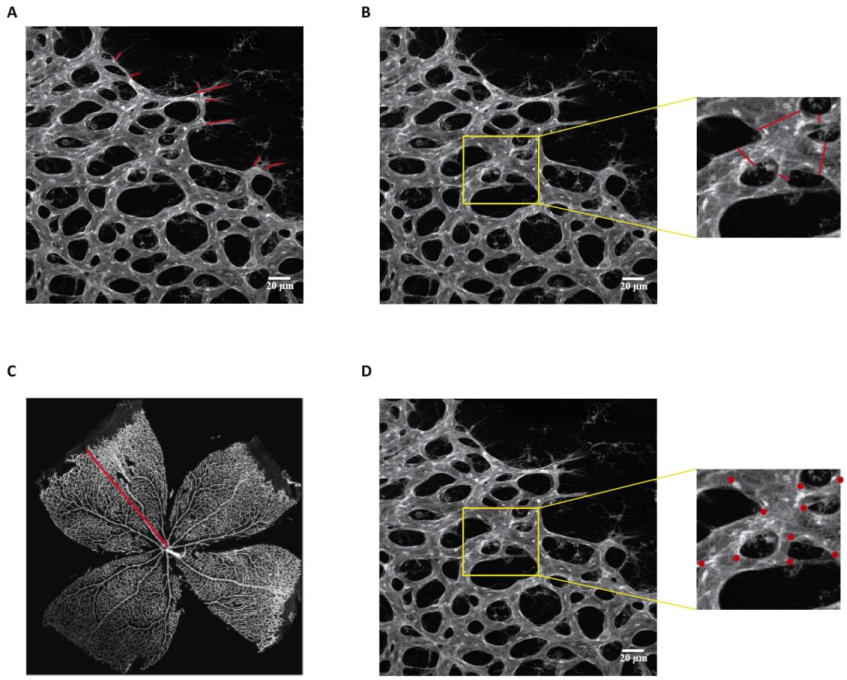

Figure M3. Quantification of vascular parameters on mouse retina immunostaining. Yellow cub determines the visual field of 100x100 µm where the quantifications of vessel width and vessel branch-point were analysed. Red lines and points represent the measure of the different parameters: A) Number of sprouts B) Vessel width C) Radial expansion and D) Vessel branching-points.

2.2.4.3 Quantification of ECs nuclei and proliferative ECs.

For the quantification of ECs nuclei and ECs proliferation per visual field, images with 40x objective were taken from retinas stained with the endothelial nuclei marker Erg1,2,3 and with EdU counterstained with isolectinB4 (following instructions in section 2.2.3). It was selected the stained cells that were strictly in contact with the sprouting membrane. Two zones were determined; first line of cells on the sprouting front of the vascular plexus and the second line just behind with 20 µm of length from the sprout, were selected of every image and the total number of ECs (Erg+) located in the two different zones separated by the template was quantified. Thereafter, it was quantified how many of those ECs were proliferating (EdU+), thus determining the percentage of proliferative ECs both in the first and the second line.

3. Cell culture

In this work we performed experiments *in vitro* with four different ovarian cell lines: The SKOV3 an ascites from a patient with an ovarian adenocarcinoma (Fogh, 1975) were obtained by ECACC (*European Collection of Cell Cultures-Sigma Aldrich*).

The SKOV3-GFP was generated by Dra. Agnès Figueras from the SKOV3 cell line infected with a lentivirus expressing GFP (*Green Fluorescent Protein)* and Luciferase under a constitutive promoter (Ibrahimi et al., 2009). The A2780p cell line, established from a human serous tumour tissue, the TOV-112D cell line, established from a human endometrioid tumour tissue (Provencher, 2000) and the OV90 cell line, established from a human serous tumour tissue (Provencher, 2000). All three cell lines were obtained from Pepita Gimenez (Universitat de Barcelona) and confirmed its identity and verification by the ECACC.

3.1 Cell line maintenance

The OV90 and TOV-112D cell lines were cultivated with 1:1 mixture of 199 medium (Gibco) and an adapted medium from the literature DMEM (lonza) instead of MCDB105 medium. The SKOV3 and SKOV3-GFP cell line was cultivated with DMEM (Lonza) medium, and the cell line A2780p was cultivated with RPMI 1640 medium (Gibco). All mediums were supplemented with inactivated 10% foetal bovine serum (Gibco). Then 50 U/mL of penicillin, 50mg/mL of streptomycin sulphate, and 2mmol/L of glutamine were added to all cell culture media.

All cells were grown at 37ºC in a humidified atmosphere with 5% CO_2.

3.2 Generation of the lentiviral IGF1R shRNA constructs.

pGIPZ-shRNA lentiviral vectors were bought in glycerol stock as bacterial cultures from DharmaconGE®. The bacteria was grown on LB with ampicillin

(50 µg/ml), afterwards, and in order to obtain the plasmid a *maxiprep* with QIAGEN® Plasmid Maxi Kit was performed.

Next, to obtain the lentiviral constructs a we did a triple transfection to 293FT; with the second-generation packaging plasmid (pPAX2), a plasmid encoding the envelope (pMD2.G) and the plasmid encoding de shRNA (Dharmacon). Cells were transfected with polyethylenimine (PEI) (25KDa, linear, powder, (Polysciences Inc.)), from a stock solution of 1mg/ml solution to a 20mM HCL, 10mM NaOH, pH7 solution, after filtration with 0.22 µm filter.

Each virus was transfected to 293FT cells on 10 cm petri dish. For each plate 2.5 µg of pMD2.G, 7.5 µg of pPAX2 and 10 µg of shRNA plasmid were mixed with 1.25ml of NaCL 150mM; and also with 1.25 ml of a solution previously generated and incubated for 5 min. (1:5 of PEI in NaCl 150mM). Both mixed solutions were added after settled at RT into the 293FT cells drop o drop. This transfection medium was changed by fresh medium after O/N incubation. After 24h from the previously change of medium, we collected the medium with the viruses already on it and it was concentrated. To asses this concentration we performed a 500G centrifugation for 2 min at 4ºC to discard cells that could remain on the medium. Supernatant was filtered by 0.45µm and centrifuged at 20.000 rpm for 90 min at 4ºC with an ultracentrifuge (Optima^{TM} L-100 XP Ultracentrifuge, Beckman Coulter).

Supernatant was eliminated by decantation and pellet was resuspended in 600µl of PBS1X, which was incubated on ice for 30 min, then, it was again centrifuged at 25.000 rpm for 90 min at 4ºC after decanted, we resuspended with 210µl and kept on ice for 2 hours afterwards, it was liquated and kept frozen at 80ºC. Lentiviral production was performed on a specific lentiviral cell culture room at IDIBELL. The generated viruses were the ones listed below:

Table M5. List of IGF1R shRNA used in this work.

Virus	Gene	Clone ID
shRNA-NS	Negative control	RHS4346
shRNA-IGF1R-V2-71	IGF1R	V2LHS_131071
shRNA-IGF1R-V2-72	IGF1R	V2LHS_131072
shRNA-IGF1R-V2-48	IGF1R	V3LHS_377848

3.3 Generation of the established cell line shRNA transduction.

When the lentiviral vectors were already produces we continued with the generation of established cell lines. To asses this lentiviral vector transduction, cells were seeded into 6 well-plates, and when cells got to a 60% confluence were transduced.

Few hours before transduction we changed for fresh medium adding 8 µg/ml of Polybrene (Santa Cruz Biotechnology, inc.) afterwards, we added 10 µl of the concentrated virus. Next day medium was changed for a fresh one and not until 48 hours post-transduction have passed that we added Puromycin (Sigma) 2µg/ml in order to select the infected cells, as these vectors express puromycin resistance and infected cells are resistant to puromycin. All control cells without lentiviral infection died while cells with lentiviral infection survive.

Dharmacon pGIPZ lentiviral vectors were used to permanently silence IGF1R expression in A2780p and SKOV3 cells. The negative vector without short hairpin RNA (shRNA) sequence (Dharmacon non silencing-pure vector) was used as negative control. Generated cell lines were constantly under puromycin presence and were expanded whenever cell grow.

3.4. Inhibitors and growth factors used *in vitro*.

Cells were treated with different inhibitors; LY2109761 was kindly provided by Lilly and Co and diluted with DMSO, IMC-A12 (Cixutumumab) was obtained from ImClone (NJ, USA).

At the same time cells were stimulated with TGFβ that was provided by R&D.

3.5. Cell viability assay by MTT incorporation

Cell viability was determined by measuring the incorporation of the methyl-thiazole-tetrazolium *(3-(4,5-dimethylthiazol-2-yl)-2,5-diphenyltetrazolium bromide*) or MTT (Sigma Chemical). This assay is based in colorimetric method using the characteristics of the MTT to be reduced into its insoluble formazan, which has a purple colour. This reduction is due to a enzymatic reaction catalysed by a mitochondrial enzyme, NAD(P)H; which is only active in metabolically an alive cells. This assay measures the metabolic activity of the cells that can be related to its cell viability (Berridge, 2005).

Cells were plated in 96-well plates, 750 cells per well, in quadruplicate, and allowed to grow for 24 hours. Cells were treated with LY2109761 (2, 5 and 10 µM), and IMC-A12 (10, 25 and 50 mg/ml), and DMSO was used as a positive control (doses are shown in logarithmic scale, 10^{-2}, 10^{-3} and 10^{-4} mg/ml).

Subsequently, after 4 days of treatment, 45 µl of MTT at 5 mg/ml was added to each well and incubated for an additional 4 hours at 37ºC on dark conditions, after that, the medium was removed and the blue MTT formazan precipitate was dissolved in 100 µl DMSO and the optical density was measured (absorbance at 570 nm) on a multiwell plate reader.

Results were expressed on percentage form, where 100% was cell control absorbance, without any inhibitor. All results were analysed and represented using GraphPad Prism 6 software.

3.6 Cell growth analysis.

To asses cell growing capacity of the shRNA clones from A2780p and SKOV3 cell lines we seeded 15.000 cells in 24 well-plates and cell number was counted post: 24, 48 and 72 hours.

Cell number was counted using the *TC20™ Automated Cell Counter* (Bio-Rad) and *Trypan blue* to count only alive cells.

3.7 Inhibitory protein synthesis analysis.

The human cell lines SKOV3 and A2780p were seeded in a 6 cm Petri dish. And allowed to recovered before pre-treat O/N with LY2109761 (2nM) or stimulate with TGF-β 10ng/ml). Then, it was added cycloheximide 10 μg/ml (Sigma) to each plate. Every 24h, cycloheximide and TGF-β or the inhibitor was added again to the medium.

Cells were lysed at 0, 8, 16 and 24 h with RIPA lysis buffer (0.1% SDS, 1% NP-40, 0.5% sodium deoxycholate, 50 mM NAF, 5mM EDTA, 40mM β-glycerolphosphate, 200 μM sodium orthovanadate, 100 μM phenylmethylsulfonyl fluoride, 1 μM pepstatin A, 1 μg/ml leupeptin, 4 μg/ml aproptin in PBS, pH 7,4) and analysed by western blot.

3.8. Analysis of the inhibition of protein degradation.

The human cell lines SKOV3 and A2780p were seed to a 6 well-plate and allowed to grow until 80% in confluence. Cells were treated alone with 2 and 10 μM of proteasome inhibitor MG132 (Sigma-Aldrich) or with 100 μM of lysosome inhibitor chloroquine for 24 h or in the presence of 2 μM of LY2109761. Cells were then lysed with RIPA buffer and analysed by western blot.

Wells without LY2109761, DMSO 1:1000 was added, with no observed toxicity as a control.

3.9 Immunofluorescence on cells

SKOV3 cells were seeded in 6 well-plate dish with glass slides and let it grow until 80% confluence. Then cells were treated with LY2109761 (2nM) or stimulation with TGF-β 10 ng/ml for 24h and DMSO diluted 1:1000 as a negative control.

After treatment cells were washed with PBS (formula) and fixed with 4% paraformaldehyde for 2 min and then washed twice with PBS 1X. Then, cells were permeabilisated with PBS 0.1% Triton X-100 for 40 minutes at room temperature. Cells were blocked with PBS-BSA 1 % for 1h at room temperature. These slides were then incubated at room temperature with a 1:250 dilution of rabbit polyclonal antibody for IGF1R (Cell signaling). Sections were washed three times with PBS 0.1% Triton X-100 and incubated with a 1:200 dilution of Alexa Fluor 588-conjugated goat anti-rabbit at room temperature for 1 h in the dark. Then were washed twice in PBS 0.1% Triton X-100 and incubation with DAPI 1/10000 (Abbot Molecular, IL) for 10 min in the dark. Cell slides were mounted using Fluoromount (Sigma).

4. Histological study of tumour samples.

4.1 Immunofluorescence studies

In the case of the study ALK5 levels on ovarian samples and the effect of the treatment over the macrophages number an IF was performed. OCT-frozen tissue (3µm) section from control and LY-treated tumours were done.

4.1.1 ALK5 staining

OCT-sections were tempered for 15 min. Then, sections were fixed with 4% paraformaldehyde for 5 min and then washed once with distilled water and twice with PBS 0.1% Triton X-100. Sections were blocked with PBS1X-goat serum 20% for 1h at RT. Next, sections were then incubated overnight at 4°C with a 1:50 dilution of rabbit polyclonal antibody for TGFβRI (Abcam).

Sections were washed twice with PBS 0.1% Triton X-100 and incubated with a 1:200 dilution of Alexa Fluor 488-conjugated goat anti-rabbit (Molecular probes) at room temperature for 1 h in the dark. Tumour slides were washed twice in PBS 0.1% Triton X-100 and cover slips were mounted using VectaShield® mounting medium for fluorescence with DAPI.

4.1.2 F4/80 - EpCAM staining

OCT-sections were tempered for 15 min. Then, sections were fixed with 4% paraformaldehyde for 2 min and then washed once with distilled water and permabilised 40 min with PBS 0.1% Triton X-100. Sections were blocked with PBS1X-goat serum 20% for 1h at RT. Next, sections were then incubated with 1:200 CD326(EpCAM)-FITC (Milteny Biotec) for 2h and next incubated overnight at 4°C with a 1:100 dilution of rat monoclonal antibody for F4/80 (Serotec). Sections were washed twice with PBS 0.1% Triton X-100 and incubated with a 1:200 dilution of Alexa Fluor 546-conjugated goat anti-rat (Molecular probes) at room temperature for 1 h in the dark. Tumour slides were washed twice in PBS 0.1% Triton X-100, then incubated with 1:3000 DAPI (Invitrogen) and cover slips were mounted using VectaShield® mounting medium.

4.1.3 ALK1 and CD31 staining

OCT-sections were tempered for 15 min. Then, sections were fixed with 4% paraformaldehyde for 2 min and then washed once with distilled water and permabilised 40 min with PBS 0.1% Triton X-100. Sections were blocked with PBS1X-goat serum 20% for 1h at RT. Next, sections were then incubated with 1:50 anti-ALK1 polyclonal antibody (Abcam) for 2h and next with 1:50 anti-CD31(human) monoclonal antibody (DAKO) incubated overnight at 4°. Sections were washed twice with PBS 0.1% Triton X-100 and incubated with a 1:200 dilution of Alexa Fluor 546-conjugated goat anti-mouse (Molecular probes) and Alexa Fluor 488-conjugated goat anti-rabbit (Molecular Probes) at room temperature for 1 h in the dark. Tumour

slides were washed twice in PBS 0.1% Triton X-100, then incubated with 1:3000 DAPI (Invitrogen) and cover slips were mounted using VectaShield® mounting medium.

4.2 Haematoxylin-eosin (H&E) staining.

Tissue sections (3-4 µm) of formalin-fixed, paraffin-embedded tumour were deparaffinised with 10 min of 4 xylene tray battery and rehydrated in graded alcohol (5 min in 3 absolute Ethanol trays, 3 Ethanol 96% and one Ethanol 70%). Afterwards, sections were washed with distilled water and were sunken on Harris' haematoxylin for 10-15 seconds. To clean the samples, slides were washed with running tap water and then 2 seconds with HCL 0.5% solution and 2 more seconds with ammonia water solution (200 ml distilled water with 1 ml ammonia 30%). Sections were again cleaned with running tap water. Then, sections were counterstained in eosin (2.5 g Eosin in 1L Ethanol 50%). After that, sections were dehydrated in graded alcohols (5 min in 3 ethanol 96%, 3 in absolute Ethanol and 10 min in 4 Xylene trays). Samples covered with cover slips mounted using DPX (Merck).

4.2.1 Necrotic area quantification.

OVA17 tumour samples from control and LY-treated mice were stained with H&E and images were taken with Stereomicroscope NIKON SMZ800 and the software NIS-ELEMENTS. With Image J software necrotic areas were quantified and its percentage by tumour total area was determined by each tumour sample.

4.3 Immunohistochemistry.

Immunohistochemistry to detect CD31, IGF1R, Ki67, ER and EpCAM followed the same protocol:

Tissue sections (3-4 µm) of formalin-fixed, paraffin-embedded tumour samples were deparaffinised in xylene and rehydrated in graded alcohols (section 4.2). After washing with distilled water antigen retrieval was performed with citrate 1X pH=6 for 5 min but 10 min for Mdm2 and incubated with 3% H_2O_2 for 10 minutes. Sections were washed with distillate water and twice with PBS 0.1% Triton X-100. Then, samples were incubated for 1 hour with protein-blocking solution (all were PBS-goat serum 20% but Ki67 that used an antibody diluten for 2 hours or ER where we used a PBS1X-BSA 3%), followed by incubation at 4ºC with primary antibodies (Table M6). Sections were washed twice with PBS 0.1% Triton X-100 and incubated 45 min with the corresponding secondary antibodies of the *DAKO invision + system HRP* (Table M6). Then sections were counterstained with haematoxylin and dehydrated in graded alcohols (5 min in 3 ethanol 96%, 3 in absolute Ethanol and 10 min in 4 Xylene trays). Then covered with cover slips and mounted using DPX (Merck).

Table M6. List of primary antibodies used for IHC.

Gene	Primary antibody		Secondary antibody	
CD31	1:80	DAKO	Anti-mouse	DAKO
Ki67 clone (MIB-1)	1:50	DAKO	Anti-mouse	DAKO
EpCAM	1:100	Abcam	Anti-rabbit	DAKO
ER	1:50	DAKO	Anti-mouse	DAKO
IGF1R	1:150	Abcam	Anti-mouse	DAKO
Mdm2 (SMP14)	1:20	St. Cruz	Anti-mouse	DAKO

4.4 pSmad2 staining

Tissue sections (3-4 µm) of formalin-fixed, paraffin-embedded tumour samples were deparaffinised in xylene and rehydrated in graded alcohols (section 4.2). Afterwards, an antigen retrieval was performed under high-

pressure and heating conditions for 20 minutes in citrate buffer, pH=6 and incubated with 3% H_2O_2 for 10 minutes.

Sections were washed with distillate water and twice with PBS 0.1% Triton X-100. Samples then were incubate with blocking solution (TBS-Tween 0,1% + BSA 5%) for 1 hour with followed by incubation at 4ºC over/night with 1:500 rabbit polyclonal antibody anti-phospho-Smad2, (Cell signaling).

The day after, sections were twice washed with TBS-Tween 0,1% and incubated with the specific secondary rabbit antibody EnVisionFLex (Dako) for 45 min. Then, samples were washed with TBS-Tween 0,1% followed by the EnVisionFLex DAB developing system (Dako) and counterstained with haematoxylin and visualized by light microscopy.

4.5 TUNEL

To identify the apoptotic cells we used the detection in situ method by the TUNEL Assay (*DeadEnd Colorimetric TUNEL System* Kit (Promega)) following its protocol.

Tissue sections (3-4 µm) of formalin-fixed, paraffin-embedded tumour xenografts were deparaffinised in xylene at 65ºC and rehydrated in graded alcohol. Then washed once with distilled water, with NaCl 0.85% for 5 min and then washed with PBS1X. Afterwards, sections were digested with proteinase K 1:100 from Proteinase 10mg/ml (from the kit) for 15 min at 37ºC on a humid chamber, and washed twice with PBS1X for 5 min each. Next, sections were incubated with the Equilibration Buffer (EB) for 10 min at RT and later with the EB mix (98µl EB + 1µl Biotinylated nucl mix + rTdT enzyme) for 1h at 37ºC. Then, it was washed with SCC 2X for 20 min at RTand washed with PBS1X. After that, sections were incubated with PBS1X-peroxidise 3% in order to inhibit peroxidises for 10 min. Then, washed with PBS1X and incubate 30 min at RT with 1:500 Streptavidin (Vecatestain), washed again with PBS1X and followed by the EnVisionFLex DAB developing system (Dako). Samples were counterstained with haematoxylin and sections were dehydrated in graded alcohols (5 min in 3 ethanol 96%, 3 in

absolute ethanol and 10 min in 4 Xylene trays). Samples covered with cover slips and mounted using DPX (Merck).

4.6 Cyclin D1 staining

Tissue sections (3-4 µm) of formalin-fixed, paraffin-embedded tumour samples were deparaffinised in xylene and rehydrated in graded alcohols (section 4.2). Retrieval was performed with EDTA pH=8 for 2 min and incubated with 3% H_2O_2 for 10 minutes. Sections were washed with distillate water and twice with PBS 0.1% Triton X-100. Then, samples were incubated for 1 hour with protein-blocking solution (PBS-goat serum 20%), followed by incubation at 4ºC with 1:50 mouse monoclonal anti-human cyclinD1 antibody (BD Biosciences, CA). Sections were washed twice with PBS 0.1% Triton X-100 and incubated 45 min with the anti-mouse secondary antibody of the *DAKO invision + system HRP*. Then sections were counterstained with haematoxylin and sections were dehydrated in graded alcohols (5 min in 3 ethanol 96%, 3 in absolute ethanol and 10 min in 4 Xylene trays). Samples covered with cover slips and mounted using DPX (Merck).

4.7 Immunohistochemistry quantification.

Images of tumour sections were obtained on NIKON-801 microscope.

To determine vessel density the ratio of the CD31-stained area to the total area and the number of vessels in each area were quantified. Quantifications were carried out in six hotspot fields of viable tissue zones at 400x magnification for each tumour, using Image J software. An average value for each tumour was obtained for each variable. Results are expressed as the means for each treatment group.

To determine cell positivity, number of cells was quantified in six hotspot fields of viable tissue zones at 400x magnification for each tumour by light microscopy NIKON Eclipse E400. An average value for each tumour was

obtained for each variable. Results are expressed as the means for each treatment group.

The intensity of pSmad2 and IGF1R stain were scored using a grading scale, defined as follows: no detectable signal (0 points), low-intensity signal (1 point), moderate-intensity signal (2 points), or high-intensity signal (3 points). Labelling frequency was scored as the percentage of positive tumoral cells. The multiplicative index of intensity and labelling frequency was used in our analysis.

5. Protein processing.

5.1 Protein extraction

5.1.1 Protein extraction of tumour samples

Protein extraction from tumour samples was done from fresh or frozen tumour pieces of 4X4 mm and was cut into smaller pieces (frozen samples were cut up on dry ice). Tumour samples were mechanically disrupted using RIPA lysis buffer (0.1% SDS, 1% NP-40, 0.5% sodium deoxycholate, 50 mM NeF, 5mM EDTA, 40mM β-glycerolphosphate, 200 µM sodium orthovanadate, 100 µM phenylmethylsulfonyl fluoride, 1 µM pepstatin A, 1 µg/ml leupeptin, 4 µg/ml aproptin in PBS, pH 7,4) and a glass homogenizer on ice. Lysates were then incubated on ice and centrifuged 12000rpm for 15 min at 4ºC. Protein concentration of its supernatants was determined using BCA assay kit (Pierce) and lysates were stored at -20C.

5.1.2 Protein extraction of cell culture samples

To extract protein from cells; cells were washed three times with cold PBS1X. With the cell plate on ice RIPA lysis buffer was added to cells and left for 15 min at 4ºC. Then, cells were scrapped on ice with a *cell scrapper.* In the case of A2780p cell line cells were sonicated at 1 cycle 100 amplitude% for 10 seconds. Then, lysates were centrifuged for 15 min at 4˚C and 13.000

rpm and protein concentration of its supernatants was determined using BCA assay kit (Pierce) and lysates were stored at -20C.

5.2 RTK Array analysis

To determine which tyrosine kinase receptors were targeted by LY2109761, a human Phospho-RTK Array (Cell signaling) was used to simultaneously detect 28 receptor tyrosine kinases and 11 important signalling nodes.

Tumour samples from control and treated group (2 per each group) were mechanically disrupted using lysis buffer (20 mM Tris-HCl (pH 7.5); 150 mM NaCl; 1 mM Na_2EDTA; 1 mM EGTA; 1% Triton; 2.5 mM sodium pyrophosphate; 1 mM beta-glycerophosphate; 1 mM $Na_3VO_{4;}$ 1 µg/ml leupeptin) and a glass homogenizer on ice. Protein concentration was determined using Bradford (Bio Rad). RTK array analysis was done according to the manufacturer's protocol. Array glass slides with 175 µg of tumour lysate were blocked with 150 µl array blocking buffer for 2 hours and incubated with overnight at 4ºC on an orbital shaker. Then, the arrays were washed; incubated with the detection antibody cocktail and HRP-linked Streptavidin and develop with LumiGLO®/ peroxidase reagent.

Average pixel density of duplicate spots was determined using the Quantity One software, and values were normalized against corner duplicate phosphotyrosine-positive control spots.

5.3 Western blotting

Proteins from tumour lysates (section 5.1) were mixed at equally volumes of total protein concentration of 25-50 µg, and loading buffer 4X (60mM Tris-HCL pH=6,8, 2% Sodium Dodecyl Sulphate (SDS), 20% glycerol, 0,01% blue of bromophenol and 5% β-Mercaptoethanol), then incubated for 5 min at 95ºC to help the denaturalisation already started for the presence of SDS and β-Mercaptoethanol.

Next, proteins were separated on an acrylamide-SDS gel. This is a size-selective technique and separate proteins by its size. These gels have two

phases: the stacking gel (4% acrylamide, 125mM Tris pH=6.8, 0,1% SDS, 1% ammonium persulfate (APS) and 0,1% TEMED), which stacks the proteins and allows the proteins to enter into the second phase at the same time. And next, the resolving gel responsible for the size-separating capacity. In this case, the acrylamide percentage is variable, choosing the percentage depending on the molecular weight of the protein of interest (9,4M Tris pH=8,8, 0,1% SDS, 1% APS, 0,1% TEMED and a % variable of acrylamide which is compensate with distilled water). In order to avoid that others characteristics but size play a role, lysates are denaturalised adding SDS and β-Mercaptoethanol. Samples were run for 1 to 2h at 100V with running buffer 1X (25mM Tris HCl pH=8,3, 192mM Glicin and 17 mM SDS) on a tray with a positive pole on the bottom and a current of 100-120V that produce the proteins to migrate into the gel.

Thereafter, proteins separated in the acrylamide gels were transferred onto to an Immobilon-P membrane, PVDF (Millipore, Billerica, MA) previously activated 1 min with Methanol. We prepared a sandwich system, where gel and membrane were next to each other, surrounded by sponges and Whatman paper tpo transfer proteins form gel to membrane. This sandwich was immersed on a transfer buffer (25 mM Tris-HCL, 0.19 M glycine, 10% methanol), with the membrane on the positive pole. Gel to membrane transference was performed at 4ºC at 100V and a maximum of 400mA for 1 hour and a half.

Next, membrane was blocked in TBS (150mM NaCl, 50 mM Tris, pH 7.4) containing 5% non-fat dry milk for 1h shaking at RT. Then, Blots were incubated with the incubation solution (TBS-1% non-fat dry milk with 0.02% sodium azide) containing the desired primary antibody at the appropriate dilution (Table M7) O/N at 4ºC.

The following day, blots were washed three times (10 min each) shacking with TBS-1% Triton X-100 (TBS-T) and then, incubated the appropriated dilution of secondary Amersham Pharmacia Biotech, (Cambridge, UK) horseradish peroxidase-linked antibodies (Table M8), in TBS 1% non-fat dry milk at RT for 1 h. After washing with TBS-T, blots were developed using an

enhanced chemiluminescence system, *ECL Western Blotting Detection Reagents* (Amersham Pharmacia Biotech).

Table M7. Primary antibodies list for Western Blot.

Antibody	Company	Origin	Dilution
pSmad2	Cell signalling, Beverly, MA	Polyclonal rabbit	1:1000
Smad2/3	BD Biosciences, CA	Monoclonal mouse	1:2000
pSmad3	Millipore, CA	Polyclonal rabbit	1:1000
IGF1Rβ	Cell signalling, Beverly, MA	Polyclonal rabbit	1:1000
pAKT Ser 473	Cell signalling, Beverly, MA	Polyclonal rabbit	1:1000
AKT	Cell signalling, Beverly, MA	Polyclonal rabbit	1:1000
pERK1/2	Cell signalling, Beverly, MA	Polyclonal rabbit	1:1000
ERK1/2	McKenzie and Pouyssegur, 1996)	Polyclonal rabbit	1:2000
P16	BD Biosciences, CA	Monoclonal mouse	1:1000
Cyclin A	Santa Cruz, CA	Monoclonal mouse	1:500
p21-WAF	BD Biosciences, CA	Monoclonal mouse	1:1000
E-cadherin	Cell signalling, Beverly, MA	Polyclonal rabbit	1:1000
c-Cbl clone 7G10	Upstate	Monoclonal mouse	1:1000
Caveolin	BD Biosciences, CA	Monoclonal rabbit	1:1000
Mdm2	Abcam	Monoclonal mouse	1:1000
Vinculin	Sigma Chemical, St Louis, MO	Monoclonal mouse	1:3000
Tubulin	Sigma Chemical, St Louis, MO	Monoclonal mouse	1:3000
β-actin	Sigma Chemical, St Louis, MO	Monoclonal mouse	1:3000

Table M8. Secondary antibodies list for Western Blot.

Antibody	Company	Origin	Dilution
Rabbit HRP	Amersham Biosciences	goat	1:5000
Mouse HRP	Amersham Biosciences	goat	1:2500

5.3.1 Quantification of protein expression levels from Western blot analysis.

Obtained signal from the Western Blot, relative to protein expression, was digitally quantified using the QuantityOne software.

6. RNA analysis

6.1 RNA extraction

RNA extraction from tumour and cell culture samples was done using the *RNeasy mini KIT* (Qiagen®) following instructions from the company.

6.2 Reverse transcription from RNA to cDNA

cDNA was obtained from the tumour or cell RNA after a reverse transcription reaction with *High Capacity cDNA Reverse Transcription Kit* (Applied Biosystems) following the protocol from the company. Depending from the obtained RNA concentration we used 1-2 μg of RNA per sample. Before that, RNA quality and to be sure that there was no DNA contamination a 1% agarose gel was run with 500 ng of RNA of each sample.

6.3 Quantitative real-time PCR (RT-PCR)

Real-time PCR is a PCR with the capacity to quantify the number of amplification products. There are two common methods for the detection of PCR products in real-time PCR that have been used in this work.

6.3.1 RT-PCR by LightCycler and Sybergreen method (Roche®)

One method of RT-PCR is the non-specific fluorescent dyes that intercalate with any double-stranded DNA method, which in our case is the *Sybergreen* dye (Roche Molecular Biochemicals).

As Sybergreen binds un-specifically to DNA is really important to work in stringent conditions using the corresponding negatives controls to be sure that our results are specific.

Due to our work with orthotopic tumours that are a mix of human tumour cells and mouse stromal cells, the primers that have been used are human specific from Invitrogen, designed by us and with its specificity tested (Table M9).

To perform this RT-PCR, we used the LC480 Sybergreen PCR mix (Roche®) that contains all the reactive needed for the RT-PCR except the DNA and the primers (Taq DNA polymerase, RT-PCR buffer, dNTPs, MgCl2 and Sybergreen). In a 384 well plate we add to each well 100ng cDNA, 5µl Sybergreen mix, primers at 0,5µM and distillate water until a total 10µl per well.

RT-PCR was carried out on a *LightCycler* instrument (Roche Molecular Biochemicals, Lewes, UK). After an initial incubation at 95ºC for 10 min, amplification cycles (40 for PDGFRα, PDGFRβ, ERB2, PDGF-A, PDGF-B and 50 for TGFβ1, 2 and 3) were performed with denaturation at 95ºC for 10 s, followed by annealing for 20 s (at 65ºC for PDGFRα, PDGFRβ and ERB2, 60ºC for PDGF-A, PDGF-B and TGFβ3; and 55ºC for TGFβ1 and 2) and extension at 72ºC for 13 s.

Obtained results are the amplification curves which are calculated by the CT (threshold cycle). CT is the cycle from which the fluorescence over the background is significant, and is inversely proportional to the copy number.

Results on this work are presented with the values $\mathbf{2^{(-\Delta\Delta Ct)}}$, where ΔΔCt are the parameters of CTs of each sample have been normalized for its corresponding actin, relative to the corresponding sensitive phenotype.

Table M9. Primers sequences used to specifically detect the mRNA expression of some determined genes.

GEN	Sequence
hTGFβ1	Fwd: 5'- GTCCTTGCGGAAGTCAATGT-3' Rev: 5'-AAGTGGACATCAACGGGTTC-3'
hTGFβ2	Fwd: 5'-GGGTTCTGCAAACGAAAGAC-3' Rev: 5'-TTGACGTCTCAGCAATGGAG-3'
hTGFβ3	Fwd: 5'-GCTACATTTACAAGACTTCAC-3' Rev: 5'-AAGTGGGTCCATGAACCTAA-3'
hPDGFRα	Fwd: 5'- AGTTCCTTCATCCATTCTGGACT-3' Rev: 5'- AATTGTAGTGTGCCCACCTCTC-3'
hPDGFRβ	Fwd: 5'-CATCACCGTGGTTGAGAGC-3 Rev: 5'-AATTGTAGTGTGCCCACCTCTC-3'
hPDGF-A	Fwd: 5'-TACTGAATTTCGCCGCCACA-3' Rev: 5'-CCAAAGAATCCTCACTCCCTACG-3'
hPDGF-B	Fwd: 5'-TGTGCGGAAGAAGCCAATCT-3' Rev: 5'-AATAACCCTGCCCACACACTC-3'
hErbB2	Fwd: 5'-AGGGGTCTTGATCCAGC-3' Rev: 5'-GGTTGGTGTCTATCAGTGTGA-3'
hActin	Fwd: 5'-GAGGCAGCCAGGGCTTA-3' Rev: 5'-AACTAAGGTGTGCACTTTTGTTCAACT-3'

6.3.1 RT-PCR by TaqMan® assay method (Applied Biosystems)

The other method is the sequence-specific DNA probes consisting of oligonucleotides that are labelled with a fluorescent reporter which permits detection only after hybridization of the probe with its complementary sequence, then the fluorescence in each well is depending on the among of final product. In this case is also possible to obtain background for this reason, we used controls to be sure of their correct specificity.

To perform this RT-PCR we used a 384 well clear plate, each well with a total volume of 20µl (16 µl MIX Probe and 4 µl MIX cDNA).

To prepare the Probe mix, we used the Master Mix TaqMan 2x, Probe TaqMan gene expression assays (Applied Biosystems)(Table M10) and distilled water to the final volume of 16ul. For the cDNA mix, we used 100ng of cDNA and distilled water to the final volume of 4ul.

RT-PCR was carried out on a HT7900 Real-Time PCR System (Applied Biosystems) where after an initial Stage 1 at 50º for 2 min, a Stage 2 at 95º for 10 min and the Stage 3 at 95º for 15 seconds and at 60º for 1 min with 40 amplifications cycles.

Obtained results are the amplification curves which are calculated by the CT (threshold cycle). CT is the cycle from which the fluorescence over the background is significant, and is inversely proportional to the copy number.

Results on this work are presented with the values $\mathbf{2^{(-\Delta\Delta Ct)}}$, where ΔΔCt are the parameters of CTs of each sample have been normalized for its corresponding 18S, relative to the corresponding sensitive phenotype.

Table M10. TaqMan Probes used to specifically detect the mRNA expression of some determined genes.

GENE	TaqMan Probe	GENE	TaqMan Probe	GENE	TaqMan Probe	GENE	Probe
hIGF1R	Hs00609583_m1	**hIGF2**	Hs00171254_m1	**hIGFBP3**	Hs00426289_m1	**hNOV (IGFBP9)**	Hs00159631_m1
hIGF2R	Hs00974474_m1	**hIGFBP1**	Hs01065514_m1	**hIGFBP5**	Hs00181213_m1	**18S**	Hs99999901_s1
hIGF1	Hs01547656_m1	**hIGFBP2**	Hs00167151_m1	**hIGFBP6**	Hs00942697_m1		

7. Statistical analysis

Statistical significance of differences between groups was determined using the Mann-Whitney U test or T-Test. Statistical analysis was carried out using GraphPad Prism 6 (GraphPad Software, Inc.). A Spearman correlation test was used to analyse the relationships between phosphoSmad2 and IGF1R protein levels. In all experiments, differences were considered statistically significant for values of *p < 0,05; **p < 0,01;*** p < 0,001 and it has been represented with this nomenclature.

Results

RESULTS

1 - Role of ALK1 in physiological angiogenesis.

1.1 Lack of ALK1 half dose expression induces hyper-vascularization.

In order to examine the role of ALK1 in physiological angiogenesis and aiming to elucidate possible treatments for *hereditary haemorrhagic telangiectasia* (HHT) patients, where mutations in the *ACVRL1*, *ENG*, and *SMAD4* genes are responsible for this disease, we took advantage of the retina vessel development mouse model. Considering that mouse retinal vasculature develops during the first days after birth (from P3 to P10), the characterization of how this retinal plexus develops in the absence of ALK1 offered an excellent tool to determine the effect of ALK1 loss on angiogenesis in vivo. Our model in homozygosis dies at E11.5 as a result of severe vascular abnormalities, for this reason our work is done with heterozygous pups. $ALK1^{+/-}$ pups survived in the same ratio as control littermates, and were also similar in size.

To asses this study we performed an immunostaining for the endothelial marker IsolectinB4 at different days after birth to evaluate the structure and organization of the vessels among $ALK1^{+/-}$ mice in comparison with WT mice. The analysis of different vascular parameters performed in $ALK1^{+/-}$ retinas showed that in the absence of half ALK1, retinal vascular plexus developed several vascular abnormalities.

We first focused our analysis on an early time point of vascular development. Images of P5 $ALK1^{+/-}$ retinas demonstrated that the vascular defects at this time point were not very severe. No significant alterations were detected when we analysed the migratory length of the retinal plexus towards the retinal periphery of $ALK1^{+/-}$ retinas compared to controls (radial expansion). The same way, the sprouts/100 µm analysis of the sprouting front and the quantification of the sprout length revealed no striking defects in the sprouting front morphology.

Nevertheless, there was an obvious increase in vein vessel width in ALK1$^{+/-}$ retinas and a striking significant increase on the number of branch points in both arteries and veins (Figure R1).

After this first characterization of vascular development using P5 retinas, we conclude that the lack of ALK1 leads to a defect in vascular normality. Moreover, these defects associated to ALK1 half inactivation were still arising at this time point. For this reason, we decided to delay the analysis to a later stage of vascular development.

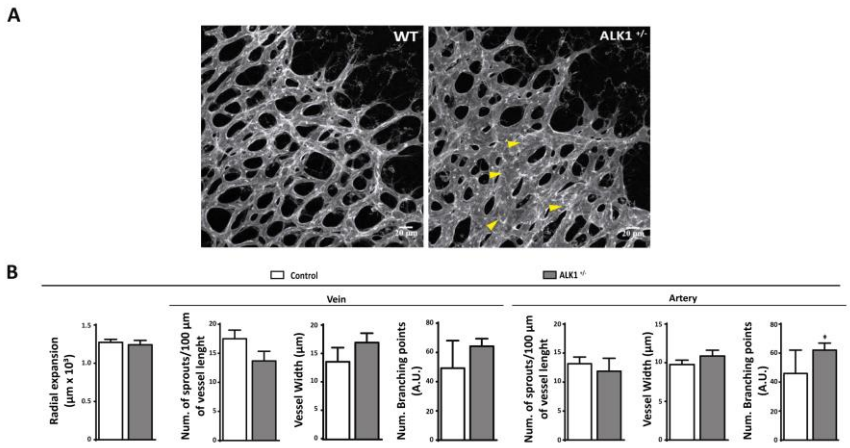

Figure R1. The analysis of P5 ALK1+/- retinas showed a mild increase in number of branch points. A) Higher magnification images of P5 retinas stained by IsolectinB4. Yellow arrowheads highlight vessels of increased calibre in ALK1 mutants. B) Statistical summary of radial expansion, number of sprouts/100 µm of vessel length, number of branch points and vessel width on arteries and veins of the respective genotypes. Control mice n=4, ALK1$^{+/-}$ n=3. Graphs represents mean values ± S.E.M. *,p< 0.05 (two-tail Mann-Whitney U test).

The analysis of P7 retinas revealed no changes in ALK1$^{+/-}$ compared to WT retinas on radial expansion or the number of sprouts/100 µm of sprouting front length. Confirming the tendency observed in P5 retinas, there was an increase in vessel width in both arteries and veins at this stage. Surprisingly, the significant difference observed in P5 retinas on branch points disappeared. We considered that this difference was not due to a loss of phenotype but a massive increase in vessel width that reduced number of branch points (Figure R2).

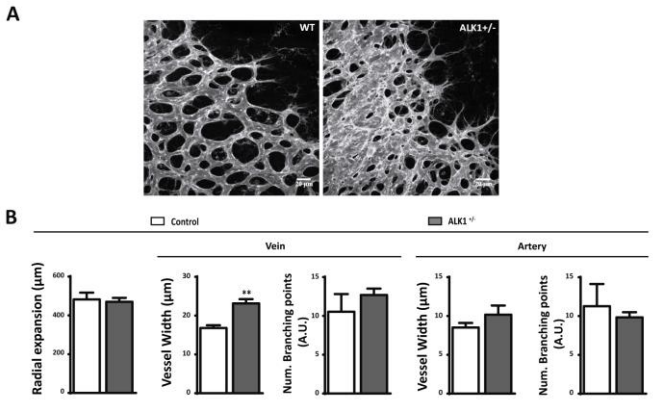

Figure R2. The analysis of P7 ALK1+/- retinas showed significant increase in vein vessel width. A) Higher magnification images of P7 retinas visualized by isolectinB4 staining. B) Statistical summary of radial expansion, vessel width and number of branch points on arteries and veins of the respective genotypes. Control mice n=10, $ALK1^{+/-}$ n=9. Graphs represents mean values ± S.E.M. **,p< 0.01 (two-tail Mann-Whitney U test).

After P5 and P7 vascular characterization we wondered what would happen at a more advanced stage, in order to determine if the effect of ALK1 was only effective at early stages or it was maintained at later stages. We decided to study the retina at P9, after the analysis we were surprised that not only the $ALK1^{+/-}$ phenotype observed at P7 was maintained but dramatically increased, and the vessel width was double in the case of P9 $ALK1^{+/-}$ retinas compared to WT ones in veins, while at this stage vessel width increase was significant in arteries as well. Furthermore, we could also confirm that no additional vascular alterations were arising aside from the ones already described at P5 and P7 (Figure R3).

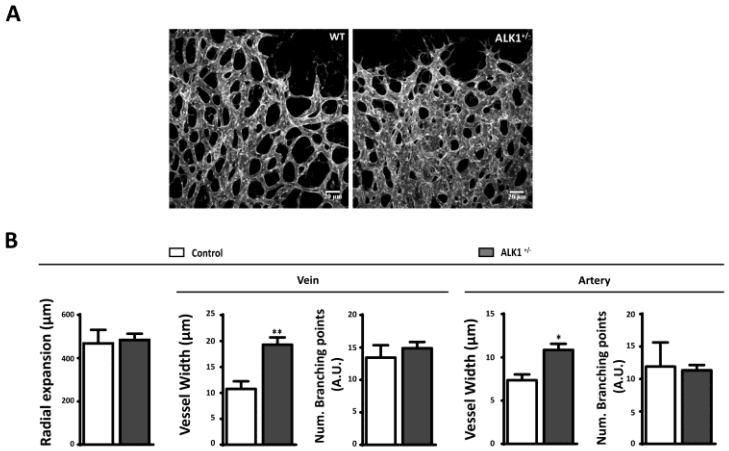

Figure R3. The analysis of P9 ALK1+/- retinas showed significant increase of vessel width in veins and arteries. A) Higher magnification images of P9 retinas visualized by isolectinB4 staining. B) Statistical summary of radial expansion, vessel width and number of branch points on arteries and veins of the respective genotypes. Control mice n=10, ALK1$^{+/-}$ n=10. Graphs represents mean values ± S.E.M. *,p< 0.05 ; **,p< 0.01 (two-tail Mann-Whitney U test).

1.1.2 Pericyte coverage is not affected in ALK1$^{+/-}$ retinas.

To assess if the effect of ALK1 loss over hyper-vascularization was due to an increase on pericyte coverage, we stained retinas at P5, P7 and P9 by Desmin, a protein express by immature and mature pericytes (Hughes and Chan-Ling, 2004). Results revealed no differences between WT and ALK1$^{+/-}$ retinas, as observed in figure R4. This experiment excluded a dysfunction in pericyte coverage able to produce this increase on vessel width. In addition, it elucidates no problems in the association between ECs and mural cells, as the co-labelling with desmin and isolectinB4 showed a tight association between both. Then, we could exclude a pericyte defect as a possible player for the vascular phenotype associated to ALK1 loss.

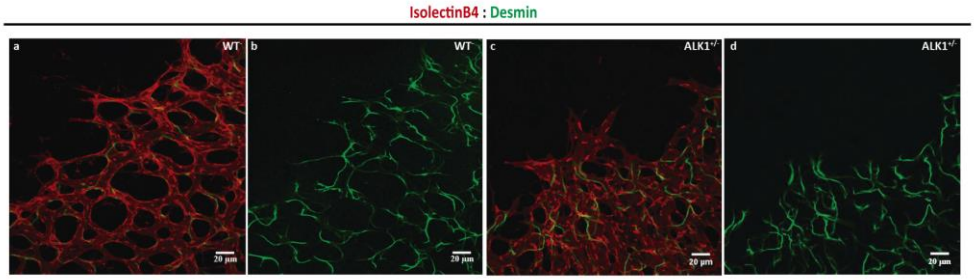

Figure R4. No alterations in perycite coverage in ALK1$^{+/-}$ retinas. Representative images of P7 control and ALK1$^{+/-}$ retinas stained with the pericyte marker desmin (green) and isolectin B4 (red).

1.1.3 Lack of ALK1 produces an increase in proliferating cells just in the second line of the vascular front.

Considering that there are no alterations in pericyte coverage, we wondered if there were changes in the number of ECs. As the analysis of ALK1$^{+/-}$ retinas had revealed stronger vascular defects at the sprouting front region, which is composed by ECs newly specified into tip and stalk phenotypes. We selected two different zones of the sprouting front: the first line with tip cells and the inmediate following stalk cells, and the second line, corresponding to only stalk cells.

First of all we quantified the number of EC by the Erg1,2,3 staining, an endothelial nuclei marker in both regions. The analysis on P7 retinas showed that in the first line of the sprouting front ALK1$^{+/-}$ mice had no changes in EC number whereas the second line ALK1$^{+/-}$ retinas showed an increased number of ECs compared to WT ones (Figure R5B). These results suggest that the increased vessel was due to a higher number of ECs. Therefore, we considered if the increase of EC was caused by an increase of EC proliferation.

To address whether the enhanced vascular density observed in ALK1$^{+/-}$ retinas were consequences of increased proliferation, we quantified the number of proliferative ECs in the growing retinas.

For this, we injected the proliferation marker EdU for 2h into P7 mice and determined EdU positive ECs after co-labelling with the endothelial nuclei marker Erg1,2,3 and isolectinB4.

The proliferation analysis revealed no defect in the first line of the sprouting front. Interestingly, at the second line of the sprouting front a significant increase in the number of proliferating ECs was observed, while the number of proliferative ECs in the rest of retina was not affected in ALK1$^{+/-}$ retinas compared to control littermates. We therefore concluded that the increased vascularization observed in ALK1$^{+/-}$ retinas was at least as a consequence of enhanced proliferation of ECs at the sprouting front, particularly at the second line (Figure R5C).

Altogether, our results suggest that while tip cell numbers (nº of sprouts) were found to be unaltered, stalk cell positions appeared to be the most affected by ALK1 half loss, as the second line lost its control on proliferation and as a result and increase on EC number and vessel width.

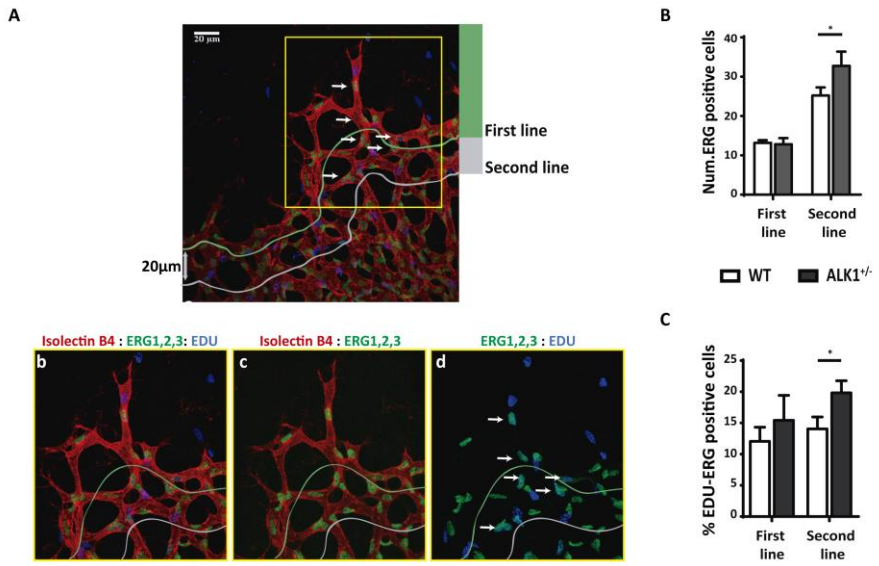

Figure R5. Endothelial cells at the second line of the sprouting front of the growing retinal vascular plexus present an increase on number of EC and an increase in proliferating EC in ALK1+/- retinas. A) (a) Representative image of P7 wild type retina immunostained with Erg1,2,3 (green), isolectinB4 (red) and EDU (blue). Green line is the limit for the first line analysis. Second line analysis corresponds to the zone between green and grey line that is always 20 µm. Yellow cub showed the region of the more amplified image (. Bar 20 µm. (b-d) Amplified images where b) have the three staining, c) only stained by IsoB4 and ERG1,2,3 and d) only stained by ERG1,2,3 and EDU, white arrows pointing out some ERG-EDU positive cells. B) Quantification of number of ECs in first and second line; Wild type mice n=6 and ALK1$^{+/-}$ mice n=4; C) Quantification of number of EDU /ERG positive cells in first and second line; Wild type mice n=5 and ALK1$^{+/-}$ mice n=4; Graphs represent mean values ± S.E.M of corresponding experiments. *,p< 0.05 (two-tail Mann-Whitney U test).

1.2 Pi3K inhibition restored ALK1$^{+/-}$ induced proliferation and hyper-vascularization.

The previous presented experiments showed a hyper-vascularization phenotype and an increase in the proliferation machinery in the sprouting front of mice lacking ALK1. These results were quite similar to the phenotype observed on PTEN$^{-/-}$ mice, where PTEN$^{-/-}$ retinas results in a hyper-vascularized phenotype and stalk pre-tip cells have increased proliferation.

Additionally, inhibition of PI3K signalling into PTEN$^{-/-}$ retinas abolished the increased angiogenesis observed in these mutants (Serra et al., 2015).

At that moment, we wondered what would happen to ALK1$^{+/-}$ phenotype upon inactivation of PI3K signalling pathway. With this purpose, we decided to genetically cross both pathways and see what happens to the ALK1$^{+/-}$ phenotype. For this study, we crossed our mice model ALK1$^{+/-}$ with the kinase-dead mice p110α^{D933A} knock-in (KI) allele from Dr. M. Graupera´s group (Foukas et al., 2006).

p110αKI/ ALK1$^{+/-}$ pups survived in the same ratio as control littermates. To evaluate if the lack on PI3K signalling had some effects over ALK1$^{+/-}$ phenotype we decided to stain retinas at p7 with isolectinB4 and analyse the vascular development in all four genotypes.

First of all, we checked radial expansion as p110αKI had reduced migratory length of the vascular plexus. As expected, ALK1$^{+/-}$ and WT retinas had the same radial expansion, whereas p110αKI reduced its migratory length of the vascular plexus (Figure R6). When we analysed radial expansion of p110αKI/ALK1$^{+/-}$ retinas we observed no changes on migratory length compared to p110αKI. These results revealed that p110αKI defect is still present after this new breeding and that there was no effect from ALK1$^{+/-}$ over PI3K signalling.

Next, we focused our study on vessel width being the most significant changes on ALK1$^{+/-}$ vascular development. Our results showed no increase in vessel width of P110αKi pups; on the contrary ALK1$^{+/-}$ retinas had a significant increase confirming our previous results. Interestingly, p110αKI/ ALK1$^{+/-}$ retinas completely restored its vascular phenotype and the vessel width was the same than in the case of WT or p110αKI pups (Figure R6). These results suggest that ALK1 controls proliferation at the sprouting front of the vascular development by affecting PI3K signalling.

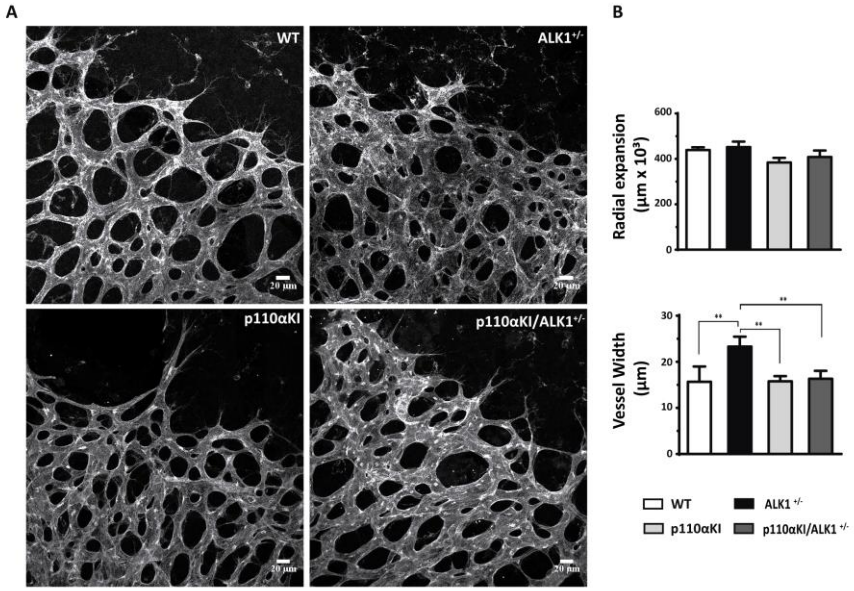

Figure R6. Genetically lack of PI3K activity normalized ALK1 phenotype in the retina mouse model. A) Images at high magnification of P7 retinas visualized by isolectinB4 staining. B) Statistical summary of radial expansion and vessel width in veins of the respective genotypes; 2 WT, 4 ALK1$^{+/-}$, 2 p110αKI and 3 p110αKI/ ALK1$^{+/-}$ mice. Mean represented ± SEM. **,p< 0.01 (two-tail Mann-Whitney U test).

At this point, taking into account all patients with HHT with need of treatment and our previously striking observations where ALK1 phenotype was restored in animals lacking PI3K activity, we decided to carry out pharmacological inhibition of PI3K signalling pathway on ALK1$^{+/-}$ or WT mice. To achieve this inhibition, we I.P. injected LY294002 or not (DMSO) to our C57BL6 model at P6 and P7. Afterwards, IsolectinB4 staining was performed as described before and P7 retinas previously injected with PI3K inhibitor or absence (DMSO) were analysed. Interestingly, injected WT retinas with the PI3K inhibitor reduced vessel width compared to control ones. Moreover, our injected ALK1$^{+/-}$ mice with the PI3K inhibitor significantly reduced vessel width to WT levels (Figure R7). Confirming our previous hypothesis and elucidating a possible therapy for HHT patient.

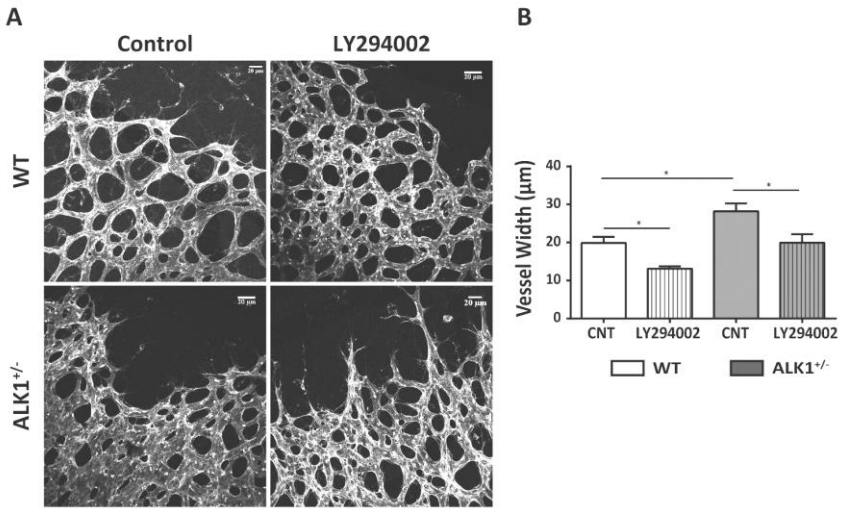

Figure R7. Pharmacologically inhibition of PI3K signalling pathway on P7 ALK1+/- retinas normalized vessel width. A) Higher magnification images of P7 retinas by isolectinB4 staining. B) Quantification of vessel width on veins of mice LY294002-treated or not (DMSO) with 5 WT mice (3 control and 2 LY294002-treated mice) and 7 ALK1$^{+/-}$ mice (3 control and 4 LY294002-treated mice). Mean represented ± S.E.M. *,p< 0.05 (two-tail Mann-Whitney U test).

2. Role of TGF-β signalling pathway in ovarian cancer

2.1 Characterisation of TGFβ signalling pathway in ovarian tumours.

It has been broadly reported that the TGFβ signalling pathway contributes to processes that involve cancer progression and dissemination, such as EMT transition, angiogenesis, extracellular matrix remodelling, migration and invasion. In addition, ALK1 and ALK5 receptors have been described to play an important role in controlling cancer development (Massague and Gomis, 2006; Massague, 2008; Ikushima and Miyazono, ; Cunha and Pietras).

2.1.1 Evaluation of ALK1 receptor in ovarian tumours.

To determine if ALK1 is important in ovarian cancer and a possible good candidate for target therapy we performed an analysis of the presence of ALK1 in human tumour samples with the collaboration of Dr. Agnès Figueras. For this analysis, we performed an immunostaining in OCT as the antibody did not work on IHC. In addition, we could co-label ALK1 and CD31, an endothelial marker, in human normal ovary or ovarian tumour samples at the same time. Our results showed no significant difference in ALK1 protein levels co-stained with CD31 between controls and tumour samples (Figure R8). Moreover, in a free survival analysis by months we observed no significant correlation with ALK1 protein levels. In addition, it showed only a mild decrease in tumour compared to normal samples (Figure R8). For this reason we abandoned ALK1 as possible target therapy for ovarian cancer and switched our ovarian cancer studies to other members of TGFβ signalling pathway.

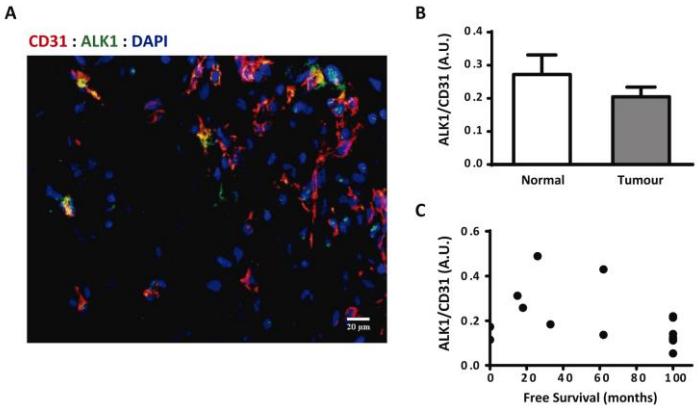

Figure R8. No differences on ALK1 protein levels comparing human tumour or normal human ovarian tissue. A) Representative's image of human ovarian tumour stained with DAPI (blue), the endothelial marker CD31 (red) and ALK1 (green). B) Quantification of the co-labelling CD31/ALK1 present in ovarian human tumour or normal tissue. Results are expressed as the mean and SEM± of 16 tumour samples and 9 control samples. C) Quantification of free survival (months) vs levels of ALK1 in 15 human tumour samples.

2.1.2 Evaluation of TGFβ signalling pathway activation in human ovarian cancer.

Subsequently, we wondered if ALK5 was present in the ovaries and if so, how active. When we analysed by immunofluorescence (IF) the presence of ALK5 (green) on ovarian tumour samples, we observed high levels of ALK5 expression (Figure R9).

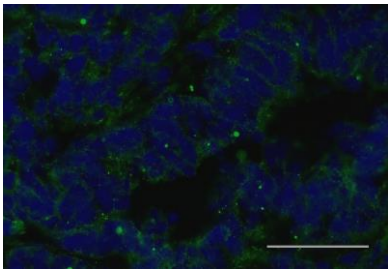

Figure R9. ALK5 receptor is present the ovarian cancer samples. Representative's amplified image of positive ALK5 staining (green) and DAPI (blue) of an endometrioid tumour ovarian sample by IF. (bar 50 µm).

Next, we detected, by immunohistochemistry (IHC), the active Smad2 (phosphoSmad2) protein levels, instead of total protein levels; as phosphoSmad2 is used as read-out of TGFβ activation from the ALK5 receptor.

First of all, we stained phosphoSmad2 in normal human ovary with the aim of having an idea of how important and active this pathway is in normal ovarian physiology. In the literature it is said that TGFβ also plays a positive role for granulose cell proliferation during normal ovarian physiology (Richards and Pangas, ; Li et al., 2008).We detected high activation levels of this protein in the normal epithelium that limits this tissue compared with parenquimal cells. As expected, phosphoSmad2 staining is nuclear, confirming the activation of the pathway (Figure R10). TGFβ signalling was highly active in normal ovary, so we were wondering if this activation was maintained in different human ovarian cancer samples, as TGFβ signalling pathway is a well-known altered pathway in cancer.

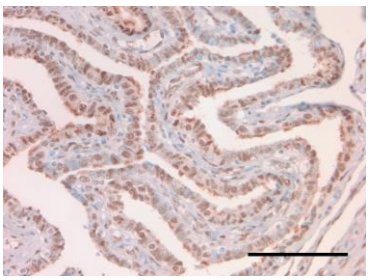

Figure R10. TGFβ signalling pathway is highly active in normal epithelium of the gynaecological tissue. Representative image of phosphoSmad2 positive IHC staining of normal human fallopian tube (400X, bar 100 µm).

To start our analysis, we used a *Tissue Macro Array (TMA*) containing samples from 66 women who were diagnosed as a high-grade serous (n = 32) or endometrioid (n = 34) epithelial ovarian carcinomas thanks to Dr. August Vidal of the Pathology Service of Hospital Universitari de Bellvitge, Barcelona. As shown in figure R11A, the main part of the tumours was stained for pSmad2 at high levels, all of them presenting nuclear localization as expected for active Smad2. No differences in pSmad2 expression levels were found when comparing serous with endometrioid tumour types indicating that TGFβ signalling pathway plays an important role on ovarian cancer progression independently of tumour cell type (Figure R11B).

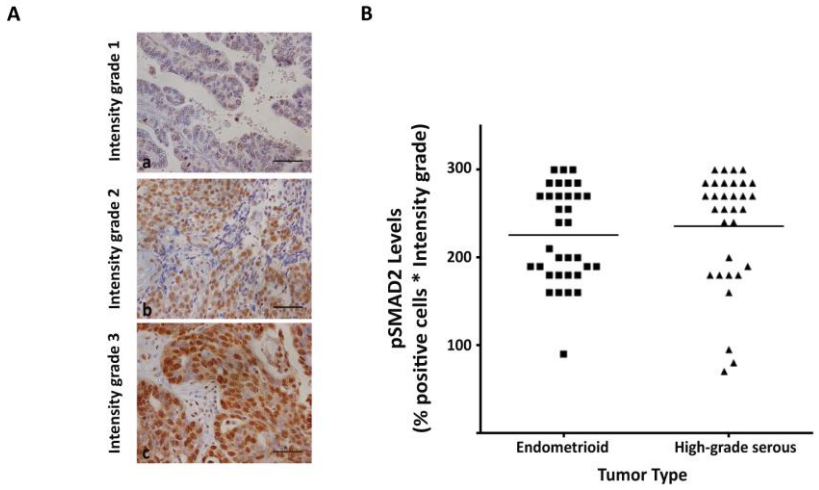

Figure R11. TGFβ signalling pathway is maintained highly active in human ovarian cancer cells independently of ovarian tumour type. A) Three representative's examples of positive phosphoSmad2 with intensity (a) low (grade 1), (b) moderate (grade 2) and (c) high (grade 3) in ovarian cancer patients samples. 400X, bar 100 µm. B) Quantification of phosphoSmad2 levels (using the multiplicative index of the intensity of the stain and the labelling frequency) in tumour tissue sections from high-grade serous or endometrioid tumour patients. Data analysed from 66 tumour patients from a TMA.

2.1.2.1 TGF-β maintains the activation in our orthotopic mouse models.

To study the role of TGFβ signalling pathway in ovarian cancer progression in both tumour subtypes in depth, we used orthotopic pre-clinical models of this tumour. They were previously generated after implantation in nude mice of tumour samples obtained from patients after surgery by Dr. Alberto Villanueva with the collaboration of the Pathology Service of Hospital Universitari de Bellvitge. Two of them were high-grade serous ovarian tumours (OVA8 and OVA17) and OVA15, an endometrioid ovarian tumour model. Particularly, the OVA17 mouse model also disseminates and metastasises to liver and lung, and then this particularity allows us to study the dissemination (Vidal et al., 2012; Vives et al., 2013). We confirmed the results of high pSmad2 levels in normal epithelial cells from human samples in those of normal mouse ovary and endometrium (Figure R12A).

To begin we compared the primary tumour and its related orthotopic mouse model to be sure that these models closely resemble the characteristics of the human patients. We observed maintenance of the histological properties, as it is shown at histological level by Haematoxylin-Eosin staining (H&E) in figure R12B. In addition, we confirmed that all three orthotopic mouse models presented high nuclear phosphoSmad2 staining, very similar to the expression pattern found in primary tumours (Figure R12B). On top of that, when we quantified phosphoSmad2 levels in our orthotopic mouse models and extrapolated into the values obtained in the *TMA* we observed that the values of OVA15 correspond to the average of the endometrioid samples (the expression levels in the TMA is 225 while OVA15 is 200) and OVA8 and OVA17 agree with the average of high-grade serous samples (the expression levels in the TMA is 235 while in OVA17 and OVA8 is 300).

After these results, we were convinced that these models were appropriate and suitable to study the role of TGFβ in ovarian cancer.

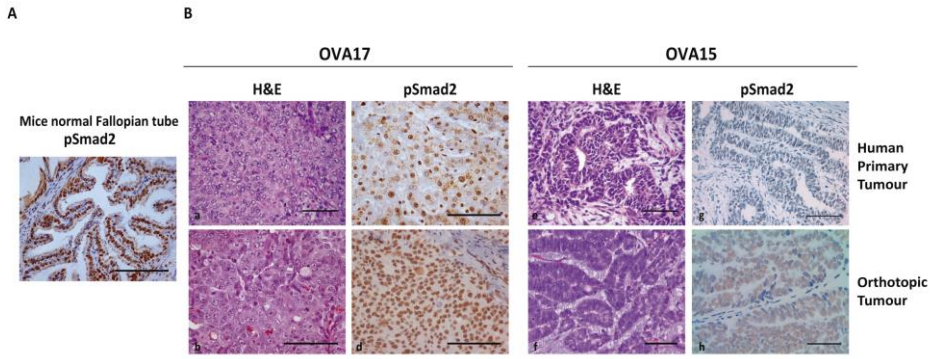

Figure R12. Orthotopic tumours maintained the same expression of TGFβ signalling pathway as in its human primary tumour. A) Representative's image of a mice normal fallopian tube stained by pSmad2. 400x, bar 100 µm. B) Representative's images of the original human tumour biopsy (a, c, e and g) and its correlated orthotopic mouse model OVA17 (b, d) and OVA15 (f, h) with the staining by H&E (a, b, e, f) and pSmad2 (c, d, g and h). a-g 400x, h 630x; bar 100 µm.

2.1.2.2 Tumour cells produce TGF-β ligands by its self as well as human normal ovarian

When we knew for sure that TGFβ signalling pathway was highly active in our orthotopics mouse models as well as primary tumours, we wondered which player could activate this pathway. To answer this question, we decided to perform mRNA analysis with the technique *Real Time polymerase chain reaction* (RT-PCR) designing human specific primers in our *in vivo* tumour samples. Normalizing later its expression with the one obtained in 4 normal human ovaries, as control of no tumour expression.

Our RT-PCR analysis indicated that human TGFβ2 was the main expressed ligand in all tumoral models, Although, human TGFβ3 was highly present in OVA15 compared to the other two (Figure R13). Nevertheless, these results indicated a predominant role for TGFβ2 stimulating the canonical TGFβ pathway in ovarian tumours, as it happens in gliomas (Rodon et al., 2014).

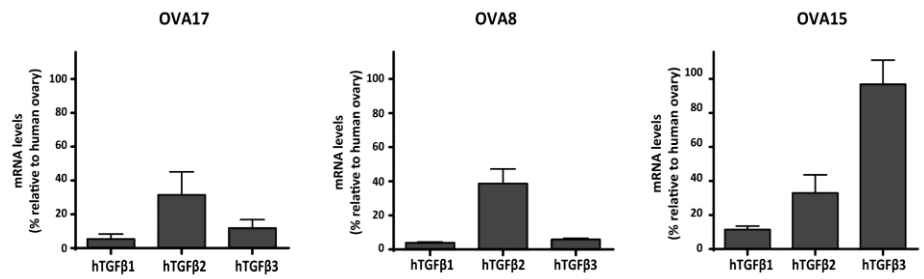

Figure R13. Ovarian orthotopic mouse models predominantly express TGFβ2. mRNA levels of human TGFβ1, 2 and 3 analysed by quantitative real-time PCR in OVA17 (3 samples), OVA8 (3 samples) and OVA15 (3 samples) orthotopic ovarian tumours. Results are expressed as the mean and SEM± of mRNA expression relative to mRNA expression levels in 3 human normal ovary samples.

2.2 Target therapy against TGFβ signalling pathway.

Having seen our previous results where TGFβ signalling through activation of pSmad2 was so active in tumour cells, we had decided to focus the target therapy on blocking TGFβ signalling pathway, and testing its blockage on our three mouse models.

2.2.1 Evaluation of the *in vivo* effect of blocking TGFβ signalling in three orthotopic mouse models.

In order to affect the activity of TGFβ signalling pathway, it was decided to use the serine/threonine kinase receptor I and II inhibitor from *Lilly and Co*, called **LY2109761** on growth of orthotopic ovarian tumours. Fragments macroscopically homogenous of OVA15, OVA17 and OVA8 were implanted to achieve this study.

First of all we evaluated the effect of TGFβRII inhibitor on the growing of the endometrioid OVA15 tumour. To this objective, we implanted the OVA15 tumour to 10 athymic mice. Mice bearing these tumours after 6 weeks of the implantation were randomized into two groups and treated twice daily by gavage with an oral dose of 100 mg/kg LY2109761 or the vehicle LY solution for one month. After 1 month of treatment tumour volume was measured and the analysis showed that LY2109761 produce a 55% decrease in tumour size, not reaching significance due to dispersion in control group (Figure R14).

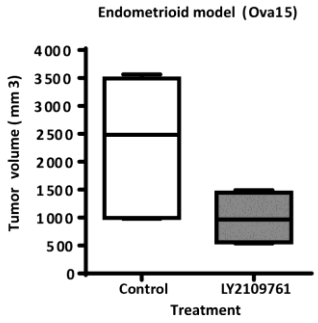

Figure R14. Blocking TGFβR activity inhibits tumour growth in the endometrioid OVA15 orthotopic mouse model. OVA15 was implanted into athymic mice; five animals were treated with LY2109761 100 mg/Kg and five with vehicle solution. Both administrations were given by gavage twice daily for one month. Final tumour volumes are illustrated by a boxplot. Median per group are 991,5 mm3 for LY and 2291 mm3 for control group.

Secondly, we decided to perform the *in vivo* experiment with the high-grade serous OVA8 animal model. Tumours were implanted to 12 mice and let grow for 5 weeks, then mice were randomized into two groups and treated the same way as OVA15 *in vivo* experiment for one month. As presented in figure R15, treatment with the inhibitor achieved a significant 46% decrease of tumour growth.

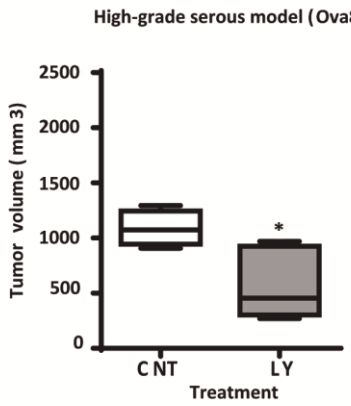

Figure R15. LY2109761 significantly inhibits tumour growth in high-grade serous OVA8 xenograft mouse model. OVA8 was implanted into athymic mice; six animals were treated with LY2109761 100 mg/Kg and six with vehicle solution. Both administrations were given by gavage twice daily for one month. Final tumour volumes are illustrated by a boxplot. Median of treated and control group correspond to 583,4 mm3 and 1088 mm3 respectively. *, $p < 0.05$ (two-tail Mann-Whitney U test).

Finally, we implanted OVA17 high-grade serous tumour into 18 mice and waited five weeks for the tumour to grow. Mice were randomized into two groups as the *in vivo* experiments above and treated for one month with the same schedule as the other two. At the end of the experiment, tumour volume was analysed and the results demonstrated a significant 60% reduction in the treated group compared to the control one (Figure R16).

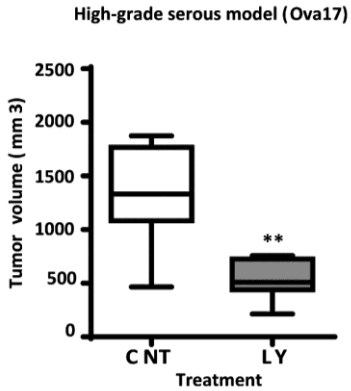

Figure R16. Inhibition of TGFβ signalling pathway significantly reduces 60% tumour volume. Ova17 was implanted into athymic mice; nine animals were treated with LY2109761 100 mg/Kg and nine with vehicle solution with the administration by gavage twice daily for one month in both groups. Final tumour volumes are illustrated by a boxplot. Median of treated is 537 mm3 and control group correspond to 1337 mm3. **,$p< 0.01$ (two-tail Mann-Whitney U test).

To confirm whether the treatment with the TGFβRII inhibitor blocked TGFβ signalling pathway, we performed Western Blot analysis to detect phosphoSmad2 protein levels. As demonstrated in figure R17; OVA15, OVA8 and OVA17 decreased phosphoSmad2 protein levels when treated with LY2109761. At this point we could conclude that the LY2109761 was effectively inhibiting TGFβ signalling pathway *in vivo* in the three orthotopic mouse models.

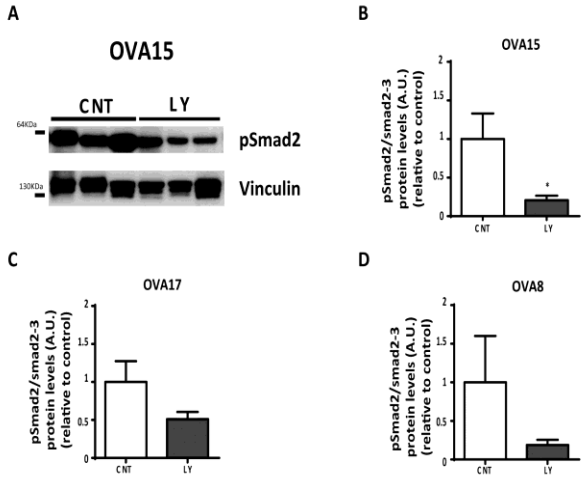

Figure R17. Blocking TGFβR activity inhibits Smad2 phosphorylation in the three xenograft orthotopic mouse models of epithelial ovarian tumours. Expression of pSmad2 and tubulin were analysed by western blot in LY2109761-treated and control tumours. A) A representative blot showing results obtained for 3 independent control tumours and 3 independent LY2109761-treated tumours from OVA15 in vivo mouse model is shown. Densitometric quantifications of phosphoSmad2 by its total smad2/3 expression relative to tubulin of B) OVA15, C) OVA17 and D) OVA8 are shown. Results are the mean ± SEM of 5 control tumours and 5 Ly2109761-treated tumours, and are represented as arbitrary units relative to the control group. *, $p < 0.05$ (two-tail Mann-Whitney U test).

As we mentioned before, OVA17 tumour has the capacity to disseminate and metastasise to lung and liver. When we checked each mouse for macroscopic nodules into the peritoneal cavity or liver, we did not observe any significant difference in number, neither in the size of these nodules between groups. Interestingly by the time of this study we did not find macroscopically nodule in the lung in any of both groups, although we could not discard microscopic dissemination (Figure R18). So the effect of LY2109761 was exclusive controlling tumour cell growth and had no effect on the capacity of the tumour to mobilise or disseminate.

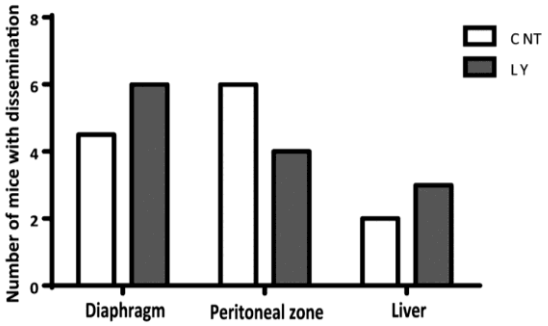

Figure R18. Inhibition of TGFβ signalling pathway had no effect on the capacity of the tumour to disseminate to other organs. Ova17 was implanted into athymic mice; nine animals were treated with LY2109761 and nine with vehicle solution as a control group. Graph represents the number of mice with nodules of dissemination for each group in different zones and organs.

In order to study the effects on dissemination and to confirm our previous results where we did not observe any effect of the TGFβ inhibitor, we took advantage of a tumour ovarian cell line previously modified by Dr. Agnès Figueras. This cell line was infected with a lentivirus expressing GFP-Luciferase (SKOV3-GFP). So that, injecting it into the mice permits us to follow its movement inside the mouse by bioimaging with *IVIS Imaging System (Caliper LifeSciences)*.

To asses this experiment, we first treated SKOV3-GFP cells with 2μM LY2109761 or absence (DMSO) for three days. Afterwards, 1 million cells where I.P injected to each mice, to a total of 6 mice per group. At 24 and 72 hours post-injection, mice were injected I.P with 3 mg luciferin and images were obtained by *IVIS* as explained in material and methods. From this experiment we could conclude that there was no effect of LY2109761 avoiding the attachment of SKOV3-GFP cell line but neither on dissemination through the body of the mice as the same result was obtained in both groups (Figure R19).

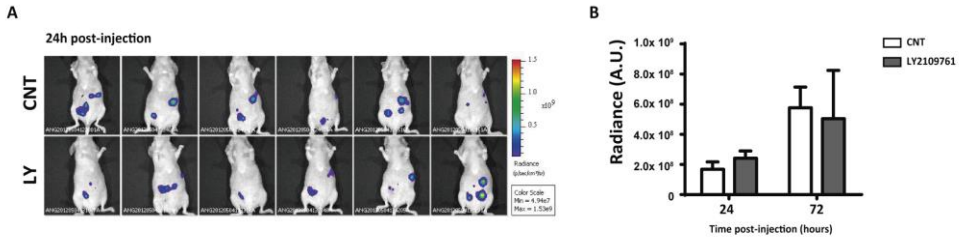

Figure R19. Inhibition of TGFβ signalling pathway has no effect on the capacity of tumour cells to attach or disseminate. SKOV3-GFP cell line were pre-treated 72h with LY2109761 (2 μM) or absence (DMSO), then injected I.P 1x106 cells to each mouse, six mice per group and the intensity and localization of luciferase positive cells was analysed by bioimaging with *IVIS Imaging System (Caliper LifeSciences)* at 24 and 72 hours. A) Image of Luci cells detected by IVIs at 24 hours. B) Quantification the radiance obtained per each mouse at 24 and 72 hours. Results are the mean ± SEM of 6 control tumours and 6 LY2109761-treated tumours, and are represented as arbitrary units.

Consequently our findings confirm our hypothesis that inhibiting TGFβ signalling pathway would affect tumour growth. We have demonstrated tumour size reduction in three different xenograft orthotopic mouse models of epithelial ovarian tumours, of which two were shown to be significant. However, no effect was observed on dissemination or metastasis. To elucidate how this inhibition works we analysed tumour samples from the in vivo OVA17 experiment in depth, as it showed the most significant reduction.

2.2.2 OVA17 tumour samples molecular analysis.

Seeking the mechanism by which LY2109761 reduced tumour size and given that the TGFβ pathway has also been implicated in regulation of cancer stem cells (CSCs)(Sakaki-Yumoto et al., 2012), we investigated whether LY2109761 treatment could affect CSC populations in our ovarian cancer model. To this end, OVA17 tumours were mechanically disaggregated and then digested with dispase and collagenase IV as described in materials and methods. Afterwards, human tumour cells were stained with CD44+ and CD133+ antibodies and analysed by flow cytometry.

Both antigens are expressed on the cell-surface and described as expressed by ovarian cancer stem cells, (Zhang et al., 2008; Conic et al., 2011). Moreover, we used the specific epithelial marker EpCAM$^+$ to discriminate between human tumour cells and mice stroma cells. Our results did not reveal any difference between groups in this cell types (Figure R20) ruling out an effect of LY2109761 on this population.

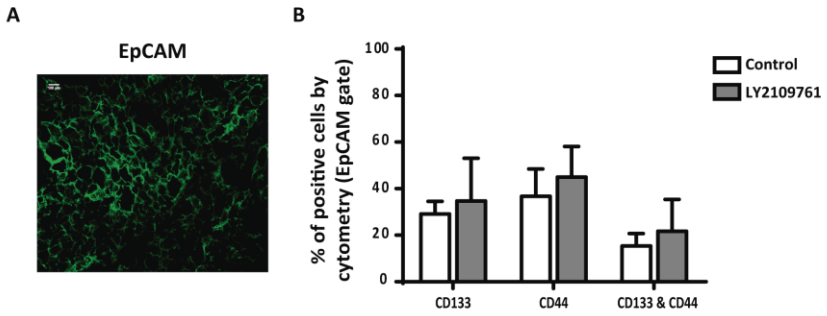

Figure R20. LY2109671 treatment had no effect on Cancer Stem Cell population. A) A representative image of EpCAM staining (green) on OVA17 tumour sample. 400x; bar 50 µm. B) OVA17 control and treated tumours were mechanically disaggregated by surgical knife, and then digested with collagenase IV and dispase for 30 min at 37ºC. Cells were stained with CD133, CD44 and EpCAM antibodies and analysed by flow cytometry. Graph represents the % of positive cells for CD133$^+$, CD44$^+$, and the double positive stained CD133$^+$ and CD44$^+$. All these numbers of cells were restricted to EpCAM$^+$ gate, for an ensured detection of only tumour cells.

Dismissing changes in CSCs and in order to determine in further detail the effect of LY2109761 on tumour biology we wanted to study the angiogenesis, as one of the oncogenic roles of TGFβ is the pro-angiogenic function (Derynck et al., 2001). With the objective to analyse the tumour vasculature we stained for CD31, in paraffin embedded tumour OVA17 samples of both groups. When we quantified the samples we did not observe any changes between groups in vessel number, indicating this was not the reason for tumour reduction (Figure R21C). Afterwards, we were wondering if the treatment was effective due to an increase on tumour cell death. TUNEL assay was used to detect apoptosis in paraffin embedded tumour OVA17 samples. In addition, the necrotic area was quantified using the H&E staining images obtained from OVA17 tumour samples. Neither

apoptosis nor necrosis had any significant change between treated and control tumour samples (Figure R21).

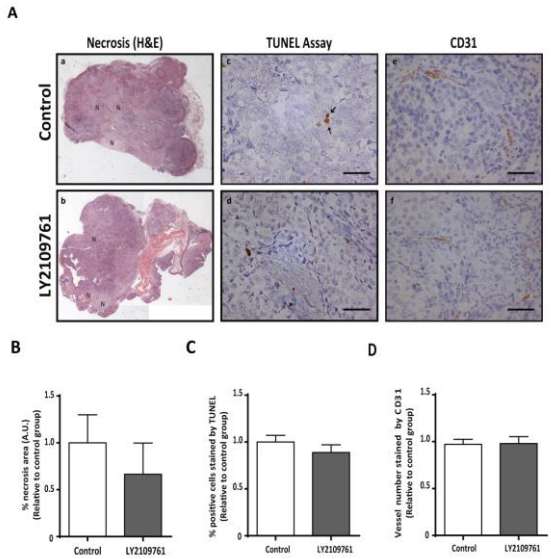

Figure R21. Blockage of TGFβ signalling pathway decreased tumour size but not through increase on cell death or angiogenesis on high-grade serous OVA17 orthotopic mouse model. A) Representative images for H&E (a,b), TUNEL assay (c,d) and CD31 (e,f) IHC staining on embedded paraffin OVA17 control and TGFβ inhibitor-treated samples. B) Quantification of % of necrosis area normalized by tumour size from H&E staining in tumour tissue sections from OVA17 control or LY2109761-treated samples. Data analysed from 4 controls and 5 treated samples. C) Quantification of the % of positive cells stained by TUNEL assay from 6 controls and 5 treated samples, with six images from a viable tumour zone for each sample of high-grade serous ova17 *in vivo* experiment. D) Quantification of number of vessels stained by CD31 from four controls and eight treated OVA17 samples. Mean represented ± SEM.

The next step was to answer if the mechanism by which LY2109761 reduced tumour growth was through affecting cell proliferation while angiogenesis and cell death were not affected. With this purpose we performed Ki67 staining by IHC, a marker of cell proliferation, in paraffin embedded control and LY2109761 treated OVA17 samples. Nucleus positivity by Ki67 staining significantly decreased 20% in treated tumours compared to control samples, indicating that the LY2109761 had an effect inhibiting tumour cell proliferation thereby causing a decrease in tumour size (Figure R22).

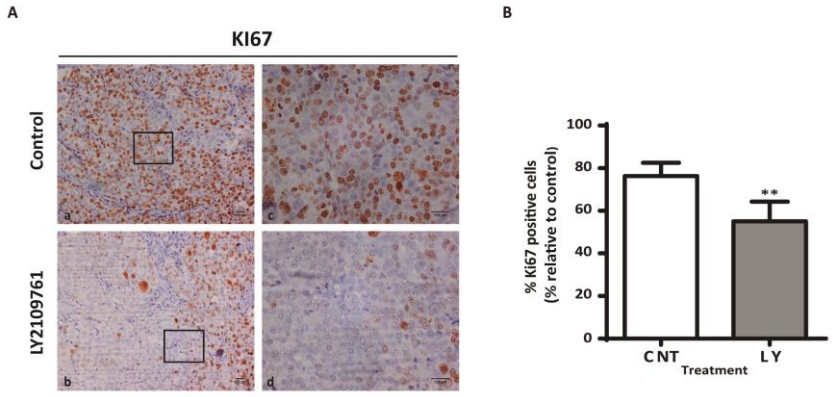

Figure R22. Blockage of TGFβ signalling decrease 20% tumour cells proliferation rate in high-grade serous OVA17 orthotopic mouse model. A) Representative's images at smaller and higher amplification of Ki67 staining by IHC on embedded paraffin OVA17 control and LY2109761 treated samples (a, b: 200X 100 µm bar; c,d: 400X 100 µm Bar). B) Quantification of the % positive cells stained with Ki67 on four controls and eight LY-treated tumour tissue sections from OVA17 samples, with eight images of viable tumour zone for each sample independently. Mean represented ± SEM. **,p< 0.01 (two-tail Mann-Whitney U test).

2.2.3 Evaluation of the mechanism to decrease cell proliferation by TGFβRII inhibition in OVA17 orthotopic mouse model.

We next sought to elucidate the mechanism by which proliferation rate had been reduced after treatment with LY2109761. To asses this characterization we performed a protein level analysis by western blot of different signalling pathways and proteins implicated in control of cell cycle in OVA17 tumour lysates. Firstly, we checked proteins directly implicated in cell cycle progression. We did not observe any changes in p21 or Cyclin A, however, a significant increase of p16, a tumour suppressor gene, protein levels was detected (Figure R23A). In contrast, Cyclin D1 levels (measured by IHC) were decreased 60 % in tumours treated with LY2109761 (Figure R22B).

Interestingly, protein levels of E-Cadherin were upregulated after one month of treatment with LY2109761 (Figure R23A). E-Cadherin is a protein expressed in epithelial cells and downregulated in the EMT process, this up regulation suggests that the inhibitor was in fact blocking TGFβ signalling and as a result avoiding the EMT process in our tumour animal models. In

addition, an up regulation of Estrogen Receptor (ER) was observed in treated samples compared to control samples, telling that tumour cells were stressed by the presence of this drug and probably as a response this receptor was increased (Figure R23C).

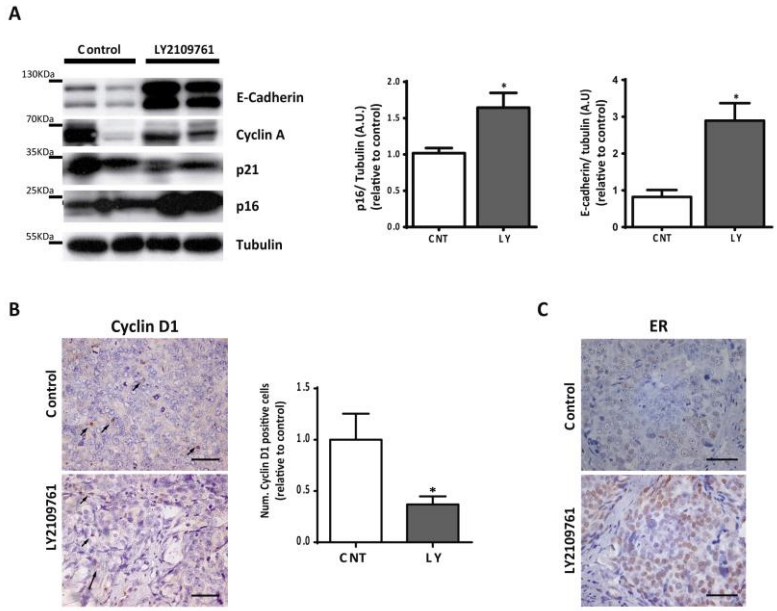

Figure R23. Treatment with LY2109761 significantly decreased Cyclin D1 but increase E-Cadherin, p16 and ER. A) Expression of E-cadherin, Cyclin A, p21, p16 and tubulin as loading control, were analysed by *Western Blot* in LY2109761-treated and control tumours from OVA17 *in vivo* experiment. A representative blot showing results obtained for 2 independent control tumours and 2 independent LY2109761-treated tumours is shown. Densitometric quantifications of 5 control and 5 LY2109761-treated tumours represented as arbitrary units (A.U.) relative to the control group for p16 and E-Cadherin are shown. B) Representative's images of cyclin D1 staining at (a) control and (b) LY-treated samples (400X, Bar 50 µm). Quantification of the percentage of tumour cyclin D1 positive cells expressed relative to control group, from 3 controls and 5 treated samples, with six images from a viable tumour zone from embedded paraffin OVA17 sections stained for cyclin D1. C) Representative's images of control and treated samples from the IHC of ER (400X, Bar 50 µm). Results are the mean + SEM. *, $p < 0.05$ (two-tail Mann-Whitney U test or T-test).

Moreover, we studied active and total levels of AKT and ERK1/2 MAPK. We did not detect any change in active or total AKT levels comparing samples from control and LY2109761-treated OVA17 tumours.

In contrast, active ERK1/2 levels were decreased by 30% with LY2109761 treatment. (Figure R24).

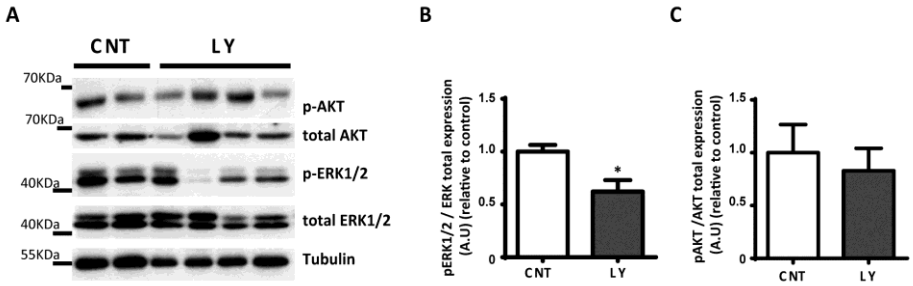

Figure R24. Treatment with the inhibitor decreased pERK1/2 protein expression whereas there were no changes in pAKT protein levels. A) Expression of total and activated form of AKT and ERK1/2 and tubulin as a loading control, were analysed by *Western Blot* in LY2109761-treated and control tumours. A representative blot showing results obtained for 2 independent control tumours and 4 independent LY2109761-treated tumours is shown. Densitometric quantifications of 4 tumour samples per group represented as arbitrary units (A.U.) relative to the control group for pERK1/2 are shown. Results are the mean + SEM. *, $p < 0.05$ (Two-tail T-test).

As the TGFβ signalling pathway by itself is not a classical stimulator of cell proliferation and does not activate the ERK1/2 - cyclin D1 axis, we hypothesized that this effect could be mediated by a different factor regulated by TGFβ. Equivalent mechanisms have already been described, for example in gliomas, in which inhibition of TGFβ reduced the size of tumours by affecting PDGF-B production and PDGFRβ-signalling pathways (Bruna et al., 2007). To establish whether this was also the case in ovarian tumours, we checked the expression of members of the PDGF family (PDGF-A, PDGF-B, PDGFRβ and PDGFRβ) at the mRNA level in our OVA17 *in vivo* control or treated tumour samples, but found no difference between the groups (Figure R25A-D). In addition, some other receptors from proliferation pathways like HER/ERBR family member ErbB2 were also checked, but no change was noted in these either (Figure R25E).

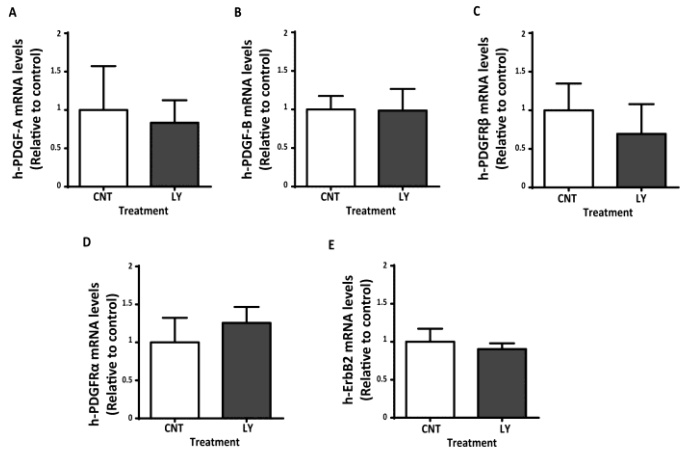

Figure R25. Blockage of TGFβ signalling does not produce any change in mRNA expression of PDGF family or ErbB2. Analysis of the human mRNA levels of PDGF family and ErbB2 in control and treated OVA17 *in vivo* tumour samples by RT-PCR, normalizing its results each one by its corresponding human normal ovary mRNA level. A) h-PDGF-A B) h-PDGF-B from 4 control and 5 LY-treated samples independently. C) h-PDGFR-β from 3 control and 4 LY-treated samples independently. D) h-PDGFR-α from 4 control and 5 LY-treated samples. E) h-ErbB2 from 5 control and 5 LY-treated samples independently. Results represented by the mean + SEM.

2.2.4 Identification of IGF1R or M-CSFR/CSF-1R as candidates for mediator factors of tumour cell proliferation regulated by TGFβ.

Ruling out the PDGF signalling pathway as mediator factor of cell proliferation regulated by TGFβ, we sought to screen tumours in order to find which could be the candidates. At that time, an *RTK Signalling Antibody Array* from *Cell signalling* was used to detect possible changes in the active levels of 11 important signalling nodes, when phosphorylated at tyrosine or other residues, in OVA17 tumours before and after LY2109761 treatment (two samples per group). Results of this array indicated that LY2109761 produced no changes in receptors like PDGFRs or those of the ErbBs, confirming our previous results on FGFR families (Figure R26).

We observed an increase in active levels of some receptors as Ephrines A1 and A2, but more interestingly, a 59% decrease in active levels of M-CSFR/CSF-1R and a 62% decrease in active levels of IGF1R (Figure R26).

At this time, we focused our studies to elucidate if one of these two receptors were responsible for TGFβ regulation on cell proliferation in ovarian cancer.

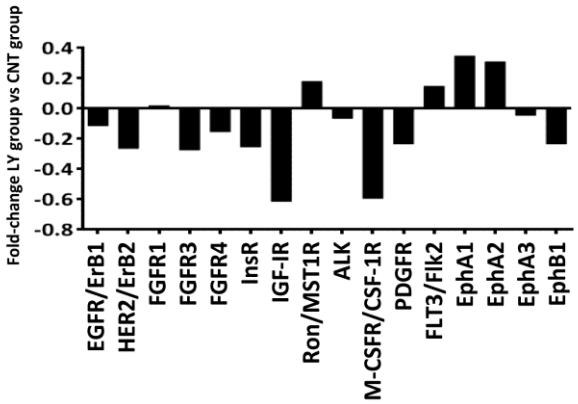

Figure R26. RTK Array showed a 59% decrease on m-CSFR/CSF-1R and a 62% decrease on IGF1R protein levels decrease after LY2109761 treatment. Phosphorylation levels of various RTKs were analysed using a human phospho-RTK array kit in LY2109761-treated and control OVA17 tumours. Results are the mean of 2 control tumours and 2 LY2109761-treated tumours, and are represented in arbitrary units (after densitometric quantification) relative to the control group.

Firstly, the Colony stimulating factor 1 receptor (CSF1R), also known as macrophage colony-stimulating factor receptor (M-CSFR) controls the production, differentiation, and function of macrophages. For this reason we analysed the number of macrophages by the staining of F4/80, a mature mouse cell surface glycoprotein, well-characterized and extensively referenced mouse macrophage marker, on OCT OVA17 samples in control and LY2109761-treated groups. The quantification did not show any change between the control and treated group, ruling out an effect of TGFβ inhibitor on macrophage number, thereby suggesting that M-CSFR/CSF-1R may not be the factor that directly reduce tumour size. Nevertheless, we can not discard a direct effect of the M-CSFR/CSF-1R on the tumour cell, and more work is still required (Figure R27).

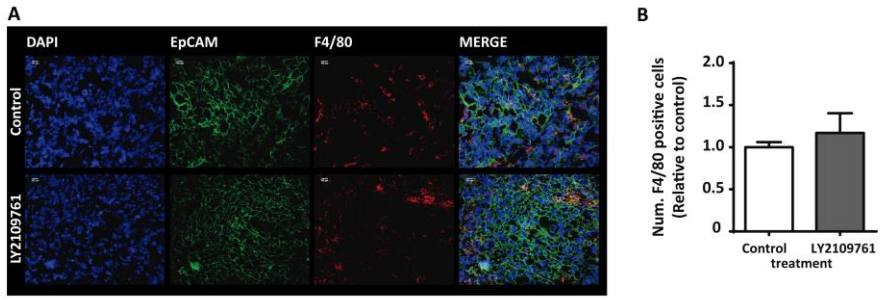

Figure R27. There is no change on macrophages number, quantified by F4/80 staining. A) Representative's image of control and treated tumour sample with the triple immunofluorescence staining in OCT of DAPI in blue detecting the nucleus, EpCAM staining tumour cells in green and F4/80 in red to stain macrophages and its respective merge image (400X, Bar 100 µm). B) Quantification of F4/80 positive cells expressed relative to control group. We analysed two control and four treated samples, with four images from a viable tumour zone for each sample independently from samples of high-grade serous OVA17 in vivo experiment. Mean represented ± SEM.

On the other hand, IGF1 signalling pathway is a well-known proliferative pathway already implicated in ovarian cancer (Cao et al., 2012; Banerjee and Kaye, 2013). As we found changes in proliferation rate, we decided to investigate in greater depth the possible role of this receptor in mediating the TGFβ effect. With this objective, first we analysed by western blot the effect caused by LY2109761 treatment on total IGF1R protein levels of OVA17 tumour samples. We observed a decrease in total levels of IGF1Rβ protein in these samples (Figure R28), indicating that the reduction in IGF1R activation levels was not caused by a lack of activation but by a decrease in the total IGF1R protein levels present in treated tumours. Furthermore, we also observed a decrease in IGF1Rβ protein levels in LY2109761-treated OVA8 and OVA15 tumours (Figure R28). These results imply a general effect of blocking of the TGFβ signalling pathway on IGF1Rβ protein expression, postulating IGF1R as mediator of cell proliferation regulated by TGFβ in our three ovarian orthotopic cancer models.

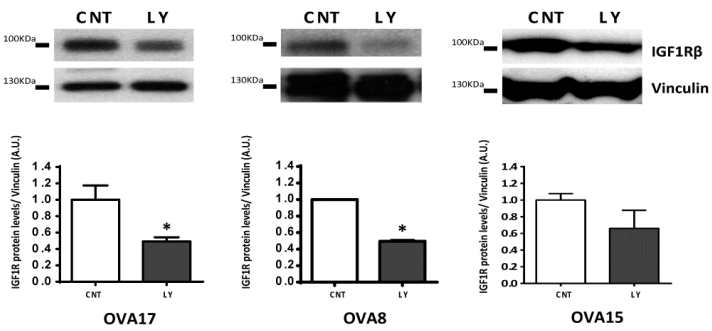

Figure R28. IGF1R protein levels decrease after LY2109761 treatment in our three mouse models. Total IGF1Rβ and vinculin expression were analysed by western blotting in independent OVA17, OVA8 and OVA15 tumours from the treatments with vehicle or LY2109761. Representative blots show the results obtained. Densitometric quantifications of IGF1Rβ relative to vinculin are shown. Results are the mean ± SD of 4 control tumours and 4 LY2109761-treated tumours in OVA17, 2 controls and 3 treated for OVA8 and 4 controls and 3 LY-treated tumours in OVA15. Results are presented in arbitrary units relative to the control group. *, $p < 0.05$ (two-tail Mann-Whitney U test or T-test).

2.3 Importance of IGF1R in ovarian cancer and in our orthotopic mouse models.

In our previous data, we had postulated IGF1R as a mediator of cell proliferation control regulated by TGFβ. IGF1R in ovarian cancer has been widely related to cancer progression; currently some clinical trials are under study. For this reason, we decided to study the importance of IGF1R in our ovarian tumour cancer models.

To this end, we orthotopically implanted 9 mice with OVA17 tumour, after 5 weeks of implantation we randomized groups and then we treated for 4 weeks four mice three times a week I.P with 12 mg/kg dose of *IMC-A12 (Cixutumumab*), a monoclonal antibody against IGF1Rβ that blocks the activity of this receptor and five mice I.P with PBS following the same schedule of the treated group. Treatment for 4 weeks with this antibody caused an 8% decrease in body weight of the animals. Given these side effects, antibody treatment resulted in a 42 % decrease in tumour size from an average of 1225 mm^3 in control tumours, to an average of 713 mm^3 in

treated tumours, (Figure R29A), indicating the great importance of this signalling pathway in this ovarian cancer model.

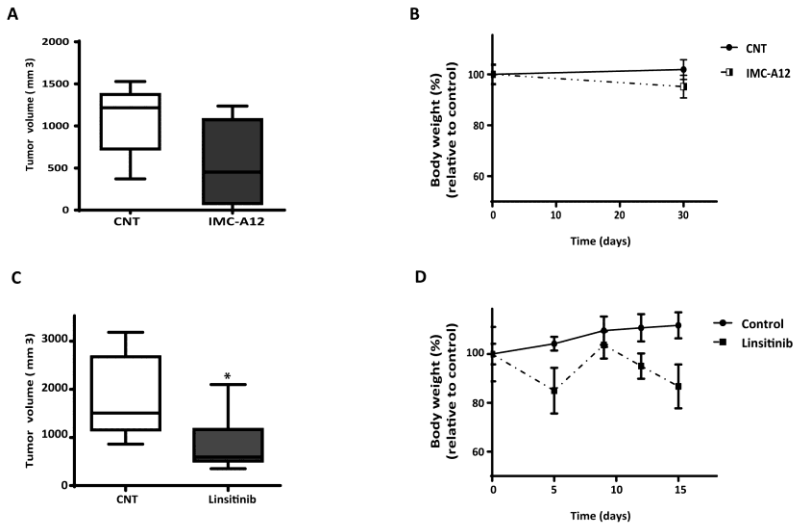

Figure R29. Blocking IGF1R activity with *IMC-A12* or *Linsitinib* inhibits tumour growth but decrease body weight as side effect. A-B) Mice with an orthotopically implanted OVA17 tumour were treated with vehicle (6 mice) or the antibody IMC-A12 i.p. three times a week for 4 weeks at a dose of 12 mg/kg (4 mice). Mice were sacrificed when control mouse tumours affected the wellbeing of the animals. (A) Final volumes are illustrated by a boxplot. (B) Mean group ± SEM of mice body weight for control or IMC-A12-treated group was represented. Values normalized for the control group. C-D) Mice with an orthotopically implanted OVA8 tumours were treated with vehicle or linsitinib with an oral dose of 40 mg/kg by gavage (as indicated in results) in an alternating regimen to six mice and 8 mice were treated with the vehicle following the same schedule. Mice were sacrificed when control mouse tumours affected the wellbeing of the animals. (C) Final volumes are illustrated by a boxplot. (D) Mean relative to control ± SEM of mice body weight for control or Linsitinib-treated group was represented. *, $p < 0.05$ (Mann-Whitney U test).

Willing to confirm this importance we also tested linsitinib (OSI-906), a tyrosine kinase inhibitor specific for IGF1R and insulin receptor on OVA8 growth (Buck et al., 2010). To asses this experiment we implanted 14 mice with OVA8 tumour model. Treatment started 4 weeks after implantation. *Linsitinib* was administered daily with an oral dose of 40 mg/kg by gavage (Leiphrakpam et al., 2013) to six mice and 8 mice were treated with the vehicle oral solution as the treated groups.

In this case we also observed side effects on mice body growth (14% decreases after 1 week of treatment). For this reason, we decided to administer linsitinib in an alternating regimen of two cycles of 5 days treatment followed by 7 days off. In all, animals were treated or not with linsitinib for 10 days. At the end of the treatment, treated animals presented a 14% decrease in body weight. Even considering these toxic effects, however, linsitinib caused a 60% decrease in tumour volume with controls, 1500 mm^3 versus treated, 600 mm^3 (Figure R29B). So, anti-IGF1R treatment impaired tumour size by 40-60%.

Next, we also took advantage of our *TMA* with samples from different patients affected by ovarian cancers to analyse IGF1R expression by IHC in order to have a widely image of this expression in human ovarian cancer. As seen in Figure R30A and similarly to pSmad2 staining, the main part of the tumours presented high levels of IGF1R and comparing high-grade serous with endometrioid tumours we did not find any differences between them. More strikingly, we found a significant correlation between the levels of pSmad2 and IGF1R in the same tumour (Figure R30B). These results indicate that IGF1R expression is dependent on the activation of the TGFβ-Smad2 pathway.

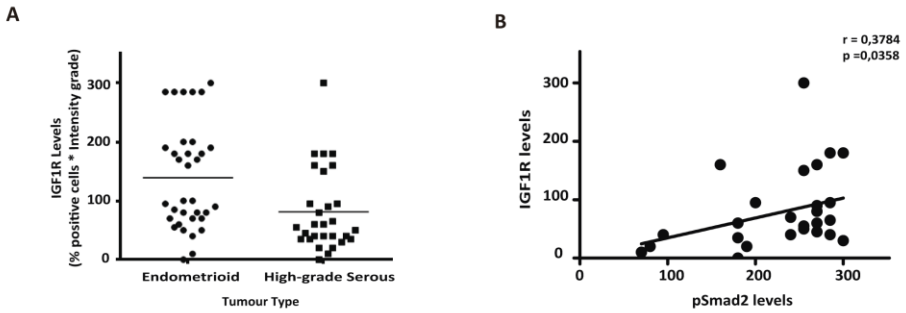

Figure R30. IGF1R is present in human ovarian cancer samples and its levels correlate with Smad2 activation. A) Quantification of IGF1R levels (using the multiplicative index of the intensity of the stain and the labelling frequency) in tumour tissue sections from high grade serous or endometrioid tumour patients. Data analysed from 65 tumour patients from our *TMA*. B) Correlation between pSmad2 and total IGF1R levels in *tissue macroarray* from high-grade serous ovarian patients analysed in Figure R10 and Figure R27A. A Spearman test was used, and the correlation coefficient is shown.

2.4 Evaluation of the control mechanism of TGFβ on IGF1R expression.

The question arises as to how the TGFβ pathway affects IGF1R levels. To answer this we measured IGF1R mRNA levels by Taqman RT-PCR in the various treated and untreated orthotopic tumours. As observed in Figure R31, LY2109761 treatment caused a decrease in IGF1R mRNA levels in OVA8 and OVA15 tumours, while no effect was observed in OVA17, implying that several TGFβ-stimulated mechanisms control IGF1R levels.

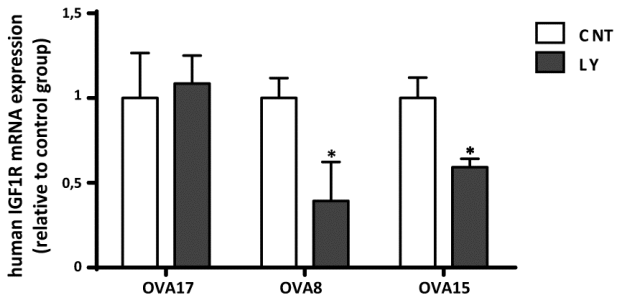

Figure R31. IGF1R is affected by LY2109761 treatment at mRNA level on OVA8 and OVA15 whereas in OVA17 mouse model IGF1R mRNA levels are not affected. mRNA levels of human IGF1R analysed by quantitative real-time PCR in OVA17 (4 control tumours and 5 LY2109761-treated tumours), OVA8 (3 control and 3 LY2109761-treated tumours samples) and OVA15 (5 control tumours and 3 LY2109761-treated tumours) orthotopic ovarian tumours. Results are expressed as the mean and SEM of mRNA expression relative to the control group. *, $p < 0.05$ (Mann-Whitney U test).

Next, we used cell culture ovarian tumoral models to analyse various ovarian cancer cell lines for IGF1R expression and TGFβ stimulation. Of the cell lines analysed, the A2780p ovarian serous cell type responded well to TGFβ stimulation, resulting in Smad2 and Smad3 phosphorylation, an effect that was inhibited by LY2109761. These cells presented low expression levels of IGF1Rβ. The SKOV3 ovarian adenocarcinoma cell line also had a good response to TGFβ but showed higher levels of IGF1Rβ expression. In the case of OV90 cell line, the cells had higher levels of pSmad3 and IGF1R at basal state so we preferred not to work with this cell line for this analysis and the TOV-112D cell line shown very low levels of IGF1R or Smad2.

At this moment, we decided to continue our studies with A2780p and SKOV3 cell lines (Figure R32).

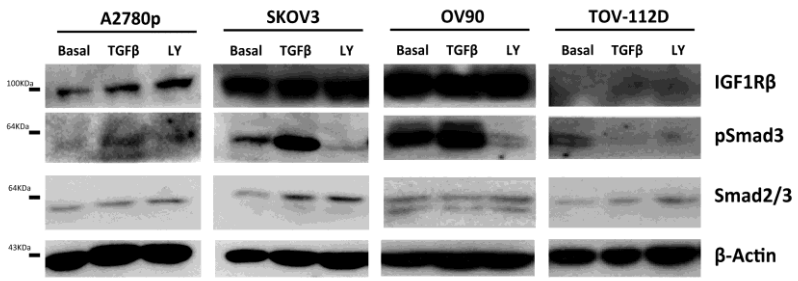

Figure R32. Different ovarian cancer cell lines respond differently to TGFβ stimulation. A2780p, SKOV3, OV90 and TOV11-2D cell lines stimulated with TGFβ 10 ng/ml for 30 min or LY2109761 (2 μM) 30 min and then TGFβ 10 ng/ml for 30 min. Cells were lysed and expression of IGF1Rβ, pSmad3, Smad2/3 total and β-actin, as a loading control, was analysed by western blot. A representative blot is shown.

We measured IGF1R protein levels in A2780p and SKOV3 cells treated for 24 h with TGFβ or LY2109761. In both cell lines TGFβ caused a 100% increase in IGF1Rβ levels, while LY2109761 treatment caused a 30% decrease in this protein (Figure R33). These results are in correspondence with results obtained in our *in vivo* models, were blockage of TGFβ signalling decreased IGF1R protein levels.

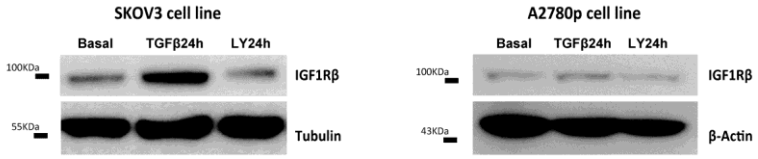

Figure R33. IGF1R protein levels decrease after LY2109761 treatment in SKOV3 and A2780p cell lines. Expression of IGF1Rβ and tubulin, as a loading control, were analysed by western blot of A2780p or SKOV3 cells lysates. Cells were incubated for 24 h with DMSO, TGFβ1 (10 ng/ml) or LY2109761 (2 μM). A representative blot of the results is shown.

Subsequently, we performed the mRNA levels analysis by Taqman RT-PCR of members of the IGFs signalling pathways (such as IGF1, IGF1R or IGF1 binding proteins) with samples of the A2780p and SKOV3 cell lines, after treatment for 8 and 24 hours with TGFβ 10 ng/μl, 2 μM LY2109761 or absence (DMSO). Results revealed different effects depending on cell type: there was TGFβ stimulation and LY2109761 inhibition of IGF1R mRNA levels in A2780p cells, but no effect in the case of SKOV3 cells. Additionally, other genes of the IGF signalling pathway (IGF1, IGF2 and IGF2R) were affected in A2780p cell line while in SKOV3 cell line were maintained upon TGFβ inhibition or stimulation (Figure R34).

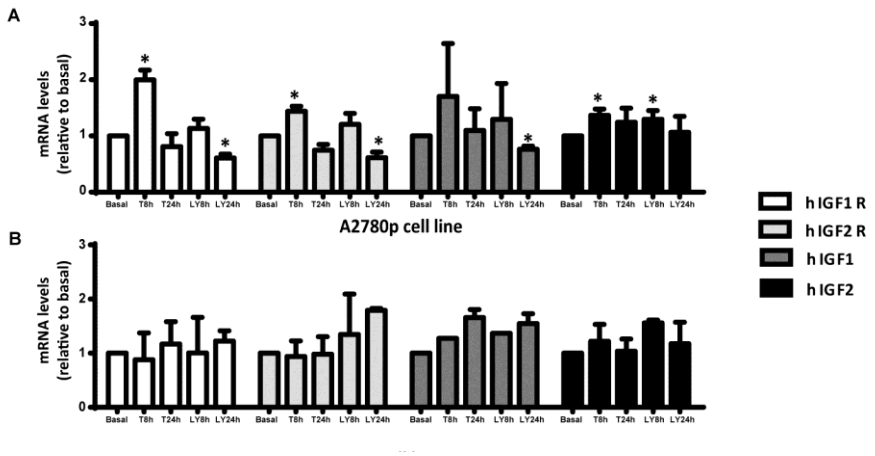

Figure R34. TGFβ stimulates IGF1R at mRNAl level in A2780p cells but does not produce any change in SKOV3 cell line. mRNA levels of human IGF1R, IGF2R, IGF1 and IGF2 were analysed by quantitative real-time PCR after treatment 8 and 24h with TGFβ 10ng/μl, 2 μM LY2109761 or absence (DMSO) in A) A2780p (4 samples) and B) SKOV3 (3 samples) cells. Results are expressed as the mean and SEM of mRNA expression relative to control condition mRNA expression. *, $p < 0.05$ (Mann-Whitney U test).

However, the IGF binding proteins analysed were not affected in either cell line (Figure R35). Overall, these results suggest that different mechanisms affecting mRNA or protein are involved in controlling IGF1R levels, which is consistent with the results obtained from orthotopic tumour models. On the basis of these results, we decided to study IGF1R protein stability in SKOV3 cells as the cell with no mRNA changes.

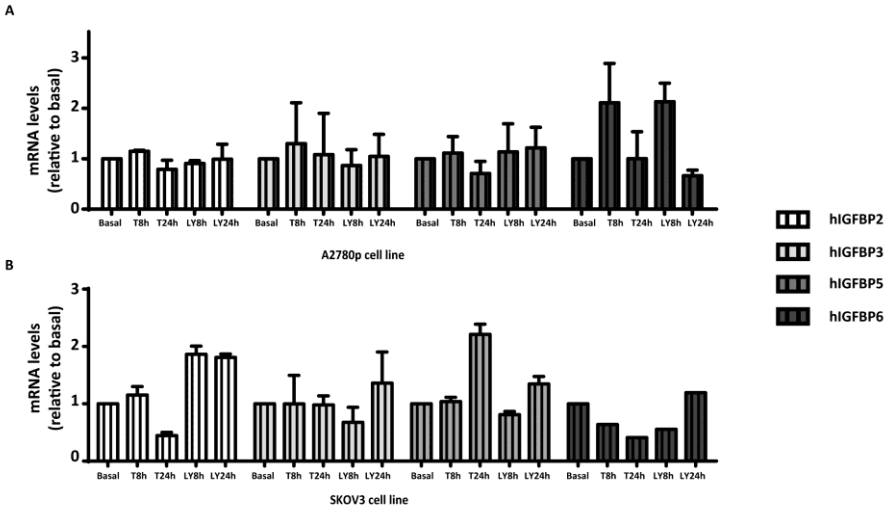

Figure R35. Any change in mRNA levels of IGFBP in any of both cells. mRNA levels of human IGFBP2, IGFBP3, IGFBP5 and IGFBP6 were analysed by quantitative real-time PCR after treatment 8 and 24h with TGFβ 10ng/µl, 2 µM LY2109761 or absence (DMSO) in A) A2780p (4 samples) and B) SKOV3 (3 samples) cells. Results are expressed as the mean and SEM of mRNA expression relative to control condition mRNA expression.

To study IGF1R protein stability in SKOV3 cells, we pre-treated SKOV3 cells with 10 ng/µl of TGFβ, 2 µM of LY2109761 or DMSO as control for 16 hours before blocking protein synthesis with *cycloheximide,* an inhibitor of protein synthesis, for 8, 16 or 24 hours. We analysed cell lysates by *Western Blot*, we found that TGFβ addition maintained IGF1Rβ protein for longer than in control samples, whereas LY2109761 treatment produced shorter duration maintenance of IGF1Rβ protein (Figure R36A). These results indicated that the TGFβ pathway regulated IGF1R protein stability in SKOV3 ovarian tumour cells.

In order to identify the mechanism involved, we blocked two systems previously described as implicated in control of IGF1R protein levels: proteasome function (through the use of MG132) and lysosomal degradation (using chloroquine) (Girnita et al., 2013). Firstly, we analysed the proteasome function by treating SKOV3 cell line with 2 µM and 10 µM of MG132, 2 µM LY2109761 or DMSO as control and the two combinations of 2 µM of LY2109761 with both concentrations of MG132 for 24 hours.

Blocking the proteasome did not affect basal IGF1Rβ levels and did not reverse the effect of LY2109761 (Figure R36B). In contrast, after adding 100 µM of *chloroquine*, 2 µM of LY2109761 or DMSO as control to the medium for 24 hours in SKOV3 cell line, chloroquine treatment increased basal IGF1Rβ protein levels and blocked the decrease induced by LY2109761 (Figure R36C).

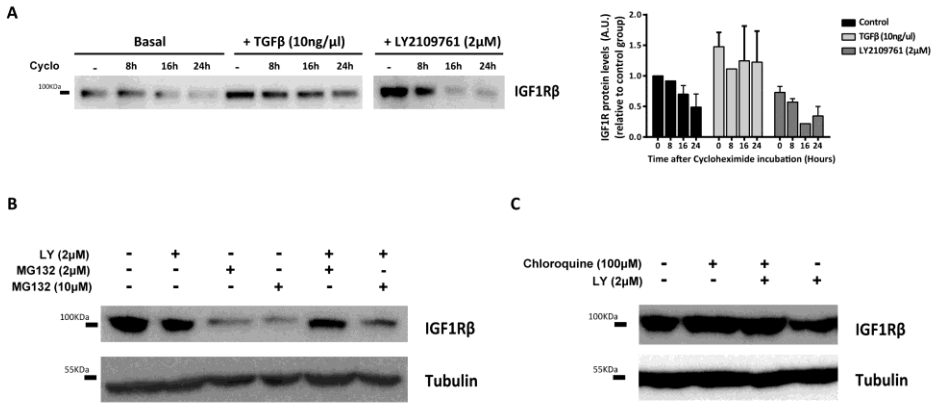

Figure R36. TGFβ stimulates IGF1R at post-transcriptional levels. A) Exponential SKOV3 cells incubated for 16h in the absence (DMSO) or presence of TGFβ1 (10 ng/ml) or LY2109761 (2 µM). After this time, *Cycloheximide* (10 µg/ml) was added for 0, 8, 16 or 24 h. Cells were lysed and IGF1Rβ expression was analysed by western blot. A blot representative of three independent experiments is shown. Densitometric quantification of IGF1Rβ is shown. B) Exponential SKOV3 cells incubated for 24h in the absence (DMSO) or presence of 2 µM and 10 µM of MG132 and 2 µM LY2109761. Cells were lysed and IGF1Rβ and tubulin expression was analysed by western blot. A blot representative of three independent experiments is shown. C) Exponential SKOV3 cells incubated for 24 h in the absence (DMSO) or presence of 100 µM *Chloroquine* and 2 µM LY2109761. Cells were lysed and IGF1Rβ and tubulin expression was analysed by western blot. A blot representative of three independent experiments is shown.

This effect was confirmed by analysing IGF1Rβ sub-cellular localization when we treated SKOV3 cell line with LY2109761 (Figure R37). Incubation with this inhibitor caused a clear internalization (2 h after inhibitor addition) and subsequent decrease of IGF1Rβ levels, confirming the TGFβ-dependent control of IGF1R recycling.

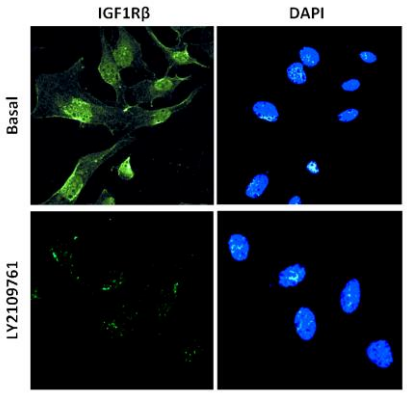

Figure R37. LY2109761 treatment produced an internalization of IGF1R in SKOV3 cell line. Immunofluorescence of SKOV3 cell line with IGF1R staining in green and DAPI in blue after incubation for 24 h in the absence (DMSO) or presence of LY2109761 (2 μM).

At that time, we moved back to our in vivo tumour samples and we decided to analyse localization of IGF1R by IHC staining in the orthotopic tumour samples. To perform this analysis we looked for localization by quantifying the percentage of IGF1R positive cells stained in different cell compartments; membrane, cytoplasm or nucleus. Interestingly, as shown in Figure R38, there are two groups of IGF1Rβ localization pattern. OVA17 pattern is different than the obtained on OVA8 and OVA15 tumour sections, where IGF1R membrane staining is only present in the first one. In contrast, nuclear staining is higher in OVA15 and OVA8 than in OVA17 tumour samples.

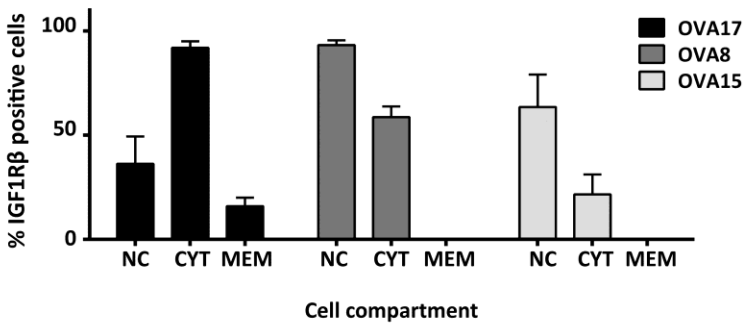

Figure R38. IGF1R protein levels are localised differently depending of tumour type. Quantification of IGF1Rβ localization presents on each cell compartment; nucleus (NC), cytoplasm (CYT) or membrane (MEM) in tumour tissue sections from control tumour samples of OVA17, OVA8 and OVA15 *in vivo* experiments. Data analysed from 6 controls in the case of OVA17 and OVA8 and 4 control samples for OVA15.

Next, as in OVA17 tumour IGF1R mRNA was no affected by LY treatment, we quantified total cell positivity stained by IGF1Rβ and the different localization of IGF1R after LY2109761 treatment between control and treated OVA17 tumour samples. Confirming results obtained by the array and by Western Blot, IGF1Rβ was significantly reduced in LY-treated samples (Figure R39). Interestingly, OVA17 LY2109761 treated samples reduced significantly the presence of IGF1Rβ in the membrane compartment (Figure R39B), corroborating results obtained in SKOV3 cell line where internalization of the receptor was observed upon TGFβ inhibitor treatment.

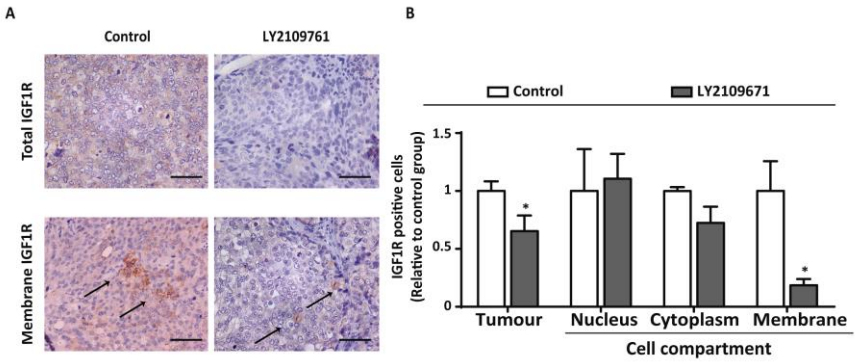

Figure R39. IGF1R protein levels are decreased after LY-treatment as well as a reduction on cell membrane presence. A) Histological IGF1Rβ staining of OVA17 orthotopic tumours. Total (top) or membrane localized (down, indicated with arrows) 400x, bar 100 µm. B) Quantification of IGF1Rβ positive cells (tumour) or localization present on each cell compartment; nucleus, cytoplasm or membrane in tumour tissue sections from OVA17 control or LY2109761-treated samples Data analysed from 6 controls and 7 treated samples. *, $p < 0.05$ (Mann-Whitney U test).

Following we evaluated our tumour samples in order to discover the player of this post-transcriptional control upon TGFβ inhibition. Hence, we started our analysis with some possible candidates already described in the literature. Unfortunately we did not find any differences that can explain the control of IGF1R recycling and degradation (Girnita et al., 2013). For example, **m**urine **d**ouble **m**inute 2 (mdm2) levels were shown to be decreased but did not increase after LY2109761 treatment.

Therefore, mdm2 could be not our candidate. Samples were analysed by Western blot and IHC to confirm and extend our results (Figure R40B-C). Another possible candidate was **C**asitas **B**-lineage **L**ymphoma (Cbl) that was not altered in our treated tumours compared with controls (Figure R40A). Unfortunately, none of these E3 ligases were responsible for TGFβ control over IGF1R. Further, caveolin was not the candidate either as protein levels were decreased after LY2109761 treatment (Figure R40B).

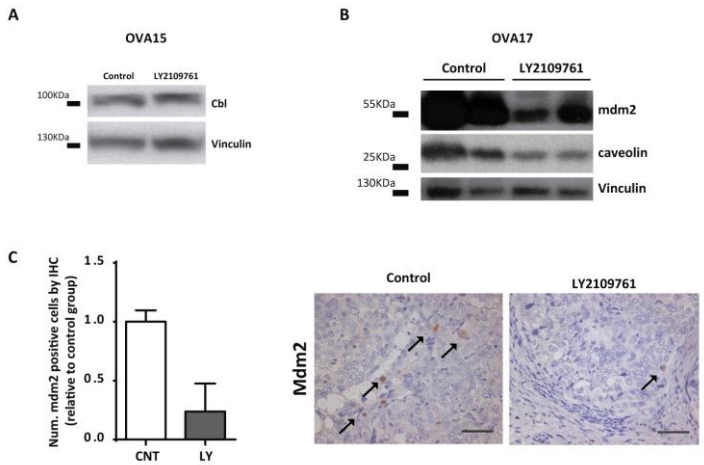

Figure R40. Mdm2, cbl or caveolin are not responsible for TGFβ control on IGF1R expression. A) Representative's WB of cbl and vinculin as a loading control of 1 control and 1 LY-treated OVA15 tumour sample. B) Representative's WB of mdm2, caveolin and vinculin as a loading control of 2 control and 2 LY-treated OVA17 tumour samples. C) Quantification of mdm2 positivity stained by mdm2 in OVA17 tumour samples. Graph represents the mean and SEM of 3 tumours per group of OVA17 tumour samples, relative to control condition. Representative's image of mdm2 staining in OVA17 embedded paraffin samples. Black arrows indicate the positive cells. (400X, Bar 50 µm).

2.5 Evaluation of the TGFβ inhibition dependence on IGF1R expression.

A further question arises as to how important IGF1R is in the observed LY2109761-effect. To address this, we evaluated the effect of LY2109761 inhibitor on cell viability in the A2780p cell line. Cells were treated for five days with LY2109761 (2, 5, 10 µM), CDDP (10^{-3} and 10^{-2} mg/ml), IMC-A12 (50 mg/ml) and DMSO was added to controls (Basal). When treatment was finished, cell viability was determined by measuring the metabolic activity

using the methyl-thiazole-tetrazolium (MTT) assay. Addition of LY2109761 caused a dose-response inhibition in the number of viable cells (Figure R41). Results also indicated a reduction in cell viability caused by IMC-A12 incubation or under CDDP, the ovarian cancer standard treatment.

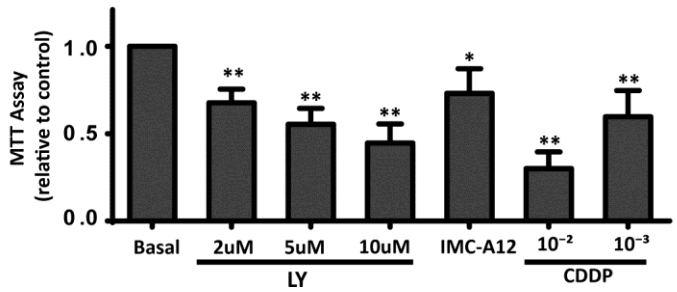

Figure R41. A2780p cell viability was significantly decreased after treatment with LY2109761. A2780p cells incubated for 5 days in the presence of the indicated concentrations of CDDP, LY2109761, 50 mg/ml IMC-A12 or in the absence (DMSO). Cell viability was measured by MTT assay. Results are expressed as relative to control condition (DMSO). Each data point represents the mean ± SEM of five independent determinations. *, $p<0.05$, **,$p< 0.01$ (two-tail Mann-Whitney U test).

To confirm that IGF1R is important for A2780p viability, we inhibited its expression in these cells. By transducing lentiviral vectors expressing either IGF1Rβ-shRNAs or a negative control using a non-silencing vector, A2780p-NS and A2780p-shIGF1R cells were generated. All four shRNA vectors express puromycin resistance that allowed us to select cells with the shRNA incorporated and maintained as a stable cell line with puromycin added to the medium. We used three independent shRNA vectors. Levels of expression were then analysed by *Western* Blot and two of them (shV2-71 and shV2-72) reduced IGF1Rβ protein expression by 70-90% (Figure R42A), while the shV2-48 vector only reduced expression by 40%. As shown in Figure R42B, the decrease of IGF1Rβ levels in A2780p cells reduced cell viability (MTT Assay) depending on the IGF1Rβ levels still expressed: 60% inhibition in shV2-71 and shV2-72, but no reduction in shV2-48.

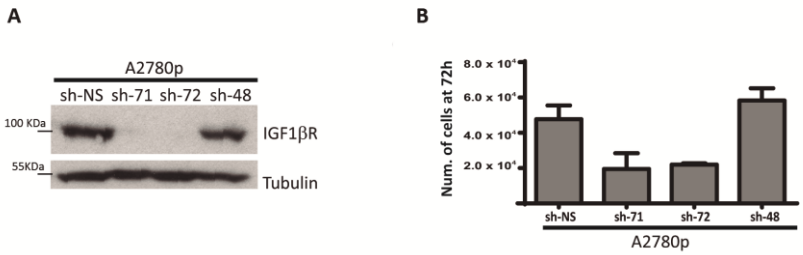

Figure R42. shIGF1R effectively inhibit IGF1R expression in two of the three A2780p cells infected, demonstrated by less protein level and reduction of its proliferation. A) IGF1R and tubulin protein levels analysed by western blot in A2780p-sh-NS, A2780p-sh71, A2780p-sh72 or A2780p-sh48 cell lysates. A blot representative of three independent experiments is shown. B) 5000 A2780p-sh-NS, A2780p-sh71, A2780p-sh72 or A2780p-sh48 cells were seeded in 24 plate dish and incubated for 3 days in normal medium. After 72h trypsinized and number of cells was counted. Each data point represents the mean and SEM± of 3 independent determinations. *, p<0.05, (T- test).

Next, knowing that levels of IGF1R were decreased and in order to determine whether the LY2109761 effect was IGF1R-dependent, we added LY2109761 inhibitor for five days to A2780p-NS cells and to A2780p-shIGF1R cells. After treatment cell viability was quantified and results showed that inhibition of IGF1Rβ expression caused a loss of LY2109761 sensitivity (Figure R43), indicating that IGF1R expression was critical for the LY2109761 effect.

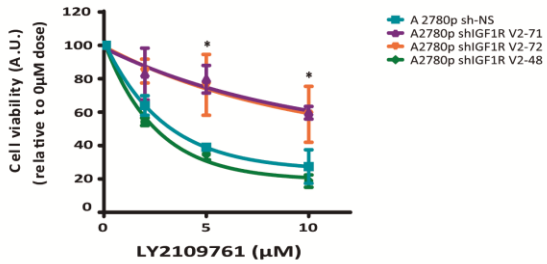

Figure R43. A2780p cell viability was significantly decreased after treatment with LY2109761. A2780p-sh-NS, A2780p-sh71, A2780p-sh72 or A2780p-sh48 cells were incubated for 5 days in the presence of the indicated concentrations of Ly2109761 or in the absence (DMSO). Cell viability was measured by MTT assay. Results are expressed as relative to control condition. Each data point represents the mean and SEM of three independent determinations. *, p<0.05 (two-tail Mann-Whitney U test).

The same experiments with shRNA vectors were performed in SKOV3 cell line and we could confirm the TGFβ inhibitor effect dependence on IGF1R expression (Figure R44). These results indicated that this connection is present independently of the mechanism of control; at mRNA or protein level and that both mechanisms can coexist depending on ovarian tumour cell.

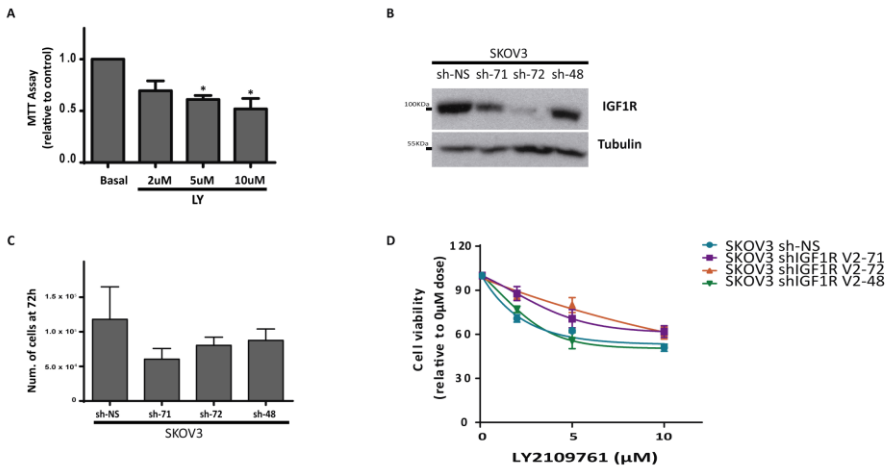

Figure R44. Cell viability was decreased after treatment with LY2109761 in SKOV3 shIGF1R clones were IGF1R was effectively inhibited. A) SKOV3 cells were incubated for 5 days in the presence of the indicated concentrations LY2109761 or in the absence (DMSO). Cell viability was measured by MTT assay. Results are expressed as relative to control condition (DMSO). Each data point represents the mean ± SEM of four independent determinations. B) IGF1R and tubulin protein levels analysed by western blot in SKOV3-sh-NS, SKOV3p-sh71, SKOV3p-sh72 or SKOV3p-sh48 cell lysates. A blot representative of three independent experiments is shown. C) 5000 SKOV3-sh-NS, SKOV3p-sh71, SKOV3p-sh72 or SKOV3p-sh48 cells were seeded in 24 plate dish and incubated for 3 days in normal medium. After 72h trypsinized and number of cells was counted. Each data point represents the mean and ±SEM of 3 independent determinations. D) SKOV3-sh-NS, SKOV3p-sh71, SKOV3p-sh72 or SKOV3p-sh48 cells were incubated for 5 days in the presence of the indicated concentrations of Ly2109761 or in the absence (DMSO). Cell viability was measured by MTT assay. Results are expressed as relative to control condition. Each data point represents the mean and SEM of three independent determinations. *, $p<0.05$, (Two-tail T- test).

Discussion

Discussion

1. Role of ALK1 on physiological angiogenesis

1.1. Lack of half dose expression induces hyper-vascularization by increasing EC proliferation.

In the first part of the presented work, we performed a study of ALK1 functions in ECs during sprouting angiogenesis. Specifically, the work presented here aimed to address the role of ALK1 in regulating angiogenesis as there are controversial results of BMP9/ALK1 signalling between *in vivo* and *in vitro* studies. However, more recently researchers have been arriving to a mutual agreement. In addition, BMP9/ALK1 signalling is also implicated in the HHT disease, where there is no effective treatment and studding the implication of BMP9/ALK1 signalling on angiogenesis should reveal new possible therapies for them.

For this, we decided to use ALK1 mutant mice to study the influence of this signalling on sprouting angiogenesis. Due to the embryonic lethally of the $ALK1^{-/-}$ mice we realized all our studies with heterozygous mice, as $ALK1^{+/-}$ pups survived in the same ratio as control littermates. Some publications suggested the importance of ALK1 on the control of angiogenesis, for example having a critical role for ALK1 signalling in regulating both developmental and pathologic blood vessel formation (Cunha and Pietras, 2011). For this reason, we chose the retinal vascular tissue, which develops during the first days after birth (from postnatal day 1 to postnatal day 10), as our model of study. Furthermore, this model allows us to stop at different time points and evaluate ALK1 influence on the vascular formation.

In this study we have demonstrated that a lack of half ALK1 expression causes hyper-vascularisation in $ALK1^{+/-}$ mutant retinas and that ALK1 is essential for a proper angiogenic development. Accordingly, half loss of ALK1 led to the development of severe vascular defects that principally enhanced vessel diameter and changed the sprouting front morphology.

In agreement with literature, we have verified that ALK1$^{+/-}$ mice reproduced the vascular malformations observed in patients with HHT (Srinivasan et al., 2003). As HHT is a dominant disorder, the lack of just one functional copy of the gene is able to develop the disease, in fact the majority of patients are heterozygous for ALK1 (Govani and Shovlin, 2009). Therefore, using mice expressing half ALK1 mimics the patient population, confirming this model for a tool to study the genetic implications of this disease and to test new possible therapies for these patients.

First, when we compared ALK1 heterozygous and WT mice we observed no changes in different vascular parameters, as radial expansion, tip cell number or tip cell length, indicating that decrease on ALK1 expression levels was not affecting migration or elongation of ECs. Similar results without changes on migration were observed in Cdh5(PAC)Cre^{ERT2};ALK1$^{fl/fl}$ mice, which produces a lack of ALK1 in endothelial cells (as Cdh5 gene is the Vascular endothelial-cadherin (VE-cadherin)) and this mutation is only Tamoxifen inducible (Tual-Chalot et al., 2014). On the contrary, these results were not similar to some results already published, where they observed filopodia and cell migration defects while blocking ALK1/BMP9 signalling, although they worked with Smad1/5 KO animals (Moya et al., 2012) instead of ALK1 mice. Since we are using diverse mutated genes from the same signalling pathway some different results may be observed. For instance, the signal from one receptor arrives to different effectors, thus we can have similar but not the same effects while blocking one or another gene. Both results can be explained as a part of the canonical pathway or several non-canonical pathways. Smad-independent signalling pathways for BMP signalling have been identified. For example, BMP signalling has been found to affect the ERK pathway, PI3K/AKT, Rho-GTPases, and others (Zhang, 2009). Therefore, inhibition of pSmad1/5 or the receptor can produce different results. Another possibility is that other BMP family members different from BMP9/10, such as BMP2/4/6 also activates Smad1/5 and all these differences can evolve in diverse altered phenotypes. These differences would be interesting to study deeply in order to better understand the BMP9/ALK1 signalling pathway.

Secondly, while other parameters were not changed, we demonstrated an increase in vessel width comparing whole-mount stained retinas of WT and ALK1 heterozygous mice at P5, P7 and P9. Similar results were observed by (Larrivee et al., 2012) where retinas from mice with postnatal injection of anti-ALK1 adenovirus that blocked ALK1 signalling increased vessel width. In addition, comparable results were obtained by (Tual-Chalot et al., 2014), where they observed that endothelial specific loss of ALK1 KO led to venous enlargement, vascular hyper-branching and arteriovenous malformations. These studies altogether indicate that blockage of ALK1 receptor or endoglin (ALK1 co-receptor) increase hyper-vascularisation on the retina mouse model, a model for pro-angiogenic vessels. A summary of the different phenotypes obtained by diverse approximations of BMP9/ALK1 signalling inhibition in the neonatal retinal vascular plexus can be viewed in the table below (Table D1):

Table D1. Summary of key phenotype differences in the neonatal retinal vascular plexus with the different approximations to induce BMP9/ALK1 signalling inhibition.

Model	Vascular parameters	Author
Eng KO^{EC}	AVM formation and increased vessel Branching only at periphery	(Mahmoud et al., 2010)
Bmp9-KO	no defects on vascularisation	(Ricard et al., 2012)
Bmp9-KO + anti-BMP10	increase in vascular density and a strong decrease in vascular radial expansion	Ricard 2012
ALK1-Fc	hyper-vascularisation and AVM formation	(Larrivee et al., 2012)
ALK1 KO ^{EC}	AVM formation and hyper-branching	(Tual-Chalot et al., 2014)
ALK1$^{+/-}$	Hyper-vascularisation and increased vessel width	This work
Smad1/5 KO^{EC}	Excessive sprouting	(Moya et al., 2012)

The overview images of whole-mount ALK1$^{+/-}$ retinas revealed that the sprouting front region of the vasculature was the most affected region by half loss of ALK1. Focusing our studies in the sprouting front, we described that this increase in vessel width was not attributable to the rise in pericyte recruitment as desmin expression levels were the same between both genotypes. In contrast, (Tual-Chalot et al., 2014), who used EC specific ALK1 mutant mice, had described that pericyte recruitment was affected in the vascular plexus. Our results discarded this effect in our approach at the sprouting front. Both results can be reliable because the analysis is done in different places of the vascular plexus and it has already been demonstrated that BMP9/ALK1 signalling controls angiogenesis in a context specific manner (Scharpfenecker et al., 2007; David et al., 2008). Besides, it is important to take into account that we do not know if half or complete block of the ALK1/BMP9 signalling pathway, can differentially influence the proper pericyte recruitment. Furthermore, in the case of Tual-Chalot the ALK1 mutation is endothelial-specific whereas in our case the mutation is present in all cells, and it is not known if this difference can influence the crosstalk between both cell types. It is also important to take into account that HHT patients have mutations in all their cells and not in specifically just one type of cells. This would be important to identify whether this different implication mimics what is happening in the patient.

Our findings showed a particular vascular defect arisen upon loss of half ALK1 signalling. In this setting, we have demonstrated that this increase in vessel width was due to an increase in endothelial cell number, observed by the endothelial marker Erg1,2,3. Furthermore, we validated that this increase in endothelial cell number was caused by an increase in endothelial cell proliferation specifically in the second line of the sprouting front and this increase in cell proliferation is responsible for the hyper-vascularisation and width vessel increase. It has already been described that BMP9/ALK1 blocks endothelial cell proliferation maintaining a quiescent endothelial state in cell cultures (David et al., 2007; Scharpfenecker et al., 2007) and in zebrafish (Roman et al., 2002).

Remarkably, the sprouting front of the growing retinal plexus is primarily integrated by newly specified tip and stalk cells and it is where the switch of tip/stalk cell specification takes place. Suitably, it has been described that BMP9/ALK1 signalling controls tip/stalk cell specification and that upon inactivation of ALK1 by ALK1-Fc, stalk ECs increase its tip cell markers (Larrivee et al., 2012). However, tip cells numbers were found to be unaltered in $ALK1^{+/-}$ retinas; as EC proliferation in the first line of the sprouting front, radial expansion, tip cell number and tip cell length were not affected in $ALK1^{+/-}$ retinas. Therefore, hinting that the stalk cell population was the most affected by ALK1 half loss as the increased endothelial cell proliferation at the sprouting front was restricted just to the second line. Consequently, these findings allowed us to reach one conclusion of this work: during sprouting angiogenesis, ALK1 was specifically required to control the proliferative behaviour of the stalk cell population controlling its quiescent stalk cell state, while not affecting its switch to tip cell as tip cells are not affected in our $ALK1^{+/-}$ retinas.

Moreover, it has been described that ALK1/Smad1/5 cooperate with Dll4/Notch dependent proliferative arrest involved in the stalk cell phenotype through a collaborative stimulation of genes such as HES1, HEY1, HEY2 and JAG1 (Larrivee et al., 2012; Moya et al., 2012). Our results *in vivo* on sprouting retinas confirmed this anti-proliferative role for the BMP9/ALK1 signalling pathway and in future work it would be interesting to analyse its molecular implications.

As the table below shows (Table D2), inhibition of the ALK1 receptor or similarly its co-receptor endoglin, produced an increase in EC proliferation whereas it is reduced with the genetic approximation of Smad1/5 KO mice. These results revealed that the control on the EC proliferation by BMP9/ALK1 signalling would not be through Smad1/5 signalling but through another factor that collaborates with the BMP9/ALK1 signalling.

Table D2. Summary of the EC proliferation results in the neonatal retinal vascular plexus with the different approximations to induce BMP9/ALK1 signalling inhibition.

Model	proliferation	Author
Eng KO^{EC}	Increased EC proliferation	(Mahmoud et al., 2010)
ALK1-Fc	Notch + ALK1 cooperate to decrease expression of the tip cell marker apelin, which induces stalk cell proliferation	(Larrivee et al., 2012)
ALK1 KO ^{EC}	Increased EC proliferation	(Tual-Chalot et al., 2014)
ALK1$^{+/-}$	Increased EC proliferation in the second line of the sprouting front	This work
Smad1/5 KO^{EC}	reduced EC proliferating	(Moya et al., 2012)

1.2 ALK1 controls EC proliferation by PI3K signalling pathway.

Similarly, recent work showed a crucial role for PTEN mediating Notch-induced stalk cell quiescence. PTEN controls stalk cell proliferation just in the sprouting front of the vascular plexus as well as an increase in vessel width at the sprouting front of PTEN $^{-/-}$ retinas (Serra et al., 2015). Altogether, these results are similar to the results obtained in this work but with Notch as inducer. For this reason, we have postulated that if ALK1 is controlling increase in vessel width at the sprouting front with similar phenotype to PTEN$^{-/-}$ mice, perhaps PTEN would be a good candidate to collaborate with BMP9/ALK1 signalling to control angiogenesis and EC proliferation in the sprouting front.

Indeed, when we have crossed our ALK1$^{+/-}$ mice with a p110α KI mice, which have less PI3K signalling activity. We have normalized to WT phenotype and ALK1$^{+/-}$ did not increase vessel width. In agreement with our hypothesis, these results suggested that the control of stalk cell proliferation was through the PI3K signalling pathway. Correspondingly, when we had affected PI3K signalling pathway, ALK1 loss was not able to generate hyper-

vascularisation. However, the migratory capacity reduced on p110α KI mice was not restored upon genetic cross with ALK1$^{+/-}$ mice, indicating that ALK1 was not required for the migratory effect of the PI3K signalling pathway, and confirming that ALK1 does not play any role on controlling tip cells. Our findings suggest that there is no crosstalk between both pathways but an effect of ALK1 on cell proliferation through PI3K signalling pathway.

In recent years, a correlation between TGFβ signalling and PI3K has been described in different cell types (Yan et al., 2009; Martinez-Palacian et al., 2013; Lamouille et al., 2014). For instance, in mouse capillary endothelial cells, TGFβ1 promotes angiogenesis by activating PI3K/AKT and p42/p44 MAPK (Viñals and Pouyssegur, 2001). Also, it has been associated with Endoglin, an ALK1 co-receptor, regulating PI3K/AKT trafficking and signalling to alter endothelial capillary stability during angiogenesis (Lee et al., 2012).

Additionally, when we pharmacologically treated ALK1$^{+/-}$ mice with PI3K inhibitor we were able to normalize the ALK1 loss phenotype in agreement with the genetic approximation, thereby elucidating a possible therapeutic treatment for HHT patients. Interestingly, when using the inhibitor on WT mice reduction in vessel width was observed whereas using the inhibitor on ALK1$^{+/-}$ mice the vessel width got to the WT levels and not to the WT + PI3K inhibitor levels. Then, PI3K inhibitor is promising as a possible treatment in HHT patients, as it normalizes vessels to WT condition and no other side effects were observed, although it is likely that there are more factors implicated in the ALK1 phenotype than only PI3K signalling. Consequently, different approaches can result in different phenotypes as it has been reviewed in this work.

Furthermore, it has been described that ALK1 and Notch signalling are both implicated in the stalk cell identity and both share some genes, but that ALK1 is not a gene downstream of Notch (Rochon et al., 2015). These transcriptional similarities between both pathways can explain the resemblance of its phenotypes due to its aberrant signalling. Some in vivo studies demonstrate that both phenotypes are additive (Larrivee et al., 2012).

Nevertheless, pharmacologically inhibition of Notch signalling does not restore AVM produced by ALK1 mutants (Rochon et al., 2015). Thus, it may be explained considering the importance of the PI3K signalling pathway in the control of EC proliferation and AVM observed in ALK1 mutants. Although both pathways share some partners, probably both have a slightly different implication on sprouting angiogenesis. In contrast, Jagged-1 peptide-mediated activation of the Notch signalling was able to suppress ALK1-Fc-induced hyper-sprouting (Larrivee et al., 2012). This suppression of the hyper-sprouting can be explained by the fact that Notch can inhibit Id1 expression stabilizing ALK1 signalling effects. In addition, Notch signalling can increase PTEN levels, which decrease PI3K signalling while avoiding ALK1 to enhance EC proliferation.

Moreover, during sprouting angiogenesis, stalk cells have been generally considered to be the ones proliferating in response to VEGF to allow the elongation of the newly formed vessels. This would partially contrast with our findings, which propose a proliferation arrest of the stalk cell population upon ALK1 induction. We believe that the ALK1-mediated stalk cell proliferation arrest might be very acute and restricted to the stalk cells immediately at the base of the growing sprouts. As it has been published BMP9/ALK1 controls the tip/stalk cell specification in early stalks collaborating with Notch signalling. In addition, it is has been demonstrated that early stalk cells BMPs/ Smad enforced Notch signalling to cooperatively activate targets genes and that upon inhibition of Smad signalling Dll4 failed to decrease in these mutant cells (Larrivee et al., 2012; Moya et al., 2012). Altogether, these findings elucidate a role for BMP9/ALK1 in controlling EC proliferation in these early stalk cells by preparing the cell with stalk cell behaviour for the next step. At this point the cell can become stalk cell by receiving Notch signalling or tip cell, to achieve the front of the sprouting again, in response to VEGF.

Our findings postulated a new mechanism of BMP9/ALK1 signalling controlling angiogenesis. Collectively, this animal model suggest a role for ALK1 in favouring stalk endothelial cell quiescence, by which ALK1 dictates endothelial stalk cell behaviour by controlling EC proliferation through PI3K

signalling pathway on pro-angiogenic vessels. Furthermore, genetic or pharmacological inhibition of the PI3K signalling pathway resulted on normalization of the EC proliferation and hyper-vascularisation upon ALK1 half loss expression (Figure D1). It remains unknown at which level of the PI3K signalling pathway is controlling ALK1 and further studies are needed. Furthermore, PTEN would be a good candidate to test its implication on hyper-vascularisation by the lack of ALK1.

Remarkably, $ALK1^{+/-}$ mice reproduce the phenotype observed in HHT patients. Currently, there is no suitable treatment to cure this disease. Right now, the only available treatment is to avoid complications by surgical intervention. Lately, new experimental clinical and pre-clinical treatments have been tested. For example, it has been observed that in mice bearing a heterozygous knock-in allele of a human BMPRII mutation, a Type II Receptor for ALK1, which also generates pulmonary arterial hypertension (PAH), administration of BMP9 reversed the established PAH, elucidating a possible treatment for this PAH (Long et al., 2015). Furthermore, an intracranial injection of an adenovirus expressing VEGF caused abnormal AVM-like structures in $ALK1^{+/-}$ mice (Hao et al., 2010). Besides, the antiangiogenic therapy using a monoclonal antibody to mouse VEGF-A promotes a restitution to normal levels of VEGF after its injection and an attenuation of their AVM and the microvasculature alterations (Han et al., 2014). Moreover, in a phase II clinical trial of bevacizumab (monoclonal antibody to VEGF) in HHT patients with severe liver disease it was reported that hyperdynamic cardiac output secondary to intrahepatic arteriovenous shunting was significantly improved in treated patients (Dupuis-Girod et al., 2012). PI3K-AKT is a key pathway for VEGF-stimulated angiogenesis (Graupera and Potente, 2013). Our data stress the importance of the PI3K pathway for the hyper-proliferation observed in $ALK1^{+/-}$ animals and let us to propose the use of PI3K or AKT inhibitors as pharmacological alternative strategies to treat HHT patients. Our work using both, genetical and pharmacological inhibition of PI3K signalling that normalize endothelial cell number in $ALK1^{+/-}$ animals, is a proof of concept for the use of these inhibitors to treat patients affected by HHT.

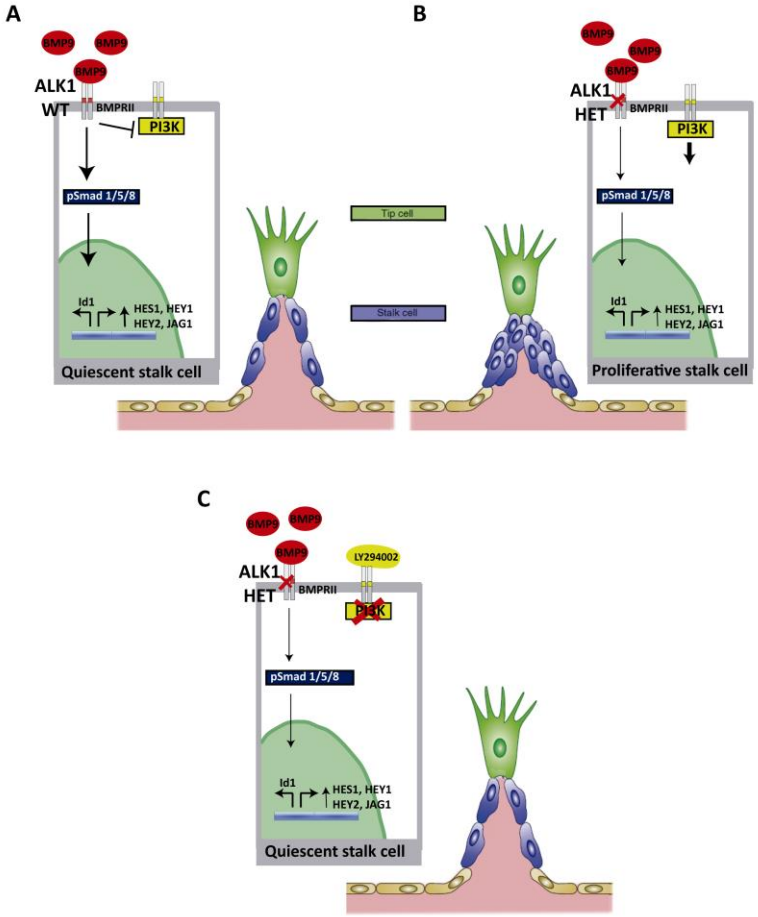

Figure D1. Schematic model of ALK1 controlling cell proliferation by PI3K. A) ALK1, after BMP9 stimulation, is inhibiting PI3K proliferation effect over stalk EC at the second line of the sprouting front. B) Half ALK1 expression, after BMP9 stimulation, is not capable of inhibiting PI3K proliferation effect over stalk EC at the second line of the sprouting front. C) Presence of PI3K inhibitor avoids the half ALK1 expression over-proliferation effect on stalk EC. Figure adapted from (Serra et al., 2015).

2. Role of TGF-β signalling members in ovarian cancer

2.1 Characterisation of TGFβ signalling pathway in ovarian tumours.

In the second part of this work we focused our studies on trying to elucidate the role of different TGFβ members in the progression of ovarian cancer. TGFβ has extensively been related with cancer progression, ovarian cancer included (Massague, 2008; Tian and Schiemann, 2009). In addition, in this thesis we evaluated if the inhibition of one of the two receptors of TGFβ signalling pathway would be a good candidate for target therapy in the treatment of ovarian cancer.

2.1.1 ALK1 receptor does not seem to effect ovarian cancer progression.

Antiangiogenic treatments have been considered really effective but with some obstacles to solve, as acquired resistance in majority of the cases. Some researchers believe that targeting of alternate angiogenic pathways, particularly in combination with VEGF pathway blockade, holds the promise of optimally inhibiting angiogenic driven tumour progression. While VEGF is important for vessel initiation, ALK1 is involved in vessel network formation. Some publication described that ALK1-Fc treated mice displayed a 70% reduction in tumour burden compared with vehicle treated mice in an orthotopic breast cancer model (Mitchell et al., 2010). Moreover, it decreased tumour growth in two renal cell carcinoma models (Cunha and Pietras, 2011; Wang et al.). On top of that, two ALK1 inhibitors have entered phase I/II clinical trials, ACE-041 (dalantercept, Acceleron Pharmaceuticals) and PF-03446962 (Pfizer).

For this reason we considered it important to evaluate the levels of ALK1 present in human ovarian tumour samples in comparison to control tissue to describe the importance of this receptor on ovarian cancer. Our analysis revealed a decrease of the receptor levels in tumour samples versus normal tissue, indicating that ALK1 expression is reduced upon tumour progression.

Moreover, a free survival analysis monitoring progression upon months (100 months) and ALK1 expression revealed no correlation between levels of ALK1 and survival. Even though, the number of patients for this study is low and before drawing conclusions it would be important to increase patient number. Our results indicate that ALK1 does not seem important for ovarian cancer progression and aggressiveness. Our results agreed with observations that in ovarian cancer cells lines, the role of BMP9 signalling goes predominantly through an ALK2/Smad1/Smad4 pathway rather than through ALK1, the major BMP9 receptor in endothelial cells (Herrera et al., 2009). For this reason, we decided to discard to continue the study of ALK1 inhibitors to treat ovarian cancer in this work.

2.1.2 Activation of TGFβ signalling pathway through ALK5/ Smad2/3 on human ovarian cancer.

The next step was to evaluate ALK5 receptor levels in ovarian cancer. When we checked ALK5 presence in ovarian cancer, we observed high levels of this receptor present in human ovarian tumoural cells. Therefore, we decided to check ALK5 activation levels. To asses this study we decided to use the *Tissue Macro Array* (TMA) with different types of ovarian cancer; high-grade serous or endometrioid and stained by pSmad2 (readout of ALK5 receptor activity).

An active TGFβ signalling pathway is characteristic of later stages of tumoural proliferation, as in squamous cell carcinomas (Oshimori et al., 2015) or gliomas (Bruna et al., 2007). In addition, in these latter tumours, high pSmad2 was correlated with poor prognosis. While TGFβ blocks cell growth in normal ovarian epithelial cells, in 40% of ovarian carcinomas TGFβ loses its cytostatic effect but maintains EMT induction and production of extracellular matrix (Helleman et al., 2010). For all these reasons, different targeted drugs have been developed against this pathway, some of which are currently in clinical trials (Seoane, 2008{Akhurst, #33; Akhurst and Hata, 2012; Neuzillet et al., 2015).

In this work, we observed that pSmad2 was present in tumoral cells, with only a few positive stromal cells. The staining also indicated that ovarian epithelial tumours maintained the activity of the TGFβ-Smad2/3 pathway, which is already active in normal fallopian tube epithelium. In fact, this pathway also plays a positive role for granulose cell proliferation during normal ovarian physiology (Richards and Pangas, ; Li et al., 2008).

Furthermore, our results confirmed highly activation of the canonical TGFβ signalling pathway (high Smad2 phosphorylation), in ovarian carcinomas with independence of their anatomical origin (high-grade serous or endometrioid). It has recently been described that in advanced high-grade serous ovarian cancers pSmad2 staining is also correlated with poor patient outcome (Parikh et al., 2014). Considering this highly positivity in all our results, this poor prognosis probably would be affecting endometrioid ovarian cancers too. Moreover, it suggests that anti-TGFβ treatment on ovarian cancer should be effective at similar levels as in the case of glioblastoma.

Previously, to start analysing the importance of TGFβ signalling pathway on our ovarian cancer animal models, we confirmed that these models maintained the characteristics of its primary tumour and were comparable to the patients' samples. In fact, tumours maintained the same features and morphology observed in the primary tumours. Indeed, we could demonstrate that pSmad2 highly activation was maintained upon passages. For this reason, we were convinced that the orthotopic ovarian cancer mouse models were a good tool to study the role of TGFβ on ovarian cancer progression and to test possible target therapies.

Subsequently, we were wondering by which mechanism TGFβ signalling pathway would be activated. Mechanisms for activating the TGFβ pathway in tumours include overexpression of the microRNA-181a and repression of the negative regulator Smad7 (Parikh et al., 2014), or the secretion of autocrine TGFβ family members by tumoral cells (Henriksen et al., 1995); (Rodon et al., 2014).

Our RT-PCR analysis indicates that human TGFβ2 was the most strongly expressed ligand in the various orthotopic tumours analysed, suggesting a major role for this factor in activating Smad2 in ovarian tumours, as occurs in gliomas (Rodon et al., 2014). Interestingly, we discovered that in the endometrioid mouse model human TGFβ2 was highly expressed and in this the tumour human TGFβ3 played a major role. At the moment, we do not know if this difference was exclusive to this tumour in particular or was depending on epithelial tumour type in general, where high-grade serous are TGFβ2-dependent whereas endometrioid type are TGFβ2 and 3-dependent.

It has been described that TGFβ isoforms are differentially expressed by the ovarian surface epithelium (OSE) and TGFβ appears to have an important role in regulating OSE and possibly stromal–OSE interactions (Nilsson et al., 2001). In addition, a skin carcinogenesis study suggested differential functions for each TGFβ isoform in epidermal carcinogenesis, such that TGFβ1 was associated with the more differentiated state, TGFβ2 with highly malignant and invading cells, and TGFβ3 with tumour stroma formation and angiogenesis (Gold et al., 2000). Whether the different expression can be explained by different tumour type or its progression state remains unknown. In any case, TGFβ signalling pathway was highly activated in our tumour ovarian cancer mouse models.

2.2 Affectivity of the TGFβ signalling target therapy on ovarian cancer.

At this point, we decided to test the TGFBRII inhibitor, LY2109761 that was so effective in the treatment of gliomas (Anido et al., 2010). Our aim was to find a possible new treatment for ovarian cancer as 80% of ovarian cancer patients relapse within five years post platinum-taxane treatment and become resistant to CDDP (Herzog, 2004; Ushijima, 2010).

Our results showed a decrease in tumour size in the LY-treated tumours compared to the control group. Indeed, in the case of high-grade serous mouse models the decrease was significant. We considered that the

observed decrease in the endometrioid model was not significant due to tumour dispersion. However, we believe that independently of epithelial ovarian tumour type, the inhibition of TGFβ signalling pathway would impair tumour growth. Although we have tested only three different tumours models, the analysis of the TMA showed medium or high levels of activation of the TGFβ pathway in the majority of the 66 tumours analysed, which gives reason to consider that the treatment may be effective in all of them.

TGFβ inhibition impaired tumour growth in our tumour mouse models in agreement with some already published pre-clinical and clinical studies of different tumour types (Lahn et al., 2005; Connolly et al., 2012; Sheen et al., 2013). Among those, for example, the antisense molecules; Trabedersen (AP12009), which blocks TGFβ2 mRNA, showed efficacy in a mouse model of pancreatic cancer and it was successfully tested in PhaseI/II study in patients with refractory high grade glioma. In ovarian cancer, a pre-clinical study was done by (Liao et al., 2011), in which they observed a blocked tumour growth in a SKOV3 cell line transfected with nanoparticle-mediated soluble extracellular domain of the transforming growth factor-β type II receptor (sTGFβRII). In particular, the efficacy of LY2109761 has been evaluated among others in a model of metastatic pancreatic cancer, hepatocellular carcinoma, prostate cancer and gliomas and a negative effect on tumour growth and an increase in survival rate was observed in all of them (Melisi et al., 2008; Mazzocca et al., 2009; Anido et al., 2010; Wan et al., 2012).

Although a drug resistance on sustained pharmacologic inhibition after long term treatment was observed by (Connolly et al., 2011), we did not observe any resistance during at least one month of treatment. In their case, they separated the study in two regimens; short term with our schedule but just for 10 days or sustained regimen with a single dose through tumour outgrowth. Our method was longer than its short treatment and it was still effective but at the time we do not know if longer treatments would develop tumour resistance. However, it is important to specify that they already observed a disruption on vascular integrity in the short treatment even without affectivity on tumour growth and in our approach we observed tumour size reduction without changes to the vascular network.

In this work we have demonstrated that TGFβ inhibition is strictly effective on the tumour but does not affect its dissemination or metastasis. Regarding the dissemination we demonstrate that TGFβ not only was unnecessary for the attachment but also for the growing of nodules. Our findings differed with other publications where dissemination was reduced using the anti-TGFβ treatment. For instance, a reduction in liver metastasis was observed in a pancreatic cancer model and a breast cancer model where treatment with the inhibitor blocked lung and bone metastasis (Melisi et al., 2008; Ganapathy et al., 2010). One reason for this difference could be the use of different cancer models which might be more dependent on TGFβ-mobilisation role than our model. Another possibility is the aggressiveness of the tumour; for example in the case of the study of the pancreatic tumours where control mice disseminate more than what our control tumours do. So probably this tumour is more invasive and as a consequence TGFβ could be more effectively blocking dissemination. In contrast, our tumour models may be less invasive and its mobilisation may not be TGFβ-dependent.

2.2.1 TGFBRII inhibitor reduced tumour cell proliferation by controlling IGF1R levels.

In order to determine by which mechanism TGFβ inhibition was impairing tumour growth, we first evaluated the influence of TGFβ on CSC as some studies suggested an effect on this cell population (Watabe and Miyazono, 2009; Kwon and Shin, 2013). For example, in paclitaxel resistant breast-cancer cells, the inhibition of TGFβ signalling reduced the numbers of CSCs cells induced by paclitaxel treatment as well as in GCS where they observed a reduction of the $CD44^{high}/Id1^{high}$ GIC population, and it was even observed in ovary (Anido et al., 2010; Cao et al., 2012; Bhola et al., 2013). Nevertheless, we observed no changes in the CSC population that could explain this reduction on tumour mass, nor on the number of $CD44^{+}$ cells where reduction was observed by (Anido et al., 2010). Altogether, in our

model TGFβ was not responsible for this CSC population, this effect again could be tumour type-dependent.

Next, we analysed the angiogenic state after treatment as some publications propose that the tumour reduction upon anti-TGFβ treatment was due to reduction in vessel density. These effects have been observed using a sTGFβRII that blocked TGFβ signalling and then reduced angiogenesis in two ovarian orthotopic mouse models generated from ovarian cancer cell lines (Liao et al., 2011). In addition, using LY2109761 on Hepatocellular carcinoma a reduction on angiogenesis was observed too (Mazzocca et al., 2009). In our case, there were no changes on angiogenesis and this does not explain its tumour size reduction. One explanation could be the activation level of tumour vessels at the start of the treatment. TGFβ is known to have both angiogenic and antiangiogenic actions depending on specific conditions (NAKAGAWA ET AL., 2004). What's more, the effects of TGFβ upon endothelial cells depends on the shape and the proliferative state of the cells and the surrounding matrix and can be dose-dependent (Sutton et al., 1991). As a consequence, TGFβ inhibition may produce variable effects depending on the context it is used in.

Furthermore, we evaluated necrosis and apoptosis but neither was affected. These results suggested that the inhibitor was not increasing tumour cell death. Some publications described that cell death was not the cause of reduction in tumour growth upon anti-TGFβ inhibition. However, some studies showed an increase in cell death when TGFβ inhibition was used in combinations with other agents like radiation or gemcitabine (Melisi et al., 2008; Zhang et al., 2011a).

When we analysed the proliferation rate by the staining with Ki67 we observed a 20% reduction in the treated samples. Furthermore, a 60% decrease of Cyclin D1 was observed in treated-tumours. These results were consistent with other studies where they determined that the effect of the treatment was due to inhibition of proliferation, although most studies did not explain why TGFβ inhibition is affecting proliferation (Wan et al., 2012).

Other proteins like p16 and E-cadherin, were shown to be up-regulated upon LY2109761 treatment:

Interestingly, p16 is a tumour suppressor gene important in the regulation of cell cycle. Lower p16 expression was also typical for chemotherapy-resistant tumours; cases of lower caspase-3 and higher Ki67 expression and represents an unfavourable prognostic factor (Surowiak et al., 2008). In addition, there is a publication that relates OVCA1, which is a tumour suppressor gene, with the inhibition of epithelial ovarian cancer cell proliferation by the decrease of cyclin D1 and the increase of p16 (Kong et al., 2011). Certainly, an increase of p16 levels is beneficial for the treatment of the tumour. In addition, these results seem to demonstrate that at this time OVA17 tumour after one month of treatment does not have at least the resistant feature that was proposed by (Connolly et al., 2011).

Another interesting up-regulation is observed in E-cadherin expression. E-cadherin plays a role in the EMT process (Kalluri and Weinberg, 2009). TGFβ induces expression of some transcription factors that, once expressed, repress E-cadherin expression (Medici et al., 2008). When we analysed our LY-treated tumour samples and observed an increase in E-Cadherin expression, we confirmed that the inhibitor was working and that we were inhibiting TGFβ signalling. Moreover, the central role played by E-cadherin loss in the EMT program facilitates acquisition of a mesenchymal phenotype, and promotes tumour progression, providing an explanation for how E-cadherin loss increases ovarian cancer metastasis (Sawada et al., 2008). Additionally, some studies suggest that E-cadherin expression inhibits cell growth by a β-catenin-dependent mechanism (Perrais et al., 2007) or by up-regulation of $p27^{Kip1}$ (St Croix et al., 1998). These results may be connected with our observed reduction on tumoral cell proliferation.

Another result that is important in our work is the observed reduction on pERK1/2 protein levels, a proliferative pathway, while pAKT a more anti-apoptotic pathway was not changed. Considering the relation of the ERK1/2-cyclin D1 axis, we hypothesis that TGFβ on its own was not performing the effect on proliferation and that TGFβ was controlling proliferation through

the control of another factor. Similar indirect mechanisms of control of cell growth and proliferation by TGFβ through other growth factors have been described, for example, in glioma models, where TGFβ stimulates production of PDGF-B and activation of PDGFRβ (Bruna et al., 2007). Firstly, we analysed mRNA levels of PDGF family and ERBB2 to evaluated if the factor was the same. The mRNA levels of the PDGFB and ERB2 were not changed, so we had to look for another player. Discarding PDGF or ERBB2 family as collaborators we performed an array to find a possible candidate that could play a role on TGFβ control of proliferation. From this array we selected two possible candidates to control tumour cell proliferation: *Colony-stimulating factor-1 receptor* (CSF-1R) and *insulin-like growth factor 1* (IGF1R).

It has already been described that TGFβ1 induces CSF-1R mRNA levels in vascular smooth muscle cells (Inaba et al., 1996) and in cervical cancer cells lines (Kirma et al., 2007). In agreement with our results, treatment with a TGFβRI inhibitor significantly decreased the CSF-1R mRNA expression of the primary tumour cells from MDA-MB-231 xenografts (Patsialou et al., 2009).

Next, it was important to evaluate if this reduction impaired tumour growth or if it was an independent event. M-CSF, a ligand of CSF-1R, is required for tissue-resident macrophage proliferation and the addition of antibody against TGFβ produce a 32% inhibition on M-CSF-dependent proliferation (Celada and Maki, 1992). Moreover, macrophage-depleted mice had a lower tumour mitotic index, microvascular density, and reduced tumour growth (Gabrusiewicz et al., 2015). Summarizing these results; a decrease in CSF-1R could reduce macrophage number and thereby reduce tumour growth. In contrast, we observed that active CSF-1R levels decreased in our samples after LY2109761 treatment but it did not affect macrophages number. Some studies postulate that TGFβ may be an important negative regulator of macrophage proliferation in the bone marrow; whereas, in the tissues, TGFβ may enhance macrophage proliferation (Davies et al., 2013).

CSF-1R is not only expressed in macrophages but also in primitive multipotent hematopoietic cells (Bartelmez et al., 1985), testis, uterus, ovary, placenta, and mammary glands and the early phase of the developing prostate (Sapi and Kacinski, 1999; Ide et al., 2002). It has been described that ovarian cancer cells produce M-CSF (Kacinski et al., 1989a). Elevated expression of CSF-1R was seen in breast, ovarian, and uterine cancers, and its elevated expression in these tumours correlates with high-grade and poor prognosis. Furthermore, high circulating levels of CSF-1 correlates with active disease in ovarian and endometrial cancers and with metastatic breast and prostate cancer (Kacinski et al., 1989b; Sapi and Kacinski, 1999). Co-expression of the macrophage colony-stimulating factor (CSF-1) and its receptor (CSF-1R) has been shown to be a predictor of poor outcome in epithelial ovarian cancer (Chambers et al., 1997). Consequently, in our case a decrease on CSF1R may deter tumour progression.

Inhibition of CSF-1R activity could therefore reduce macrophage infiltration and cause a delay in tumour progression, as macrophage recruitment is enhanced by overexpression of CSF-1 in the tumour, which correlates with accelerated tumour malignant transformation and angiogenesis (Murray et al., 2003; Toy et al., 2009). Our results do not shown any change in macrophage numbers, suggesting that it is not affecting macrophage infiltration. In addition, it has been described that there is a paracrine and autocrine loop of M-CSF between macrophages and breast cancer cells and this tumour cell autocrine loop is generally important for tumour invasion, but we have not observed changes on the levels of invasion (Patsialou et al., 2009). Altogether, our study suggests that although CSF-1R changes would be remarkable, probably the CSF-1R decrease does not directly explain the observed proliferation rate reduction in our mouse models.

The candidate IGF1R has been shown to be important in ovarian cancer cell proliferation and that targeting IGF1R suppresses cell proliferation (King et al., 2011; Guo et al., 2013). IGF1R in turn stimulates the ERK subset of MAPKs: extracellular-related kinase ERK1/2 and ERK also mediates transcriptional induction of the cyclin D1 gene (Peeper et al., 1997). For example, it has been described in SKOV3 cell line that inhibition of the gen

OVA66 let to decreased tumour growth, by inhibition of IGF1R and its extracellular signalling ERK1/2 (Rao et al., 2014). Altogether, it reinforces the hypothesis of IGF1R as an important candidate to control cell proliferation regulated by TGFβ reducing ERK activation and cyclin D1 expression levels.

Our results suggest that IGF1R mediates the TGFβ effects on ovarian cancer cells. This TGFβ-IGF1R link was confirmed by the decrease of total IGF1R protein levels observed by Western Blot detection in LY-treated samples compared to their control samples on all three *in vivo* experiments. In addition, we observed a significant correlation between pSmad2 and total IGF1R levels in the human cancer samples of the TMA analysed here. These results extrapolate our *in vivo* results with a correlation maintained in the clinic.

Positive effects of TGFβ on the IGF1R pathway have been described in osteosarcoma cells, where TGFβ increases IGFBP3 protein, in turn boosting IGF1R signalling (Schedlich et al., 2013). In normal prostate cells the IGF axis and TGFβ are both up-regulated during normal prostate epithelial differentiation and down-regulated in local prostate cancer. After TGFβ treatment, the expression of the IGF axis was enhanced in prostate cells expressing TGFβ receptors (Massoner et al., 2011). It is noteworthy, that in this work we have demonstrated the direct relation of TGFβ controlling IGF1R levels, in comparison with the other studies where this relation was mediated by other implicated genes, for instance the IGFBP3 in the case of osteosarcoma cells (Schedlich et al., 2013).

In addition, we have demonstrated that TGFβ inhibition controls proliferation by IGF1R and that the effect of LY2109761 was IGF1R-dependent. We observed that adding LY2109761 inhibitor to A2780p and SKOV3 with IGF1R expression inhibited caused a loss of LY2109761 sensitivity, indicating that IGF1R expression was critical for the LY2109761 effect. Altogether, these results confirmed the role of TGFβ in the control of tumour cell proliferation via the IGF1 signalling pathway.

2.2.2 TGFβ regulates IGF1R expression levels.

Our findings suggest that the control of IGF1R levels by TGFβ includes a control at the mRNA and protein level. We observed in the A2780p cell line that IGF1R mRNA levels were modified upon inhibition or stimulation of the TGFβ signalling pathway. In agreement, OVA15 and OVA8 LY-treated tumour samples decreased IGF1R mRNA levels too. Still, IGFBP3 mRNA was not affected upon LY2109761 treatment; these results diverged with a study where they observed changes in IGFBP3 upon TGFβ stimulation (Schedlich et al., 2013). Thus, this may indicate that our mechanism of action is different than the mechanism in the osteosarcoma cell line.

One possibility could be a transcriptional mechanism that involves Smads, given that Smad binding sites are present in the conserved promoter region of the human IGF1R gene. Another possibility could be the control of miR that represses or stimulates IGF1R mRNA expression. One example was observed in SKOV3 generated tumours where miR133a suppresses cell proliferation by inhibiting IGF1R transcription, interestingly TGFβ stimulation down-regulates miR133a during liver fibrosis (Roderburg et al., 2012; Guo et al., 2013). Further studies are necessary to elucidate by which mechanism TGFβ is controlling IGF1R mRNA levels.

In addition to the mRNA control, our results also identify a positive control of TGFβ signalling pathway on IGF1R protein recycling. We observed changes in its localization upon TGFβRII inhibitor in OVA17 tumour samples and SKOV3 cell line. To be sure that these changes were post-traductional we added cycloheximide to the medium and evaluated the IGF1R life span in the SKOV3 cell line upon TGFβ or LY2109761 treatment. R results demonstrated that after LY addition IGF1R protein was degraded faster whereas, TGFβ addition prolonged IGF1R protein levels.

In general, IGF1R degradation is mediated by two systems; the proteasome and the lysosomal pathway, although the relative roles of each are not clear (Girnita et al., 2013). Degradation of the IGF1R by a proteasome mediated route was prevented by proteasome inhibitors while being insensitive to lysosome inhibitors (Sepp-Lorenzino et al., 1995) and vice versa in the

lysosome mediated route. The IGF1R has been demonstrated to be a substrate of three E3 ubiquitin ligases: Mdm2 (Girnita et al., 2003), Nedd4 (Vecchione et al., 2003), and c-Cbl (Sehat et al., 2008). Ubiquitination of a single RTK by different E3 ligases may result in different functional outcomes.

Our results then revealed that TGFβ increased IGF1R internalization and degradation by the lysosome mechanism as chloroquine inhibition prevented its internalization. Receptors and transporters require post-endocytic delivery to lysosomes. This process can be signalled by ubiquitination; conjugation of a single Ub (mono-Ub), multiple mono-Ub (multimeric-Ub) or Ub chains (polymeric-Ub or poly-Ub) are associated with efficient endocytic cargo recognition in animal cells (Dupre et al., 2004) (Lefkowitz, 1998). Therefore, this trafficking step is highly sensitive to the regulation of the ubiquitination and deubiquitinating (DUB) systems (Goh and Sorkin, 2013). Hence, it is in this regulation that TGFβ may play a role.

The IGF1R has been shown to be ubiquitinated and internalized, through both clathrin and caveolin routes, in a ligand-dependent manner (Girnita et al., 2003; Vecchione et al., 2003; Sehat et al., 2007; Sehat et al., 2008). In this work we evaluated caveolin expression levels and we observed a decrease of expression upon TGFβRII inhibition. Thus, in our models the caveolin route must not play a role on the IGF1R internalization controlled by TGFβ. In future studies, it would be good to evaluate clathrin protein levels to elucidate the internalization processes implicated.

With the intention to find the E3 ligase implicated in IGF1R internalization by TGFβ, we evaluated Mdm2; it has been described that a post-transcriptional mechanism which evidenced that p53-Mdm2 is involved in the ubiquitination and degradation of the IGF1R (Girnita et al., 2003). Subsequent research revealed the mechanism of Mdm2 binding to the IGF1R by identifying β-arrestins; which serves as adaptors to bring the E3 ligase Mdm2 to the IGF-1R (Girnita et al., 2005). Recently, β-arrestin was recognized not only as help on IGF1R internalization and signal cessation but to initiate its own second wave of signalling through the MAPK/ ERK

pathway (Girnita et al., 2007). For instance, similar to our results with LY2109761, it has been described that Sunitinib mediates ubiquitination of IGF1R through Mdm2 (Shen et al., 2012). However, in our case was not only Mdm2 not increased but even decreased. Thus, Mdm2 did not explain the internalization regulated by TGFβ on ovarian cancer.

Afterwards, we evaluated c-cbl levels and its levels were maintained upon treatment with LY2109761 discarding this ligase of controlling IGF1R by TGFβ. Moreover, while Mdm2-mediated IGF1R ubiquitination targeted the receptor to endosomes, c-Cbl–mediated IGF1R ubiquitination was internalized via the caveolin/lipid raft route in a depending manner (Sehat et al., 2008; Goh and Sorkin, 2013), therefore results were consistent as caveolin was not increased either.

Finally, there are several leads for future studies. For example, the other E3 that could be responsible for IGF1R internalization is Nedd4. It has been shown that Grb10 binds the E3 ubiquitin ligase Nedd4 and promotes IGF1-stimulated ubiquitination, internalization, and degradation of the IGF1R, thereby giving rise to long-term attenuation of the signalling (Monami et al., 2008). Another mechanism that exists is the DUB system, which can control this lysosomal trafficking. It has been seen in gliomas that a DUB stabilizes TGFβRII (Eichhorn et al., 2012). By now, we do not know if a similar system is controlling IGF1R internalization in our case. Although, we do not know which factor is controlling the internalization of IGF1R by TGFβ signalling, there are still some mechanisms to evaluate in the future. Another question that remains unanswered until we identify the target is if stimulation or inhibition of TGFβ is affecting the effector at transcriptional or post-transcriptional level.

Right now, what we know for sure is that the two molecular mechanisms of controlling IGF1R levels can coexist in some tumoral cell types or one can predominate over the other. Thus, in OVA17 tumours and the SKOV3 cell line, mRNA levels are not affected by TGFβ while post-translational mechanisms are predominant. In contrast, in OVA8, OVA15 and A2780 cells TGFβ controls both IGF1R mRNA levels and protein recycling (Figure D2).

Interestingly, OVA8 and OVA15 tumours have high percentatge of IGF1R positivity in the nuclear cell compartment but no presence in the membrane compartment. In contrast, OVA17 tumour samples have IGF1R membrane localization and low percentatge of IGF1R positivity in the nuclear compartment. At that moment, the implication of IGF1R in different cell compartments remained unanswered. Nevertheless, these results suggest that TGFβ control of proliferation through IGF1R by one mechanism or the other can be determined depending on IGF1R inicial localization.

However, the important point is that TGFβ always positively controls IGF1R levels in ovarian cancer cells. To our knowledge, this is one of the first times that TGFβ has been shown to directly control IGF1R protein levels in tumoral cells.

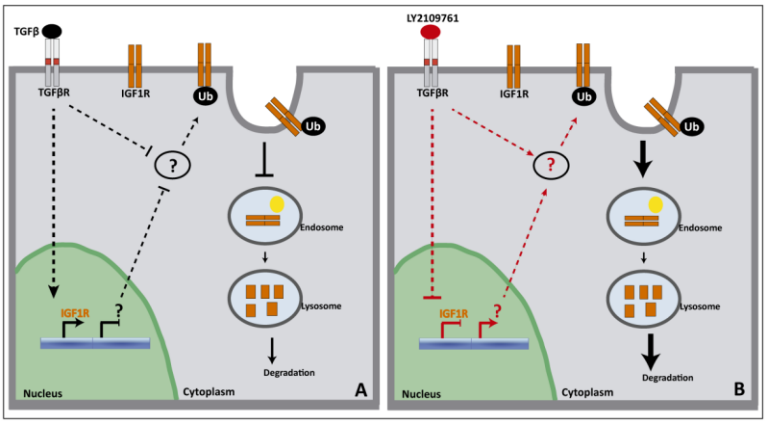

Figure D2. Schematic representation of how TGFβ controls IGF1R expression levels through mRNA and Lysosomal degradation. A) TGFβ stimulation is up-regulating IGF1R mRNA levels on some cells and in other type of cells is affecting a modulator that decreases protein IGF1R degradation levels or both mechanisms can coexist in some tumoral cell types. B) TGFβ inhibition is t down-regulating IGF1R mRNA levels in some cells and in other type of cells is affecting a modulator that increases IGF1R degradation or both mechanisms can coexist in some tumoral cell types.

2.3 Ovarian cancer cells are IGF1R-dependent.

IGF1R plays an important role in the progression of various cancers, including those of the ovary (Pollak, 2012; Bruchim and Werner, 2013),

which is confirmed in our ovarian cancer models. Several clinical trials are evaluating the effect of IGF1R inhibitors in different tumours, ovarian cancers included.

In order to confirm the dependence of the orthotopics tumour mouse models on IGF1R, we evaluated the effect of the anti-IGF1R treatment on two of the three mouse models. We obtained the same result in our mouse experiments treating animals with inhibitors against IGF1R, the blocking antibody IMC-A12 (Cixutumumab) and linsitinib (OSI-906), an inhibitor of the tyrosine kinase of the insulin and IGF1 receptors as both treatments reduced tumour growth by 40 and 60% respectively. Although, it is important to emphasise that both treatments decreased mouse body weight by 8-14%, an important reduction, which can be considered as an important side effect that must be considered in the clinic. Taking these unwanted effects into account, our results indicate that TGFβ inhibitors could be considered for treatment as it showed less toxicity than other treatments, proved in our mouse models, while producing similar anti-tumoral effects (40-60% tumour size reduction), at least in ovarian carcinomas.

Interestingly, it has been published that EMT predicts sensitivity to OSI-906 treatment and that increased phosphorylation of IGF1R/IR and sensitivity to OSI-906 is associated with an epithelial phenotype (Buck et al., 2008). In addition, highly expression of E-cadherin positively correlated with cell sensitivity to OSI-906 and induction of EMT upon treatment with TGFβ reduced sensitivity to OSI-906 (Zhao et al., 2012). This reinforces our results that both pathways are related and we believe that in this case TGFβ is playing a more important role on OSI-906 sensitivity than just the induction of the EMT phenotype.

To sum up, we have demonstrated that ovarian cancer tumours have TGFβ signalling pathway highly activated and for this reason, treatment with TGFβRII inhibitor reduced tumour size by a decrease in cell proliferation rate in two high-grade serous and one endometrioid tumour models. In addition, we have described that TGFβ control of proliferation is attributable to IGF1R

expression levels which is controlled by TGFβ signalling at transcriptional and post-transcriptional level through the lysosome.

It would be appropriate to confirm if the affectivity of the inhibitor depends on pathway activation of either TGFβ or IGF1R, or both pathways at the same time. Through our work we know that lack of IGF1R in tumour patients would result in loss of LY2109761 affectivity. At which activation level of the pathway LY2109761 will continue being effective is still unknown. Overall, our results indicate that inhibitors of the TGFβ signalling pathway could be a therapeutic alternative for the treatment of ovarian tumours in which IGF1R plays a key role. However, it would be critical to better understand the mechanism of action.

A better knowledge of the treatment and its molecular mechanism would be essential in order to provide better patient stratification and elucidate possible resistance that may arise. In other therapies, when pre-clinical studies, with promising results, got into the clinic, they failed due to a bad stratification or wrong target detection. It is known that not all patients respond the same way to some target therapies and in the case of ovarian cancer it is even worse, as all patients are treated the same even though we know that there are different histological subtypes. Moreover, it is often clear that one therapy would not be enough to cure cancer and a combination of different drugs will be needed to improve the survival of cancer patients. Recently, it has been demonstrated in ovarian cancer cell lines that a combination of LY2109761 and CDDP had more anti-proliferative effects than the sum of each treatment alone and promoted tumour regression in established parental and resistant ovarian cancer xenograft models. Thus, LY2109761 may enhance the treatment benefit of the CDDP, which is the standard treatment to date, for ovarian cancer patients (Gao et al., 2015).

For all, we hope that more pre-clinical and clinical trials with new possible therapies will be carried out for ovarian cancer patients because new therapies are even more essential as 80% of patients of ovarian cancer relapse within five years.

Conclusions

Conclusions

The lack of ALK1 half dose causes hyper-vascularisation and an increase in vessel width. This effect is the result of an increase in endothelial cell number due to an increase on endothelial cell proliferation in the second line of the sprouting front.

ALK1 represses endothelial cell proliferation through the negative control of PI3K activity. Pharmacological o genetic inhibition of PI3K signalling pathway produces a vessel normalisation on $ALK1^{+/-}$ retinas. This postulates PI3K or AKT inhibitors for the treatment of HHT patients.

The TGFβ signalling pathway is present on human normal gynaecological tissue and ovarian cancer samples as indicated by high pSmad2 expression levels.

The inhibition of TGFβ signalling pathway impaired ovarian tumour growth by controlling tumour cell proliferation in three orthotopic ovarian cancer mouse models.

TGFβ controls cell proliferation by regulating IGF1R mRNA and protein levels. In addition, IGF1R expression is required for TGFβ inhibition to decrease tumour growth.

References

References

Adams RH, Alitalo K. 2007. Molecular regulation of angiogenesis and lymphangiogenesis. Nat Rev Mol Cell Biol 8:464-478.

Adams TE, Epa VC, Garrett TP, Ward CW. 2000. Structure and function of the type 1 insulin-like growth factor receptor. Cell Mol Life Sci 57:1050-1093.

Akhurst RJ, Hata A. 2012. Targeting the TGFbeta signalling pathway in disease. Nat Rev Drug Discov 11:790-811.

Alberts DS, Liu PY, Wilczynski SP, Clouser MC, Lopez AM, Michelin DP, Lanzotti VJ, Markman M. 2008. Randomized trial of pegylated liposomal doxorubicin (PLD) plus carboplatin versus carboplatin in platinum-sensitive (PS) patients with recurrent epithelial ovarian or peritoneal carcinoma after failure of initial platinum-based chemotherapy (Southwest Oncology Group Protocol S0200). Gynecol Oncol 108:90-94.

Anido J, Saez-Borderias A, Gonzalez-Junca A, Rodon L, Folch G, Carmona MA, Prieto-Sanchez RM, Barba I, Martinez-Saez E, Prudkin L, Cuartas I, Raventos C, Martinez-Ricarte F, Poca MA, Garcia-Dorado D, Lahn MM, Yingling JM, Rodon J, Sahuquillo J, Baselga J, Seoane J. 2010. TGF-beta Receptor Inhibitors Target the CD44(high)/Id1(high) Glioma-Initiating Cell Population in Human Glioblastoma. Cancer Cell 18:655-668.

Backen A, Renehan AG, Clamp AR, Berzuini C, Zhou C, Oza A, Bannoo S, Scherer SJ, Banks RE, Dive C, Jayson GC. 2014. The combination of circulating Ang1 and Tie2 levels predicts progression-free survival advantage in bevacizumab-treated patients with ovarian cancer. Clin Cancer Res 20:4549-4558.

Bakin AV, Tomlinson AK, Bhowmick NA, Moses HL, Arteaga CL. 2000. Phosphatidylinositol 3-kinase function is required for transforming growth factor beta-mediated epithelial to mesenchymal transition and cell migration. J Biol Chem 275:36803-36810.

Banerjee S, Kaye SB. 2013. New strategies in the treatment of ovarian cancer: current clinical perspectives and future potential. Clin Cancer Res 19:961-968.

Bartelmez SH, Sacca R, Stanley ER. 1985. Lineage specific receptors used to identify a growth factor for developmentally early hemopoietic cells: assay of hemopoietin-2. J Cell Physiol 122:362-369.

Baserga R. 1999. The IGF-I receptor in cancer research. Exp Cell Res 253:1-6.

Bast RC, Jr., Feeney M, Lazarus H, Nadler LM, Colvin RB, Knapp RC. 1981. Reactivity of a monoclonal antibody with human ovarian carcinoma. J Clin Invest 68:1331-1337.

Bell D, Berchuck A, Birrer M, Chien J, Cramer D, Dao F. 2011. Integrated genomic analyses of ovarian carcinoma. Nature 474:609-615.

Bernabeu C, Lopez-Novoa JM, Quintanilla M. 2009. The emerging role of TGF-beta superfamily coreceptors in cancer. Biochim Biophys Acta 1792:954-973.

Berrino F, De Angelis R, Sant M, Rosso S, Bielska-Lasota M, Coebergh JW, Santaquilani M. 2007. Survival for eight major cancers and all cancers

combined for European adults diagnosed in 1995-99: results of the EUROCARE-4 study. Lancet Oncol 8:773-783.

Bertolino P, Deckers M, Lebrin F, ten Dijke P. 2005. Transforming growth factor-beta signal transduction in angiogenesis and vascular disorders. Chest 128:585S-590S.

Bhola NE, Balko JM, Dugger TC, Kuba MG, Sanchez V, Sanders M, Stanford J, Cook RS, Arteaga CL. 2013. TGF-beta inhibition enhances chemotherapy action against triple-negative breast cancer. J Clin Invest 123:1348-1358.

Blanco R, Gerhardt H. 2013. VEGF and Notch in tip and stalk cell selection. Cold Spring Harb Perspect Med 3:a006569.

Bogdahn U, Hau P, Stockhammer G, Venkataramana NK, Mahapatra AK, Suri A, Balasubramaniam A, Nair S, Oliushine V, Parfenov V, Poverennova I, Zaaroor M, Jachimczak P, Ludwig S, Schmaus S, Heinrichs H, Schlingensiepen KH. 2011. Targeted therapy for high-grade glioma with the TGF-beta2 inhibitor trabedersen: results of a randomized and controlled phase IIb study. Neuro Oncol 13:132-142.

Bouquet F, Pal A, Pilones KA, Demaria S, Hann B, Akhurst RJ, Babb JS, Lonning SM, DeWyngaert JK, Formenti SC, Barcellos-Hoff MH. 2011. TGFbeta1 inhibition increases the radiosensitivity of breast cancer cells in vitro and promotes tumor control by radiation in vivo. Clin Cancer Res 17:6754-6765.

Bruchim I, Werner H. 2013. Targeting IGF-1 signaling pathways in gynecologic malignancies. Expert Opin Ther Targets 17:307-320.

Bruna A, Darken RS, Rojo F, Ocana A, Penuelas S, Arias A, Paris R, Tortosa A, Mora J, Baselga J, Seoane J. 2007. High TGFbeta-Smad activity confers poor prognosis in glioma patients and promotes cell proliferation depending on the methylation of the PDGF-B gene. Cancer Cell 11:147-160.

Buck E, Eyzaguirre A, Rosenfeld-Franklin M, Thomson S, Mulvihill M, Barr S, Brown E, O'Connor M, Yao Y, Pachter J, Miglarese M, Epstein D, Iwata KK, Haley JD, Gibson NW, Ji QS. 2008. Feedback mechanisms promote cooperativity for small molecule inhibitors of epidermal and insulin-like growth factor receptors. Cancer Res 68:8322-8332.

Buck E, Gokhale PC, Koujak S, Brown E, Eyzaguirre A, Tao N, Rosenfeld-Franklin M, Lerner L, Chiu MI, Wild R, Epstein D, Pachter JA, Miglarese MR. 2010. Compensatory insulin receptor (IR) activation on inhibition of insulin-like growth factor-1 receptor (IGF-1R): rationale for cotargeting IGF-1R and IR in cancer. Mol Cancer Ther 9:2652-2664.

Cabanes A, Vidal E, Aragones N, Perez-Gomez B, Pollan M, Lope V, Lopez-Abente G. 2010. Cancer mortality trends in Spain: 1980-2007. Ann Oncol 21 Suppl 3:iii14-20.

Cannistra SA. 2004. Cancer of the ovary. N Engl J Med 351:2519-2529.

Cannistra SA. 2007. BRCA-1 in sporadic epithelial ovarian cancer: lessons learned from the genetics of hereditary disease. Clin Cancer Res 13:7225-7227.

Cao L, Shao M, Schilder J, Guise T, Mohammad KS, Matei D. 2012. Tissue transglutaminase links TGF-beta, epithelial to mesenchymal transition and a stem cell phenotype in ovarian cancer. Oncogene 31:2521-2534.

Carmeliet P. 2000. Mechanisms of angiogenesis and arteriogenesis. Nat Med 6:389-395.

Carmeliet P, De Smet F, Loges S, Mazzone M. 2009. Branching morphogenesis and antiangiogenesis candidates: tip cells lead the way. Nat Rev Clin Oncol 6:315-326.

Carmeliet P, Ferreira V, Breier G, Pollefeyt S, Kieckens L, Gertsenstein M, Fahrig M, Vandenhoeck A, Harpal K, Eberhardt C, Declercq C, Pawling J, Moons L, Collen D, Risau W, Nagy A. 1996. Abnormal blood vessel development and lethality in embryos lacking a single VEGF allele. Nature 380:435-439.

Casagrande JT, Louie EW, Pike MC, Roy S, Ross RK, Henderson BE. 1979. "Incessant ovulation" and ovarian cancer. Lancet 2:170-173.

Catasus L, Bussaglia E, Rodrguez I, Gallardo A, Pons C, Irving JA, Prat J. 2004. Molecular genetic alterations in endometrioid carcinomas of the ovary: similar frequency of beta-catenin abnormalities but lower rate of microsatellite instability and PTEN alterations than in uterine endometrioid carcinomas. Hum Pathol 35:1360-1368.

Celada A, Maki RA. 1992. Transforming growth factor-beta enhances the M-CSF and GM-CSF-stimulated proliferation of macrophages. J Immunol 148:1102-1105.

Clayton PE, Banerjee I, Murray PG, Renehan AG. 2011. Growth hormone, the insulin-like growth factor axis, insulin and cancer risk. Nat Rev Endocrinol 7:11-24.

Conic I, Dimov I, Tasic-Dimov D, Djordjevic B, Stefanovic V. 2011. Ovarian epithelial cancer stem cells. ScientificWorldJournal 11:1243-1269.

Connolly EC, Freimuth J, Akhurst RJ. 2012. Complexities of TGF-beta targeted cancer therapy. Int J Biol Sci 8:964-978.

Connolly EC, Saunier EF, Quigley D, Luu MT, De Sapio A, Hann B, Yingling JM, Akhurst RJ. 2011. Outgrowth of drug-resistant carcinomas expressing markers of tumor aggression after long-term TbetaRI/II kinase inhibition with LY2109761. Cancer Res 71:2339-2349.

Cuatrecasas M, Villanueva A, Matias-Guiu X, Prat J. 1997. K-ras mutations in mucinous ovarian tumors: a clinicopathologic and molecular study of 95 cases. Cancer 79:1581-1586.

Cullen KJ, Yee D, Sly WS, Perdue J, Hampton B, Lippman ME, Rosen N. 1990. Insulin-like growth factor receptor expression and function in human breast cancer. Cancer Res 50:48-53.

Cunha SI, Pietras K. 2011. ALK1 as an emerging target for antiangiogenic therapy of cancer. Blood 117:6999-7006.

Chambers SK, Kacinski BM, Ivins CM, Carcangiu ML. 1997. Overexpression of epithelial macrophage colony-stimulating factor (CSF-1) and CSF-1

receptor: a poor prognostic factor in epithelial ovarian cancer, contrasted with a protective effect of stromal CSF-1. Clin Cancer Res 3:999-1007.

Chan WY, Cheung KK, Schorge JO, Huang LW, Welch WR, Bell DA, Berkowitz RS, Mok SC. 2000. Bcl-2 and p53 protein expression, apoptosis, and p53 mutation in human epithelial ovarian cancers. Am J Pathol 156:409-417.

Chavan A, Schumann-Binarsch S, Luthe L, Nickau B, Elsasser A, Kuhnel T, Geisthoff U, Kohne H. 2013. Systemic therapy with bevacizumab in patients with hereditary hemorrhagic telangiectasia (HHT). Vasa 42:106-110.

Cheifetz S, Massague J. 1989. Transforming growth factor-beta (TGF-beta) receptor proteoglycan. Cell surface expression and ligand binding in the absence of glycosaminoglycan chains. J Biol Chem 264:12025-12028.

Chi DS, Musa F, Dao F, Zivanovic O, Sonoda Y, Leitao MM, Levine DA, Gardner GJ, Abu-Rustum NR, Barakat RR. 2011. An analysis of patients with bulky advanced stage ovarian, tubal, and peritoneal carcinoma treated with primary debulking surgery (PDS) during an identical time period as the randomized EORTC-NCIC trial of PDS vs neoadjuvant chemotherapy (NACT). Gynecol Oncol 124:10-14.

Cho KR, Shih Ie M. 2009. Ovarian cancer. Annu Rev Pathol 4:287-313.

Choi SH, Kwon OJ, Park JY, Kim do Y, Ahn SH, Kim SU, Ro SW, Kim KS, Park JH, Kim S, Yun CO, Han KH. 2014. Inhibition of tumour angiogenesis and growth by small hairpin HIF-1alpha and IL-8 in hepatocellular carcinoma. Liver Int 34:632-642.

Christiansen J, Rajasekaran AK. 2004. Biological impediments to monoclonal antibody-based cancer immunotherapy. Mol Cancer Ther 3:1493-1501.

Daniilidis A, Karagiannis V. 2007. Epithelial ovarian cancer. Risk factors, screening and the role of prophylactic oophorectomy. Hippokratia 11:63-66.

David L, Mallet C, Keramidas M, Lamande N, Gasc JM, Dupuis-Girod S, Plauchu H, Feige JJ, Bailly S. 2008. Bone morphogenetic protein-9 is a circulating vascular quiescence factor. Circ Res 102:914-922.

David L, Mallet C, Vailhe B, Lamouille S, Feige JJ, Bailly S. 2007. Activin receptor-like kinase 1 inhibits human microvascular endothelial cell migration: potential roles for JNK and ERK. J Cell Physiol 213:484-489.

Davies LC, Rosas M, Jenkins SJ, Liao CT, Scurr MJ, Brombacher F, Fraser DJ, Allen JE, Jones SA, Taylor PR. 2013. Distinct bone marrow-derived and tissue-resident macrophage lineages proliferate at key stages during inflammation. Nat Commun 4:1886.

De Bock K, De Smet F, Leite De Oliveira R, Anthonis K, Carmeliet P. 2009. Endothelial oxygen sensors regulate tumor vessel abnormalization by instructing phalanx endothelial cells. J Mol Med (Berl) 87:561-569.

Dejana E, Orsenigo F, Molendini C, Baluk P, McDonald DM. 2009. Organization and signaling of endothelial cell-to-cell junctions in various regions of the blood and lymphatic vascular trees. Cell Tissue Res 335:17-25.

Della Pepa C, Tonini G, Pisano C, Di Napoli M, Cecere SC, Tambaro R, Facchini G, Pignata S. 2015. Ovarian cancer standard of care: are there real alternatives? Chin J Cancer 34:17-27.

Denton CP, Merkel PA, Furst DE, Khanna D, Emery P, Hsu VM, Silliman N, Streisand J, Powell J, Akesson A, Coppock J, Hoogen F, Herrick A, Mayes MD, Veale D, Haas J, Ledbetter S, Korn JH, Black CM, Seibold JR. 2007. Recombinant human anti-transforming growth factor beta1 antibody therapy in systemic sclerosis: a multicenter, randomized, placebo-controlled phase I/II trial of CAT-192. Arthritis Rheum 56:323-333.

Derynck R, Akhurst RJ, Balmain A. 2001. TGF-beta signaling in tumor suppression and cancer progression. Nat Genet 29:117-129.

Derynck R, Feng XH. 1997. TGF-beta receptor signaling. Biochim Biophys Acta 1333:F105-150.

Diaz-Padilla I, Malpica AL, Minig L, Chiva LM, Gershenson DM, Gonzalez-Martin A. 2012. Ovarian low-grade serous carcinoma: a comprehensive update. Gynecol Oncol 126:279-285.

Dixelius J, Makinen T, Wirzenius M, Karkkainen MJ, Wernstedt C, Alitalo K, Claesson-Welsh L. 2003. Ligand-induced vascular endothelial growth factor receptor-3 (VEGFR-3) heterodimerization with VEGFR-2 in primary lymphatic endothelial cells regulates tyrosine phosphorylation sites. J Biol Chem 278:40973-40979.

Doufekas K, Olaitan A. 2014. Clinical epidemiology of epithelial ovarian cancer in the UK. Int J Womens Health 6:537-545.

du Bois A, Luck HJ, Meier W, Adams HP, Mobus V, Costa S, Bauknecht T, Richter B, Warm M, Schroder W, Olbricht S, Nitz U, Jackisch C, Emons G, Wagner U, Kuhn W, Pfisterer J. 2003. A randomized clinical trial of cisplatin/paclitaxel versus carboplatin/paclitaxel as first-line treatment of ovarian cancer. J Natl Cancer Inst 95:1320-1329.

Dupre S, Urban-Grimal D, Haguenauer-Tsapis R. 2004. Ubiquitin and endocytic internalization in yeast and animal cells. Biochim Biophys Acta 1695:89-111.

Dupuis-Girod S, Ginon I, Saurin JC, Marion D, Guillot E, Decullier E, Roux A, Carette MF, Gilbert-Dussardier B, Hatron PY, Lacombe P, Lorcerie B, Riviere S, Corre R, Giraud S, Bailly S, Paintaud G, Ternant D, Valette PJ, Plauchu H, Faure F. 2012. Bevacizumab in patients with hereditary hemorrhagic telangiectasia and severe hepatic vascular malformations and high cardiac output. JAMA 307:948-955.

Eichhorn PJ, Rodon L, Gonzalez-Junca A, Dirac A, Gili M, Martinez-Saez E, Aura C, Barba I, Peg V, Prat A, Cuartas I, Jimenez J, Garcia-Dorado D, Sahuquillo J, Bernards R, Baselga J, Seoane J. 2012. USP15 stabilizes TGF-beta receptor I and promotes oncogenesis through the activation of TGF-beta signaling in glioblastoma. Nat Med 18:429-435.

Engelman JA, Luo J, Cantley LC. 2006. The evolution of phosphatidylinositol 3-kinases as regulators of growth and metabolism. Nat Rev Genet 7:606-619.

Fang S, Salven P. 2011. Stem cells in tumor angiogenesis. J Mol Cell Cardiol 50:290-295.

Farley J, Brady WE, Vathipadiekal V, Lankes HA, Coleman R, Morgan MA, Mannel R, Yamada SD, Mutch D, Rodgers WH, Birrer M, Gershenson DM. 2012. Selumetinib in women with recurrent low-grade serous carcinoma of the ovary or peritoneum: an open-label, single-arm, phase 2 study. Lancet Oncol 14:134-140.

Feeley KM, Wells M. 2001. Precursor lesions of ovarian epithelial malignancy. Histopathology 38:87-95.

Ferlay J, Parkin DM, Steliarova-Foucher E. 2010. Estimates of cancer incidence and mortality in Europe in 2008. Eur J Cancer 46:765-781.

Ferrara N. 1996. Vascular endothelial growth factor. Eur J Cancer 32A:2413-2422.

Fogh J. 1975. **Human Tumor Cells In Vitro**. Plenum Press: New York pp. 115–159.

Foley OW, Rauh-Hain JA, del Carmen MG. 2013. Recurrent epithelial ovarian cancer: an update on treatment. Oncology (Williston Park) 27:288-294, 298.

Foukas LC, Claret M, Pearce W, Okkenhaug K, Meek S, Peskett E, Sancho S, Smith AJ, Withers DJ, Vanhaesebroeck B. 2006. Critical role for the p110alpha phosphoinositide-3-OH kinase in growth and metabolic regulation. Nature 441:366-370.

Fountain J, Trimble E, Birrer MJ. 2006. Summary and discussion of session recommendations. Gynecol Oncol 103:S23-25.

Frasca F, Pandini G, Sciacca L, Pezzino V, Squatrito S, Belfiore A, Vigneri R. 2008. The role of insulin receptors and IGF-I receptors in cancer and other diseases. Arch Physiol Biochem 114:23-37.

Fritsche HA, Bast RC. 1998. CA 125 in ovarian cancer: advances and controversy. Clin Chem 44:1379-1380.

Fruttiger M, Calver AR, Kruger WH, Mudhar HS, Michalovich D, Takakura N, Nishikawa S, Richardson WD. 1996. PDGF mediates a neuron-astrocyte interaction in the developing retina. Neuron 17:1117-1131.

Funaki B. 2007. Embolization of pulmonary arteriovenous malformations. Semin Intervent Radiol 24:350-355.

Gabrusiewicz K, Hossain MB, Cortes-Santiago N, Fan X, Kaminska B, Marini FC, Fueyo J, Gomez-Manzano C. 2015. Macrophage Ablation Reduces M2-Like Populations and Jeopardizes Tumor Growth in a MAFIA-Based Glioma Model. Neoplasia 17:374-384.

Galic V, Willner J, Wollan M, Garg R, Garcia R, Goff BA, Gray HJ, Swisher EM. 2007. Common polymorphisms in TP53 and MDM2 and the relationship to TP53 mutations and clinical outcomes in women with ovarian and peritoneal carcinomas. Genes Chromosomes Cancer 46:239-247.

Galluzzi L, Senovilla L, Vitale I, Michels J, Martins I, Kepp O, Castedo M, Kroemer G. 2012. Molecular mechanisms of cisplatin resistance. Oncogene 31:1869-1883.

Ganapathy V, Ge R, Grazioli A, Xie W, Banach-Petrosky W, Kang Y, Lonning S, McPherson J, Yingling JM, Biswas S, Mundy GR, Reiss M. 2010. Targeting the Transforming Growth Factor-beta pathway inhibits human basal-like breast cancer metastasis. Mol Cancer 9:122.

Gao Y, Shan N, Zhao C, Wang Y, Xu F, Li J, Yu X, Gao L, Yi Z. 2015. LY2109761 enhances cisplatin antitumor activity in ovarian cancer cells. Int J Clin Exp Pathol 8:4923-4932.

George SH, Shaw P. 2014. BRCA and Early Events in the Development of Serous Ovarian Cancer. Front Oncol 4:5.

Gerhardt H, Golding M, Fruttiger M, Ruhrberg C, Lundkvist A, Abramsson A, Jeltsch M, Mitchell C, Alitalo K, Shima D, Betsholtz C. 2003. VEGF guides angiogenic sprouting utilizing endothelial tip cell filopodia. J Cell Biol 161:1163-1177.

Girnita L, Girnita A, Larsson O. 2003. Mdm2-dependent ubiquitination and degradation of the insulin-like growth factor 1 receptor. Proc Natl Acad Sci U S A 100:8247-8252.

Girnita L, Shenoy SK, Sehat B, Vasilcanu R, Girnita A, Lefkowitz RJ, Larsson O. 2005. {beta}-Arrestin is crucial for ubiquitination and down-regulation of the insulin-like growth factor-1 receptor by acting as adaptor for the MDM2 E3 ligase. J Biol Chem 280:24412-24419.

Girnita L, Shenoy SK, Sehat B, Vasilcanu R, Vasilcanu D, Girnita A, Lefkowitz RJ, Larsson O. 2007. Beta-arrestin and Mdm2 mediate IGF-1 receptor-stimulated ERK activation and cell cycle progression. J Biol Chem 282:11329-11338.

Girnita L, Worrall C, Takahashi S, Seregard S, Girnita A. 2013. Something old, something new and something borrowed: emerging paradigm of insulin-like growth factor type 1 receptor (IGF-1R) signaling regulation. Cell Mol Life Sci 71:2403-2427.

Goff BA, Mandel L, Muntz HG, Melancon CH. 2000. Ovarian carcinoma diagnosis. Cancer 89:2068-2075.

Goh LK, Sorkin A. 2013. Endocytosis of receptor tyrosine kinases. Cold Spring Harb Perspect Biol 5:a017459.

Gold LI, Jussila T, Fusenig NE, Stenback F. 2000. TGF-beta isoforms are differentially expressed in increasing malignant grades of HaCaT keratinocytes, suggesting separate roles in skin carcinogenesis. J Pathol 190:579-588.

Gooch JL, Van Den Berg CL, Yee D. 1999. Insulin-like growth factor (IGF)-I rescues breast cancer cells from chemotherapy-induced cell death--proliferative and anti-apoptotic effects. Breast Cancer Res Treat 56:1-10.

Goumans MJ, Mummery C. 2000. Functional analysis of the TGFbeta receptor/Smad pathway through gene ablation in mice. Int J Dev Biol 44:253-265.

Govani FS, Shovlin CL. 2009. Hereditary haemorrhagic telangiectasia: a clinical and scientific review. Eur J Hum Genet 17:860-871.

Graupera M, Potente M. 2013. Regulation of angiogenesis by PI3K signaling networks. Exp Cell Res 319:1348-1355.

Guo J, Xia B, Meng F, Lou G. 2013. miR-133a suppresses ovarian cancer cell proliferation by directly targeting insulin-like growth factor 1 receptor. Tumour Biol 35:1557-1564.

Halme J, Hammond MG, Hulka JF, Raj SG, Talbert LM. 1984. Retrograde menstruation in healthy women and in patients with endometriosis. Obstet Gynecol 64:151-154.

Han C, Choe SW, Kim YH, Acharya AP, Keselowsky BG, Sorg BS, Lee YJ, Oh SP. 2014. VEGF neutralization can prevent and normalize arteriovenous malformations in an animal model for hereditary hemorrhagic telangiectasia 2. Angiogenesis 17:823-830.

Hao Q, Zhu Y, Su H, Shen F, Yang GY, Kim H, Young WL. 2010. VEGF Induces More Severe Cerebrovascular Dysplasia in Endoglin than in Alk1 Mice. Transl Stroke Res 1:197-201.

Hassan AB, Macaulay VM. 2002. The insulin-like growth factor system as a therapeutic target in colorectal cancer. Ann Oncol 13:349-356.

Heldin CH, Miyazono K, ten Dijke P. 1997. TGF-beta signalling from cell membrane to nucleus through SMAD proteins. Nature 390:465-471.

Helleman J, Smid M, Jansen MP, van der Burg ME, Berns EM. 2010. Pathway analysis of gene lists associated with platinum-based chemotherapy resistance in ovarian cancer: the big picture. Gynecol Oncol 117:170-176.

Henriksen R, Gobl A, Wilander E, Oberg K, Miyazono K, Funa K. 1995. Expression and prognostic significance of TGF-beta isotypes, latent TGF-beta 1 binding protein, TGF-beta type I and type II receptors, and endoglin in normal ovary and ovarian neoplasms. Lab Invest 73:213-220.

Herrera B, van Dinther M, Ten Dijke P, Inman GJ. 2009. Autocrine bone morphogenetic protein-9 signals through activin receptor-like kinase-2/Smad1/Smad4 to promote ovarian cancer cell proliferation. Cancer Res 69:9254-9262.

Herzog TJ. 2004. Recurrent ovarian cancer: how important is it to treat to disease progression? Clin Cancer Res 10:7439-7449.

Higano CS, Berlin J, Gordon M, LoRusso P, Tang S, Dontabhaktuni A, Schwartz JD, Cosaert J, Mehnert JM. 2015. Safety, tolerability, and pharmacokinetics of single and multiple doses of intravenous cixutumumab (IMC-A12), an inhibitor of the insulin-like growth factor-I receptor, administered weekly or every 2 weeks in patients with advanced solid tumors. Invest New Drugs 33:450-462.

Hsu CY, Bristow R, Cha MS, Wang BG, Ho CL, Kurman RJ, Wang TL, Shih Ie M. 2004. Characterization of active mitogen-activated protein kinase in ovarian serous carcinomas. Clin Cancer Res 10:6432-6436.

Huang F, Chen YG. 2012. Regulation of TGF-beta receptor activity. Cell Biosci 2:9.

Huang X, Huang G, Song H, Chen L. 2010. Preconditioning chemotherapy with paclitaxel and cisplatin enhances the antitumor activity of cytokine induced-killer cells in a murine lung carcinoma model. Int J Cancer 129:648-658.

Huse M, Muir TW, Xu L, Chen YG, Kuriyan J, Massague J. 2001. The TGF beta receptor activation process: an inhibitor- to substrate-binding switch. Mol Cell 8:671-682.

Ibrahimi A, Vande Velde G, Reumers V, Toelen J, Thiry I, Vandeputte C, Vets S, Deroose C, Bormans G, Baekelandt V, Debyser Z, Gijsbers R. 2009. Highly efficient multicistronic lentiviral vectors with peptide 2A sequences. Hum Gene Ther 20:845-860.

Ide H, Seligson DB, Memarzadeh S, Xin L, Horvath S, Dubey P, Flick MB, Kacinski BM, Palotie A, Witte ON. 2002. Expression of colony-stimulating factor 1 receptor during prostate development and prostate cancer progression. Proc Natl Acad Sci U S A 99:14404-14409.

Ikushima H, Miyazono K. 2010. TGFbeta signalling: a complex web in cancer progression. Nat Rev Cancer 10:415-424.

Illum P, Bjerring P. 1988. Hereditary hemorrhagic telangiectasia treated by laser surgery. Rhinology 26:19-24.

Inaba T, Ishibashi S, Harada K, Osuga J, Yagyu H, Ohashi K, Yazaki Y, Yamada N. 1996. Synergistic effects of transforming growth factor-beta on the expression of c-fms, macrophage colony-stimulating factor receptor gene, in vascular smooth muscle cells. FEBS Lett 399:207-210.

Jakobsson L, Franco CA, Bentley K, Collins RT, Ponsioen B, Aspalter IM, Rosewell I, Busse M, Thurston G, Medvinsky A, Schulte-Merker S, Gerhardt H. 2010. Endothelial cells dynamically compete for the tip cell position during angiogenic sprouting. Nat Cell Biol 12:943-953.

Jensen MM, Jorgensen JT, Binderup T, Kjaer A. 2008. Tumor volume in subcutaneous mouse xenografts measured by microCT is more accurate and reproducible than determined by 18F-FDG-microPET or external caliper. BMC Med Imaging 8:16.

Johnson DW, Berg JN, Baldwin MA, Gallione CJ, Marondel I, Yoon SJ, Stenzel TT, Speer M, Pericak-Vance MA, Diamond A, Guttmacher AE, Jackson CE, Attisano L, Kucherlapati R, Porteous ME, Marchuk DA. 1996. Mutations in the activin receptor-like kinase 1 gene in hereditary haemorrhagic telangiectasia type 2. Nat Genet 13:189-195.

Jussila L, Alitalo K. 2002. Vascular growth factors and lymphangiogenesis. Physiol Rev 82:673-700.

Kacinski BM, Carter D, Kohorn EI, Mittal K, Bloodgood RS, Donahue J, Kramer CA, Fischer D, Edwards R, Chambers SK, et al. 1989a. Oncogene expression in vivo by ovarian adenocarcinomas and mixed-mullerian tumors. Yale J Biol Med 62:379-392.

Kacinski BM, Stanley ER, Carter D, Chambers JT, Chambers SK, Kohorn EI, Schwartz PE. 1989b. Circulating levels of CSF-1 (M-CSF) a lymphohematopoietic cytokine may be a useful marker of disease status in patients with malignant ovarian neoplasms. Int J Radiat Oncol Biol Phys 17:159-164.

Kaipainen A, Korhonen J, Mustonen T, van Hinsbergh VW, Fang GH, Dumont D, Breitman M, Alitalo K. 1995. Expression of the fms-like tyrosine kinase 4

gene becomes restricted to lymphatic endothelium during development. Proc Natl Acad Sci U S A 92:3566-3570.

Kaku T, Ogawa S, Kawano Y, Ohishi Y, Kobayashi H, Hirakawa T, Nakano H. 2003. Histological classification of ovarian cancer. Med Electron Microsc 36:9-17.

Kalluri R, Weinberg RA. 2009. The basics of epithelial-mesenchymal transition. J Clin Invest 119:1420-1428.

King ER, Zu Z, Tsang YT, Deavers MT, Malpica A, Mok SC, Gershenson DM, Wong KK. 2011. The insulin-like growth factor 1 pathway is a potential therapeutic target for low-grade serous ovarian carcinoma. Gynecol Oncol 123:13-18.

Kirma N, Hammes LS, Liu YG, Nair HB, Valente PT, Kumar S, Flowers LC, Tekmal RR. 2007. Elevated expression of the oncogene c-fms and its ligand, the macrophage colony-stimulating factor-1, in cervical cancer and the role of transforming growth factor-beta1 in inducing c-fms expression. Cancer Res 67:1918-1926.

Kong F, Tong R, Jia L, Wei W, Miao X, Zhao X, Sun W, Yang G, Zhao C. 2011. OVCA1 inhibits the proliferation of epithelial ovarian cancer cells by decreasing cyclin D1 and increasing p16. Mol Cell Biochem 354:199-205.

Koti M, Gooding RJ, Nuin P, Haslehurst A, Crane C, Weberpals J, Childs T, Bryson P, Dharsee M, Evans K, Feilotter HE, Park PC, Squire JA. 2013. Identification of the IGF1/PI3K/NF kappaB/ERK gene signalling networks associated with chemotherapy resistance and treatment response in high-grade serous epithelial ovarian cancer. BMC Cancer 13:549.

Kuhn E, Meeker AK, Visvanathan K, Gross AL, Wang TL, Kurman RJ, Shih Ie M. 2011. Telomere length in different histologic types of ovarian carcinoma with emphasis on clear cell carcinoma. Mod Pathol 24:1139-1145.

Kukk E, Lymboussaki A, Taira S, Kaipainen A, Jeltsch M, Joukov V, Alitalo K. 1996. VEGF-C receptor binding and pattern of expression with VEGFR-3 suggests a role in lymphatic vascular development. Development 122:3829-3837.

Kupryjanczyk J, Thor AD, Beauchamp R, Merritt V, Edgerton SM, Bell DA, Yandell DW. 1993. p53 gene mutations and protein accumulation in human ovarian cancer. Proc Natl Acad Sci U S A 90:4961-4965.

Kurman R. 2002. Blaustein's pathology of the female genital tract. . ed. New York: Springer-Verlag 5th.

Kwon MJ, Shin YK. 2013. Regulation of ovarian cancer stem cells or tumor-initiating cells. Int J Mol Sci 14:6624-6648.

Lacher MD, Tiirikainen MI, Saunier EF, Christian C, Anders M, Oft M, Balmain A, Akhurst RJ, Korn WM. 2006. Transforming growth factor-beta receptor inhibition enhances adenoviral infectability of carcinoma cells via up-regulation of Coxsackie and Adenovirus Receptor in conjunction with reversal of epithelial-mesenchymal transition. Cancer Res 66:1648-1657.

Lahn M, Kloeker S, Berry BS. 2005. TGF-beta inhibitors for the treatment of cancer. Expert Opin Investig Drugs 14:629-643.

Lambert HE, Berry RJ. 1985. High dose cisplatin compared with high dose cyclophosphamide in the management of advanced epithelial ovarian

cancer (FIGO stages III and IV): report from the North Thames Cooperative Group. Br Med J (Clin Res Ed) 290:889-893.

Lamouille S, Xu J, Derynck R. 2014. Molecular mechanisms of epithelial-mesenchymal transition. Nat Rev Mol Cell Biol 15:178-196.

Larrivee B, Prahst C, Gordon E, del Toro R, Mathivet T, Duarte A, Simons M, Eichmann A. 2012. ALK1 signaling inhibits angiogenesis by cooperating with the Notch pathway. Dev Cell 22:489-500.

Ledermann JA, Raja FA, Fotopoulou C, Gonzalez-Martin A, Colombo N, Sessa C. 2013. Newly diagnosed and relapsed epithelial ovarian carcinoma: ESMO Clinical Practice Guidelines for diagnosis, treatment and follow-up. Ann Oncol 24 Suppl 6:vi24-32.

Lee NY, Golzio C, Gatza CE, Sharma A, Katsanis N, Blobe GC. 2012. Endoglin regulates PI3-kinase/Akt trafficking and signaling to alter endothelial capillary stability during angiogenesis. Mol Biol Cell 23:2412-2423.

Lee Y, Miron A, Drapkin R, Nucci MR, Medeiros F, Saleemuddin A, Garber J, Birch C, Mou H, Gordon RW, Cramer DW, McKeon FD, Crum CP. 2007. A candidate precursor to serous carcinoma that originates in the distal fallopian tube. J Pathol 211:26-35.

Lefkowitz RJ. 1998. G protein-coupled receptors. III. New roles for receptor kinases and beta-arrestins in receptor signaling and desensitization. J Biol Chem 273:18677-18680.

Leiphrakpam PD, Agarwal E, Mathiesen M, Haferbier KL, Brattain MG, Chowdhury S. 2013. In vivo analysis of insulin-like growth factor type 1 receptor humanized monoclonal antibody MK-0646 and small molecule kinase inhibitor OSI-906 in colorectal cancer. Oncol Rep 31:87-94.

Li Q, Pangas SA, Jorgez CJ, Graff JM, Weinstein M, Matzuk MM. 2008. Redundant roles of SMAD2 and SMAD3 in ovarian granulosa cells in vivo. Mol Cell Biol 28:7001-7011.

Liao S, Liu J, Lin P, Shi T, Jain RK, Xu L. 2011. TGF-beta blockade controls ascites by preventing abnormalization of lymphatic vessels in orthotopic human ovarian carcinoma models. Clin Cancer Res 17:1415-1424.

Liu P, Cheng H, Roberts TM, Zhao JJ. 2009. Targeting the phosphoinositide 3-kinase pathway in cancer. Nat Rev Drug Discov 8:627-644.

Long L, Ormiston ML, Yang X, Southwood M, Graf S, Machado RD, Mueller M, Kinzel B, Yung LM, Wilkinson JM, Moore SD, Drake KM, Aldred MA, Yu PB, Upton PD, Morrell NW. 2015. Selective enhancement of endothelial BMPR-II with BMP9 reverses pulmonary arterial hypertension. Nat Med 21:777-785.

Lu Y, Ponton A, Okamoto H, Takasawa S, Herrera PL, Liu JL. 2006. Activation of the Reg family genes by pancreatic-specific IGF-I gene deficiency and after streptozotocin-induced diabetes in mouse pancreas. Am J Physiol Endocrinol Metab 291:E50-58.

Lund B, Hansen OP, Theilade K, Hansen M, Neijt JP. 1994. Phase II study of gemcitabine (2',2'-difluorodeoxycytidine) in previously treated ovarian cancer patients. J Natl Cancer Inst 86:1530-1533.

Mackay HJ, Provencheur D, Heywood M, Tu D, Eisenhauer EA, Oza AM, Meyer R. 2011. Phase ii/iii study of intraperitoneal chemotherapy after neoadjuvant chemotherapy for ovarian cancer: ncic ctg ov.21. Curr Oncol 18:84-90.

Mahmoud M, Allinson KR, Zhai Z, Oakenfull R, Ghandi P, Adams RH, Fruttiger M, Arthur HM. 2010. Pathogenesis of arteriovenous malformations in the absence of endoglin. Circ Res 106:1425-1433.

Makanya AN, Hlushchuk R, Djonov VG. 2009. Intussusceptive angiogenesis and its role in vascular morphogenesis, patterning, and remodeling. Angiogenesis 12:113-123.

Mani SA, Guo W, Liao MJ, Eaton EN, Ayyanan A, Zhou AY, Brooks M, Reinhard F, Zhang CC, Shipitsin M, Campbell LL, Polyak K, Brisken C, Yang J, Weinberg RA. 2008. The epithelial-mesenchymal transition generates cells with properties of stem cells. Cell 133:704-715.

Manning BD, Cantley LC. 2007. AKT/PKB signaling: navigating downstream. Cell 129:1261-1274.

Martinez-Palacian A, del Castillo G, Suarez-Causado A, Garcia-Alvaro M, de Morena-Frutos D, Fernandez M, Roncero C, Fabregat I, Herrera B, Sanchez A. 2013. Mouse hepatic oval cells require Met-dependent PI3K to impair TGF-beta-induced oxidative stress and apoptosis. PLoS One 8:e53108.

Massague J. 2008. TGFbeta in Cancer. Cell 134:215-230.

Massague J, Gomis RR. 2006. The logic of TGFbeta signaling. FEBS Lett 580:2811-2820.

Massoner P, Ladurner Rennau M, Heidegger I, Kloss-Brandstatter A, Summerer M, Reichhart E, Schafer G, Klocker H. 2011. Expression of the IGF axis is decreased in local prostate cancer but enhanced after benign prostate epithelial differentiation and TGF-beta treatment. Am J Pathol 179:2905-2919.

Mazzocca A, Fransvea E, Lavezzari G, Antonaci S, Giannelli G. 2009. Inhibition of transforming growth factor beta receptor I kinase blocks hepatocellular carcinoma growth through neo-angiogenesis regulation. Hepatology 50:1140-1151.

McCluggage WG. 2011. Immunohistochemistry in the distinction between primary and metastatic ovarian mucinous neoplasms. J Clin Pathol 65:596-600.

McCluggage WG. 2012. Immunohistochemistry in the distinction between primary and metastatic ovarian mucinous neoplasms. J Clin Pathol 65:596-600.

McGuire WP, Hoskins WJ, Brady MF, Kucera PR, Partridge EE, Look KY, Clarke-Pearson DL, Davidson M. 1996. Cyclophosphamide and cisplatin compared with paclitaxel and cisplatin in patients with stage III and stage IV ovarian cancer. N Engl J Med 334:1-6.

Medeiros F, Muto MG, Lee Y, Elvin JA, Callahan MJ, Feltmate C, Garber JE, Cramer DW, Crum CP. 2006. The tubal fimbria is a preferred site for early adenocarcinoma in women with familial ovarian cancer syndrome. Am J Surg Pathol 30:230-236.

Medici D, Hay ED, Olsen BR. 2008. Snail and Slug promote epithelial-mesenchymal transition through beta-catenin-T-cell factor-4-dependent expression of transforming growth factor-beta3. Mol Biol Cell 19:4875-4887.

Meinhold-Heerlein I, Bauerschlag D, Hilpert F, Dimitrov P, Sapinoso LM, Orlowska-Volk M, Bauknecht T, Park TW, Jonat W, Jacobsen A, Sehouli J, Luttges J, Krajewski M, Krajewski S, Reed JC, Arnold N, Hampton GM. 2005. Molecular and prognostic distinction between serous ovarian carcinomas of varying grade and malignant potential. Oncogene 24:1053-1065.

Melisi D, Ishiyama S, Sclabas GM, Fleming JB, Xia Q, Tortora G, Abbruzzese JL, Chiao PJ. 2008. LY2109761, a novel transforming growth factor beta receptor type I and type II dual inhibitor, as a therapeutic approach to suppressing pancreatic cancer metastasis. Mol Cancer Ther 7:829-840.

Mitchell D, Pobre EG, Mulivor AW, Grinberg AV, Castonguay R, Monnell TE, Solban N, Ucran JA, Pearsall RS, Underwood KW, Seehra J, Kumar R. 2010. ALK1-Fc inhibits multiple mediators of angiogenesis and suppresses tumor growth. Mol Cancer Ther 9:379-388.

Monami G, Emiliozzi V, Morrione A. 2008. Grb10/Nedd4-mediated multiubiquitination of the insulin-like growth factor receptor regulates receptor internalization. J Cell Physiol 216:426-437.

Morgan SL, Medina JE, Taylor MM, Dinulescu DM. 2014. Targeting platinum resistant disease in ovarian cancer. Curr Med Chem 21:3009-3020.

Moustakas A, Heldin CH. 2009. The regulation of TGFbeta signal transduction. Development 136:3699-3714.

Moya IM, Umans L, Maas E, Pereira PN, Beets K, Francis A, Sents W, Robertson EJ, Mummery CL, Huylebroeck D, Zwijsen A. 2012. Stalk cell phenotype depends on integration of Notch and Smad1/5 signaling cascades. Dev Cell 22:501-514.

Muggia FM, Jeffers S, Muderspach L, Roman L, Rosales R, Groshen S, Safra T, Morrow CP. 1997. Phase I/II study of intraperitoneal floxuridine and platinums (cisplatin and/or carboplatin). Gynecol Oncol 66:290-294.

Murray LJ, Abrams TJ, Long KR, Ngai TJ, Olson LM, Hong W, Keast PK, Brassard JA, O'Farrell AM, Cherrington JM, Pryer NK. 2003. SU11248 inhibits tumor growth and CSF-1R-dependent osteolysis in an experimental breast cancer bone metastasis model. Clin Exp Metastasis 20:757-766.

Nagaraj NS, Datta PK. 2010. Targeting the transforming growth factor-beta signaling pathway in human cancer. Expert Opin Investig Drugs 19:77-91.

Nakagawa T, Li JH, Garcia G, Mu W, Piek E, Bottinger EP, Chen Y, Zhu HJ, Kang DH, Schreiner GF, Lan HY, Johnson RJ. 2004. TGF-beta induces proangiogenic and antiangiogenic factors via parallel but distinct Smad pathways. Kidney Int 66:605-613.

Neuzillet C, Tijeras-Raballand A, Cohen R, Cros J, Faivre S, Raymond E, de Gramont A. 2015. Targeting the TGFbeta pathway for cancer therapy. Pharmacol Ther 147:22-31.

Nickerson T, Chang F, Lorimer D, Smeekens SP, Sawyers CL, Pollak M. 2001. In vivo progression of LAPC-9 and LNCaP prostate cancer models to androgen independence is associated with increased expression of insulin-like growth factor I (IGF-I) and IGF-I receptor (IGF-IR). Cancer Res 61:6276-6280.

Nilsson E, Doraiswamy V, Parrott JA, Skinner MK. 2001. Expression and action of transforming growth factor beta (TGFbeta1, TGFbeta2, TGFbeta3) in normal bovine ovarian surface epithelium and implications for human ovarian cancer. Mol Cell Endocrinol 182:145-155.

Obata K, Morland SJ, Watson RH, Hitchcock A, Chenevix-Trench G, Thomas EJ, Campbell IG. 1998. Frequent PTEN/MMAC mutations in endometrioid but not serous or mucinous epithelial ovarian tumors. Cancer Res 58:2095-2097.

Oberaigner W, Minicozzi P, Bielska-Lasota M, Allemani C, de Angelis R, Mangone L, Sant M. 2012. Survival for ovarian cancer in Europe: the across-country variation did not shrink in the past decade. Acta Oncol 51:441-453.

Oh SP, Seki T, Goss KA, Imamura T, Yi Y, Donahoe PK, Li L, Miyazono K, ten Dijke P, Kim S, Li E. 2000. Activin receptor-like kinase 1 modulates transforming growth factor-beta 1 signaling in the regulation of angiogenesis. Proc Natl Acad Sci U S A 97:2626-2631.

Olsson AK, Dimberg A, Kreuger J, Claesson-Welsh L. 2006. VEGF receptor signalling - in control of vascular function. Nat Rev Mol Cell Biol 7:359-371.

Oshimori N, Oristian D, Fuchs E. 2015. TGF-beta promotes heterogeneity and drug resistance in squamous cell carcinoma. Cell 160:963-976.

Ozguroglu M, Ersavasti G, Ilvan S, Hatemi G, Demir G, Demirelli FH. 1999. Bilateral inflammatory breast metastases of epithelial ovarian cancer. Am J Clin Oncol 22:408-410.

Ozols RF, Bundy BN, Greer BE, Fowler JM, Clarke-Pearson D, Burger RA, Mannel RS, DeGeest K, Hartenbach EM, Baergen R. 2003. Phase III trial of carboplatin and paclitaxel compared with cisplatin and paclitaxel in patients with optimally resected stage III ovarian cancer: a Gynecologic Oncology Group study. J Clin Oncol 21:3194-3200.

Palacios J, Gamallo C. 1998. Mutations in the beta-catenin gene (CTNNB1) in endometrioid ovarian carcinomas. Cancer Res 58:1344-1347.

Parikh A, Lee C, Joseph P, Marchini S, Baccarini A, Kolev V, Romualdi C, Fruscio R, Shah H, Wang F, Mullokandov G, Fishman D, D'Incalci M, Rahaman J, Kalir T, Redline RW, Brown BD, Narla G, DiFeo A. 2014. microRNA-181a has a critical role in ovarian cancer progression through the regulation of the epithelial-mesenchymal transition. Nat Commun 5:2977.

Pasanisi P, Venturelli E, Morelli D, Fontana L, Secreto G, Berrino F. 2008. Serum insulin-like growth factor-I and platelet-derived growth factor as biomarkers of breast cancer prognosis. Cancer Epidemiol Biomarkers Prev 17:1719-1722.

Patsialou A, Wyckoff J, Wang Y, Goswami S, Stanley ER, Condeelis JS. 2009. Invasion of human breast cancer cells in vivo requires both paracrine and autocrine

loops involving the colony-stimulating factor-1 receptor. Cancer Res 69:9498-9506.

Pearce LR, Sommer EM, Sakamoto K, Wullschleger S, Alessi DR. 2011. Protor-1 is required for efficient mTORC2-mediated activation of SGK1 in the kidney. Biochem J 436:169-179.

Peeper DS, Upton TM, Ladha MH, Neuman E, Zalvide J, Bernards R, DeCaprio JA, Ewen ME. 1997. Ras signalling linked to the cell-cycle machinery by the retinoblastoma protein. Nature 386:177-181.

Perrais M, Chen X, Perez-Moreno M, Gumbiner BM. 2007. E-cadherin homophilic ligation inhibits cell growth and epidermal growth factor receptor signaling independently of other cell interactions. Mol Biol Cell 18:2013-2025.

Perren TJ, Swart AM, Pfisterer J, Ledermann JA, Pujade-Lauraine E, Kristensen G, Carey MS, Beale P, Cervantes A, Kurzeder C, du Bois A, Sehouli J, Kimmig R, Stahle A, Collinson F, Essapen S, Gourley C, Lortholary A, Selle F, Mirza MR, Leminen A, Plante M, Stark D, Qian W, Parmar MK, Oza AM. 2011. A phase 3 trial of bevacizumab in ovarian cancer. N Engl J Med 365:2484-2496.

Phng LK, Gerhardt H. 2009. Angiogenesis: a team effort coordinated by notch. Dev Cell 16:196-208.

Pitulescu ME, Schmidt I, Benedito R, Adams RH. 2010. Inducible gene targeting in the neonatal vasculature and analysis of retinal angiogenesis in mice. Nat Protoc 5:1518-1534.

Pollak M. 2008. Insulin and insulin-like growth factor signalling in neoplasia. Nat Rev Cancer 8:915-928.

Pollak M. 2012. The insulin and insulin-like growth factor receptor family in neoplasia: an update. Nat Rev Cancer 12:159-169.

Pollak MN. 2004. Insulin-like growth factors and neoplasia. Novartis Found Symp 262:84-98; discussion 98-107, 265-108.

Poveda A, Vergote I, Tjulandin S, Kong B, Roy M, Chan S, Filipczyk-Cisarz E, Hagberg H, Kaye SB, Colombo N, Lebedinsky C, Parekh T, Gomez J, Park YC, Alfaro V, Monk BJ. 2010. Trabectedin plus pegylated liposomal doxorubicin in relapsed ovarian cancer: outcomes in the partially platinum-sensitive (platinum-free interval 6-12 months) subpopulation of OVA-301 phase III randomized trial. Ann Oncol 22:39-48.

Prat J. 2012. Ovarian carcinomas: five distinct diseases with different origins, genetic alterations, and clinicopathological features. Virchows Arch 460:237-249.

Press JZ, De Luca A, Boyd N, Young S, Troussard A, Ridge Y, Kaurah P, Kalloger SE, Blood KA, Smith M, Spellman PT, Wang Y, Miller DM, Horsman D, Faham M, Gilks CB, Gray J, Huntsman DG. 2008. Ovarian carcinomas with genetic and epigenetic BRCA1 loss have distinct molecular abnormalities. BMC Cancer 8:17.

Provencher D. 2000. Characterization of four novel epithelial cancer cell lines. In Vitro Cell. Dev. Biol. Anim.:357-361.

Rao W, Li H, Song F, Zhang R, Yin Q, Wang Y, Xi Y, Ge H. 2014. OVA66 increases cell growth, invasion and survival via regulation of IGF-1R-MAPK signaling in human cancer cells. Carcinogenesis 35:1573-1581.

Ricard N, Ciais D, Levet S, Subileau M, Mallet C, Zimmers TA, Lee SJ, Bidart M, Feige JJ, Bailly S. 2012. BMP9 and BMP10 are critical for postnatal retinal vascular remodeling. Blood 119:6162-6171.

Richards JS, Pangas SA. The ovary: basic biology and clinical implications. J Clin Invest 120:963-972.

Risau W. 1997. Mechanisms of angiogenesis. Nature 386:671-674.

Rochon ER, Wright DS, Schubert MM, Roman BL. 2015. Context-specific interactions between Notch and ALK1 cannot explain ALK1-associated arteriovenous malformations. Cardiovasc Res 107:143-152.

Roderburg C, Luedde M, Vargas Cardenas D, Vucur M, Mollnow T, Zimmermann HW, Koch A, Hellerbrand C, Weiskirchen R, Frey N, Tacke F, Trautwein C, Luedde T. 2012. miR-133a mediates TGF-beta-dependent derepression of collagen synthesis in hepatic stellate cells during liver fibrosis. J Hepatol 58:736-742.

Rodon J, Carducci MA, Sepulveda-Sanchez JM, Azaro A, Calvo E, Seoane J, Brana I, Sicart E, Gueorguieva I, Cleverly AL, Pillay NS, Desaiah D, Estrem ST, Paz-Ares L, Holdhoff M, Blakeley J, Lahn MM, Baselga J. 2014. First-in-human dose study of the novel transforming growth factor-beta receptor I kinase inhibitor LY2157299 monohydrate in patients with advanced cancer and glioma. Clin Cancer Res 21:553-560.

Roman BL, Pham VN, Lawson ND, Kulik M, Childs S, Lekven AC, Garrity DM, Moon RT, Fishman MC, Lechleider RJ, Weinstein BM. 2002. Disruption of acvrl1 increases endothelial cell number in zebrafish cranial vessels. Development 129:3009-3019.

Romanelli RJ, LeBeau AP, Fulmer CG, Lazzarino DA, Hochberg A, Wood TL. 2007. Insulin-like growth factor type-I receptor internalization and recycling mediate the sustained phosphorylation of Akt. J Biol Chem 282:22513-22524.

Rothenberg ML, Liu PY, Wilczynski S, Nahhas WA, Winakur GL, Jiang CS, Moinpour CM, Lyons B, Weiss GR, Essell JH, Smith HO, Markman M, Alberts DS. 2004. Phase II trial of vinorelbine for relapsed ovarian cancer: a Southwest Oncology Group study. Gynecol Oncol 95:506-512.

Rubtsov YP, Rudensky AY. 2007. TGFbeta signalling in control of T-cell-mediated self-reactivity. Nat Rev Immunol 7:443-453.

Sakaki-Yumoto M, Katsuno Y, Derynck R. 2012. TGF-beta family signaling in stem cells. Biochim Biophys Acta 1830:2280-2296.

Santarpia L, Lippman SM, El-Naggar AK. 2012. Targeting the MAPK-RAS-RAF signaling pathway in cancer therapy. Expert Opin Ther Targets 16:103-119.

Sapi E, Kacinski BM. 1999. The role of CSF-1 in normal and neoplastic breast physiology. Proc Soc Exp Biol Med 220:1-8.

Sato N, Tsunoda H, Nishida M, Morishita Y, Takimoto Y, Kubo T, Noguchi M. 2000. Loss of heterozygosity on 10q23.3 and mutation of the tumor suppressor gene PTEN in benign endometrial cyst of the ovary: possible sequence progression from benign endometrial cyst to endometrioid carcinoma and clear cell carcinoma of the ovary. Cancer Res 60:7052-7056.

Sawada K, Mitra AK, Radjabi AR, Bhaskar V, Kistner EO, Tretiakova M, Jagadeeswaran S, Montag A, Becker A, Kenny HA, Peter ME, Ramakrishnan V, Yamada SD, Lengyel E. 2008. Loss of E-cadherin promotes ovarian cancer metastasis via alpha 5-integrin, which is a therapeutic target. Cancer Res 68:2329-2339.

Scharpfenecker M, van Dinther M, Liu Z, van Bezooijen RL, Zhao Q, Pukac L, Lowik CW, ten Dijke P. 2007. BMP-9 signals via ALK1 and inhibits bFGF-induced endothelial cell proliferation and VEGF-stimulated angiogenesis. J Cell Sci 120:964-972.

Schedlich LJ, Yenson VM, Baxter RC. 2013. TGF-beta-induced expression of IGFBP-3 regulates IGF1R signaling in human osteosarcoma cells. Mol Cell Endocrinol 377:56-64.

Sehat B, Andersson S, Girnita L, Larsson O. 2008. Identification of c-Cbl as a new ligase for insulin-like growth factor-I receptor with distinct roles from Mdm2 in receptor ubiquitination and endocytosis. Cancer Res 68:5669-5677.

Sehat B, Andersson S, Vasilcanu R, Girnita L, Larsson O. 2007. Role of ubiquitination in IGF-1 receptor signaling and degradation. PLoS One 2:e340.

Seki T, Hong KH, Oh SP. 2006. Nonoverlapping expression patterns of ALK1 and ALK5 reveal distinct roles of each receptor in vascular development. Lab Invest 86:116-129.

Seoane J. 2008. The TGFBeta pathway as a therapeutic target in cancer. Clin Transl Oncol 10:14-19.

Sepp-Lorenzino L, Ma Z, Lebwohl DE, Vinitsky A, Rosen N. 1995. Herbimycin A induces the 20 S proteasome- and ubiquitin-dependent degradation of receptor tyrosine kinases. J Biol Chem 270:16580-16587.

Serra H, Chivite I, Angulo-Urarte A, Soler A, Sutherland JD, Arruabarrena-Aristorena A, Ragab A, Lim R, Malumbres M, Fruttiger M, Potente M, Serrano M, Fabra A, Viñals F, Casanovas O, Pandolfi PP, Bigas A, Carracedo A, Gerhardt H, Graupera M. 2015. PTEN mediates Notch-dependent stalk cell arrest in angiogenesis. Nat Commun 6:7935.

Sheen YY, Kim MJ, Park SA, Park SY, Nam JS. 2013. Targeting the Transforming Growth Factor-beta Signaling in Cancer Therapy. Biomol Ther (Seoul) 21:323-331.

Shen H, Fang Y, Dong W, Mu X, Liu Q, Du J. 2012. IGF-1 receptor is down-regulated by sunitinib induces MDM2-dependent ubiquitination. FEBS Open Bio 2:1-5.

Shi Y, Massague J. 2003. Mechanisms of TGF-beta signaling from cell membrane to the nucleus. Cell 113:685-700.

Shibuya M. 2013. Vascular endothelial growth factor and its receptor system: physiological functions in angiogenesis and pathological roles in various diseases. J Biochem 153:13-19.

Shin I, Bakin AV, Rodeck U, Brunet A, Arteaga CL. 2001. Transforming growth factor beta enhances epithelial cell survival via Akt-dependent regulation of FKHRL1. Mol Biol Cell 12:3328-3339.

Shipitsin M, Campbell LL, Argani P, Weremowicz S, Bloushtain-Qimron N, Yao J, Nikolskaya T, Serebryiskaya T, Beroukhim R, Hu M, Halushka MK, Sukumar S, Parker LM, Anderson KS, Harris LN, Garber JE, Richardson AL, Schnitt SJ, Nikolsky Y, Gelman RS, Polyak K. 2007. Molecular definition of breast tumor heterogeneity. Cancer Cell 11:259-273.

Shovlin CL. 2010. Hereditary haemorrhagic telangiectasia: pathophysiology, diagnosis and treatment. Blood Rev 24:203-219.

Siegel PM, Massague J. 2003. Cytostatic and apoptotic actions of TGF-beta in homeostasis and cancer. Nat Rev Cancer 3:807-821.

Siegel PM, Shu W, Massague J. 2003. Mad upregulation and Id2 repression accompany transforming growth factor (TGF)-beta-mediated epithelial cell growth suppression. J Biol Chem 278:35444-35450.

Siekmann AF, Affolter M, Belting HG. 2013. The tip cell concept 10 years after: new players tune in for a common theme. Exp Cell Res 319:1255-1263.

Singer G, Stohr R, Cope L, Dehari R, Hartmann A, Cao DF, Wang TL, Kurman RJ, Shih Ie M. 2005. Patterns of p53 mutations separate ovarian serous borderline tumors and low- and high-grade carcinomas and provide support for a new model of ovarian carcinogenesis: a mutational analysis with immunohistochemical correlation. Am J Surg Pathol 29:218-224.

Singh RK, Gaikwad SM, Jinager A, Chaudhury S, Maheshwari A, Ray P. 2014. IGF-1R inhibition potentiates cytotoxic effects of chemotherapeutic agents in early stages of chemoresistant ovarian cancer cells. Cancer Lett 354:254-262.

Skates SJ, Jacobs IJ, Knapp RC. 2001. Tumor markers in screening for ovarian cancer. Methods Mol Med 39:61-73.

Sonpavde G, Hutson TE. 2007. Pazopanib: a novel multitargeted tyrosine kinase inhibitor. Curr Oncol Rep 9:115-119.

Srinivasan S, Hanes MA, Dickens T, Porteous ME, Oh SP, Hale LP, Marchuk DA. 2003. A mouse model for hereditary hemorrhagic telangiectasia (HHT) type 2. Hum Mol Genet 12:473-482.

St Croix B, Sheehan C, Rak JW, Florenes VA, Slingerland JM, Kerbel RS. 1998. E-Cadherin-dependent growth suppression is mediated by the cyclin-dependent kinase inhibitor p27(KIP1). J Cell Biol 142:557-571.

Stahl A, Connor KM, Sapieha P, Chen J, Dennison RJ, Krah NM, Seaward MR, Willett KL, Aderman CM, Guerin KI, Hua J, Lofqvist C, Hellstrom A, Smith LE. 2010. The mouse retina as an angiogenesis model. Invest Ophthalmol Vis Sci 51:2813-2826.

Steelman LS, Chappell WH, Abrams SL, Kempf RC, Long J, Laidler P, Mijatovic S, Maksimovic-Ivanic D, Stivala F, Mazzarino MC, Donia M, Fagone P,

Malaponte G, Nicoletti F, Libra M, Milella M, Tafuri A, Bonati A, Basecke J, Cocco L, Evangelisti C, Martelli AM, Montalto G, Cervello M, McCubrey JA. 2011. Roles of the Raf/MEK/ERK and PI3K/PTEN/Akt/mTOR pathways in controlling growth and sensitivity to therapy-implications for cancer and aging. Aging (Albany NY) 3:192-222.

Stewart BW KP. 2003. World Cancer Report. Lyon: IARC Press.

Sugiyama T, Kamura T, Kigawa J, Terakawa N, Kikuchi Y, Kita T, Suzuki M, Sato I, Taguchi K. 2000. Clinical characteristics of clear cell carcinoma of the ovary: a distinct histologic type with poor prognosis and resistance to platinum-based chemotherapy. Cancer 88:2584-2589.

Surowiak P, Materna V, Maciejczyk A, Pudelko M, Suchocki S, Kedzia W, Nowak-Markwitz E, Dumanska M, Spaczynski M, Zabel M, Dietel M, Lage H. 2008. Decreased expression of p16 in ovarian cancers represents an unfavourable prognostic factor. Histol Histopathol 23:531-538.

Sutton AB, Canfield AE, Schor SL, Grant ME, Schor AM. 1991. The response of endothelial cells to TGF beta-1 is dependent upon cell shape, proliferative state and the nature of the substratum. J Cell Sci 99 (Pt 4):777-787.

Takano M, Kikuchi Y, Yaegashi N, Kuzuya K, Ueki M, Tsuda H, Suzuki M, Kigawa J, Takeuchi S, Moriya T, Sugiyama T. 2006. Clear cell carcinoma of the ovary: a retrospective multicentre experience of 254 patients with complete surgical staging. Br J Cancer 94:1369-1374.

ten Bokkel Huinink W, Gore M, Carmichael J, Gordon A, Malfetano J, Hudson I, Broom C, Scarabelli C, Davidson N, Spanczynski M, Bolis G, Malmstrom H, Coleman R, Fields SC, Heron JF. 1997. Topotecan versus paclitaxel for the treatment of recurrent epithelial ovarian cancer. J Clin Oncol 15:2183-2193.

Tian M, Neil JR, Schiemann WP. 2011. Transforming growth factor-beta and the hallmarks of cancer. Cell Signal 23:951-962.

Tian M, Schiemann WP. 2009. PGE2 receptor EP2 mediates the antagonistic effect of COX-2 on TGF-beta signaling during mammary tumorigenesis. FASEB J 24:1105-1116.

Toy EP, Azodi M, Folk NL, Zito CM, Zeiss CJ, Chambers SK. 2009. Enhanced ovarian cancer tumorigenesis and metastasis by the macrophage colony-stimulating factor. Neoplasia 11:136-144.

Tual-Chalot S, Mahmoud M, Allinson KR, Redgrave RE, Zhai Z, Oh SP, Fruttiger M, Arthur HM. 2014. Endothelial depletion of Acvrl1 in mice leads to arteriovenous malformations associated with reduced endoglin expression. PLoS One 9:e98646.

Tual-Chalot S, Oh SP, Arthur HM. 2015. Mouse models of hereditary hemorrhagic telangiectasia: recent advances and future challenges. Front Genet 6:25.

Urness LD, Sorensen LK, Li DY. 2000. Arteriovenous malformations in mice lacking activin receptor-like kinase-1. Nat Genet 26:328-331.

Ushijima K. 2010. Treatment for recurrent ovarian cancer-at first relapse. J Oncol 2010:497429.

Vadgama JV, Wu Y, Datta G, Khan H, Chillar R. 1999. Plasma insulin-like growth factor-I and serum IGF-binding protein 3 can be associated with the progression of breast cancer, and predict the risk of recurrence and the probability of survival in African-American and Hispanic women. Oncology 57:330-340.

Vallieres L. 2009. Trabedersen, a TGFbeta2-specific antisense oligonucleotide for the treatment of malignant gliomas and other tumors overexpressing TGFbeta2. IDrugs 12:445-453.

Vecchione A, Marchese A, Henry P, Rotin D, Morrione A. 2003. The Grb10/Nedd4 complex regulates ligand-induced ubiquitination and stability of the insulin-like growth factor I receptor. Mol Cell Biol 23:3363-3372.

Vidal A, Munoz C, Guillen MJ, Moreto J, Puertas S, Martinez-Iniesta M, Figueras A, Padulles L, Garcia-Rodriguez FJ, Berdiel-Acer M, Pujana MA, Salazar R, Gil-Martin M, Marti L, Ponce J, Mollevi DG, Capella G, Condom E, Viñals F, Huertas D, Cuevas C, Esteller M, Aviles P, Villanueva A. 2012. Lurbinectedin (PM01183), a new DNA minor groove binder, inhibits growth of orthotopic primary graft of cisplatin-resistant epithelial ovarian cancer. Clin Cancer Res 18:5399-5411.

Vinals F, Pouyssegur J. 2001. Transforming growth factor beta1 (TGF-beta1) promotes endothelial cell survival during in vitro angiogenesis via an autocrine mechanism implicating TGF-alpha signaling. Mol Cell Biol 21:7218-7230.

Viñals F, Pouyssegur J. 2001. Transforming growth factor beta1 (TGF-beta1) promotes endothelial cell survival during in vitro angiogenesis via an autocrine mechanism implicating TGF-alpha signaling. Mol Cell Biol 21:7218-7230.

Vives M, Ginesta MM, Gracova K, Graupera M, Casanovas O, Capella G, Serrano T, Laquente B, Viñals F. 2013. Metronomic chemotherapy following the maximum tolerated dose is an effective anti-tumour therapy affecting angiogenesis, tumour dissemination and cancer stem cells. Int J Cancer 133:2464-2472.

Wan X, Li ZG, Yingling JM, Yang J, Starbuck MW, Ravoori MK, Kundra V, Vazquez E, Navone NM. 2012. Effect of transforming growth factor beta (TGF-beta) receptor I kinase inhibitor on prostate cancer bone growth. Bone 50:695-703.

Wang L, Park P, Zhang H, La Marca F, Claeson A, Than K, Rahman S, Lin CY. 2014. BMP-2 inhibits tumor growth of human renal cell carcinoma and induces bone formation. Int J Cancer 131:1941-1950.

Watabe T, Miyazono K. 2009. Roles of TGF-beta family signaling in stem cell renewal and differentiation. Cell Res 19:103-115.

Weber B, Bamias A, Pereira D, Ray-Coquard AP, Pujade-Lauraine E, Mirza MR, Hilpert F, Reuss A, Kristensen G, SorioI R, Vergote B, Witteveen P, Wimberger P, Oaknin A, Follana P, Bollag DT. 2012. A randomized phase III

trial evaluating bevacizumab (BEV) plus chemotherapy (CT) for platinum (PT)-resistant recurrent ovarian cancer (OC). J Clin Oncol 30.

Weiss A, Attisano L. 2013. The TGFbeta superfamily signaling pathway. Wiley Interdiscip Rev Dev Biol 2:47-63.

Wen WH, Reles A, Runnebaum IB, Sullivan-Halley J, Bernstein L, Jones LA, Felix JC, Kreienberg R, el-Naggar A, Press MF. 1999. p53 mutations and expression in ovarian cancers: correlation with overall survival. Int J Gynecol Pathol 18:29-41.

Woolas RP, Xu FJ, Jacobs IJ, Yu YH, Daly L, Berchuck A, Soper JT, Clarke-Pearson DL, Oram DH, Bast RC, Jr. 1993. Elevation of multiple serum markers in patients with stage I ovarian cancer. J Natl Cancer Inst 85:1748-1751.

Wu L, Derynck R. 2009. Essential role of TGF-beta signaling in glucose-induced cell hypertrophy. Dev Cell 17:35-48.

Yan X, Liu Z, Chen Y. 2009. Regulation of TGF-beta signaling by Smad7. Acta Biochim Biophys Sin (Shanghai) 41:263-272.

Yaniv E, Preis M, Shevro J, Nageris B, Hadar T. 2011. Anti-estrogen therapy for hereditary hemorrhagic telangiectasia - a long-term clinical trial. Rhinology 49:214-216.

Yi JY, Shin I, Arteaga CL. 2005. Type I transforming growth factor beta receptor binds to and activates phosphatidylinositol 3-kinase. J Biol Chem 280:10870-10876.

Young K, Conley B, Romero D, Tweedie E, O'Neill C, Pinz I, Brogan L, Lindner V, Liaw L, Vary CP. 2012. BMP9 regulates endoglin-dependent chemokine responses in endothelial cells. Blood 120:4263-4273.

Yuan Z WY, Cragun JM, Chambers SK and Zheng W. 2013. Cell origin of endometriosis: contribution by the fallopian tube epithelium. Am J Clin Exp Obstet Gynecol 1:37-42.

Zhang M, Herion TW, Timke C, Han N, Hauser K, Weber KJ, Peschke P, Wirkner U, Lahn M, Huber PE. 2011a. Trimodal glioblastoma treatment consisting of concurrent radiotherapy, temozolomide, and the novel TGF-beta receptor I kinase inhibitor LY2109761. Neoplasia 13:537-549.

Zhang M, Kleber S, Rohrich M, Timke C, Han N, Tuettenberg J, Martin-Villalba A, Debus J, Peschke P, Wirkner U, Lahn M, Huber PE. 2011b. Blockade of TGF-beta signaling by the TGFbetaR-I kinase inhibitor LY2109761 enhances radiation response and prolongs survival in glioblastoma. Cancer Res 71:7155-7167.

Zhang S, Balch C, Chan MW, Lai HC, Matei D, Schilder JM, Yan PS, Huang TH, Nephew KP. 2008. Identification and characterization of ovarian cancer-initiating cells from primary human tumors. Cancer Res 68:4311-4320.

Zhang YE. 2009. Non-Smad pathways in TGF-beta signaling. Cell Res 19:128-139.

Zhao H, Desai V, Wang J, Epstein DM, Miglarese M, Buck E. 2012. Epithelial-mesenchymal transition predicts sensitivity to the dual IGF-1R/IR inhibitor OSI-906 in hepatocellular carcinoma cell lines. Mol Cancer Ther 11:503-513.